Energy & Environmental Science

ROYAL SOCIETY OF CHEMISTRY

REVIEW

View Article Online
View Journal

Cite this: DOI: 10.1039/d0ee00039f

Flexible metal–gas batteries: a potential option for next-generation power accessories for wearable electronics

Jingwen Zhou,[a] Jianli Cheng,*[a] Bin Wang,*[a] Huisheng Peng[b] and Jun Lu[c]

Flexible metal–gas batteries have become increasingly attractive for use in wearable electronics in the recent years due to their large theoretical energy density and superior adaptability to irregular geometric surfaces, such as the human body. With continuous improvements in design strategies and assembly technologies, the fabrication of various advanced flexible metal–gas batteries has been attempted. In spite of these efforts, the synchronous integration of high flexibility, safety, comfort, and high performance into flexible metal–gas batteries with specifically functionalized configurations still remains a formidable challenge. To resolve these dilemmas, the redesign of cathode catalysts, gel polymer electrolyte, and battery configurations/components has been investigated. In this paper, we review the recent technical advances together with the major dilemmas facing currently available flexible metal–gas batteries, highlighting how flexible cathodes and gel polymer electrolytes with various structures and components can affect the electrochemical performance and functionality of flexible metal–gas batteries. Flexible Zn–air, Li–O_2/air, and Li–CO_2 batteries are mainly exemplified to elucidate their promising potential. Finally, based on our considerations, unresolved technical hurdles and future research perspectives involving flexible metal–gas batteries for wearable electronics are proposed.

Received 5th January 2020,
Accepted 10th March 2020

DOI: 10.1039/d0ee00039f

rsc.li/ees

Broader context

With the increasing popularity of flexible electronics, higher requirements are imposed on energy supply and space adaptability of their power accessories. Due to the high energy densities, metal–gas batteries seem to be a potential option for use as next-generation energy storage systems in flexible consumer electronic products, particularly appropriate for wearable electronics characterized by long-term low-power operation. Despite numerous efforts being made to enhance the electrochemical performance of cathode catalysts, the synchronous integration of high flexibility and superior performance into metal–gas batteries still remains unresolved. In fact, the properties of gas cathodes, metal anodes, electrolytes, and battery configurations have a significant impact on the electrochemical performance and functionality of flexible metal–gas batteries, which should be carefully designed and optimized to accommodate various deformations. Besides flexibility, some other factors such as fire/water resistance, stretchability, safety, and comfort are also noteworthy. This article reviews the development status and discusses the recent technical advances, unresolved challenges, expected functionalities, and application opportunities of flexible metal–gas batteries for wearable electronics. It is hoped that some new insights and proposed methodology can drive the advance of flexible metal–gas batteries toward practical applications and provide design inspiration for other flexible energy storage devices.

1. Introduction

Over the past few decades, the global economy has flourished but at the cost of rapid natural resource consumption, which is far beyond human imagination.[1–4] This is particularly the case when fossil fuels, the dominant resources that are utilized to produce electricity and serve as power for vehicles, are taken into consideration. It has been predicted that fossil fuels will be totally exhausted by the year 2050 based on the current consumption rates.[1,5,6] Therefore, numerous efforts have been devoted toward exploiting alternative resources to ensure the sustainable development of the earth, such as solar power, geothermal energy, winds, and tides.

Among them, in the early 1970s, lithium-ion batteries (LIBs) emerged as one of the most representative applications of clean electrochemical energy.[7–10] With the gradual development of commercial technology, LIBs do provide much convenience for

[a] Institute of Chemical Materials, China Academy of Engineering Physics, Mianyang, Sichuan, 621900, P. R. China. E-mail: Jianlicheng@caep.cn, binwang@caep.cn
[b] Department of Macromolecular Science and Laboratory of Advanced Materials, Fudan University, Shanghai, 200438, China
[c] Chemical Sciences and Engineering Division, Argonne National Laboratory, Argonne, IL, 60439, USA

the daily lives of humans and even stimulate the revolution of electronic devices toward portability and miniaturization. Nowadays, the applications of LIBs have even been extended to electric vehicles (EVs). A long driving range ($\geq$500 km) requires power batteries with energy densities in excess of 500 W h kg^{-1}, provided that the battery pack system including indispensable ancillaries weighs no more than 300 kg per vehicle.[11,12] However, conventional LIBs based on $LiCoO_2$/graphite cannot satisfy this requirement due to their theoretical limitation of 350 W h kg^{-1}. It is generally accepted that a 30% improvement in energy density is the upper limit that can be achieved by optimizing the current technology, which means that endurance mileage is difficult to significantly increase when driving a conventional-LIB-powered EV.[13–16] Hence, developing next-generation high-performance energy storage systems with novel electrochemistry seems to be an inevitable choice if we want to break through the intrinsic obstacles of current batteries, such that our targets of energy density exceeding 500 W h kg^{-1} and fabrication cost of less than \$100 kW h^{-1} can be achieved.[17–19]

Metal–gas batteries have attracted significant attention in the recent years considering their much higher energy density.[33] For example, Li–O_2 batteries possess a theoretical energy density of approximately 3500 W h kg^{-1} based on the discharge product of Li_2O_2, which is nearly ten times as high as that of LIBs.[17,34] On the basis of the long development history of over 100 years, numerous categories of metal–gas couples have already been investigated to realize effective electrochemical energy transformation. According to the different characteristics of the metals and electrolytes employed, metal–gas batteries can be divided into two main types: aqueous and nonaqueous. Theoretical energy densities together with equilibrium potentials of earlier known metal–gas batteries are shown in Fig. 1, which provide a general comparison.[20–32] On average, the energy storage capability of nonaqueous metal–gas batteries is higher than that of their aqueous counterparts. The exceptionally high gravimetric energy density originates from the considerable free energy release of metal ions–gas molecules reactions occurring on the surface of the cathode catalyst.[18,34] The gases acting as

Jingwen Zhou

Jingwen Zhou is working as a Research Assistant at the Institute of Chemical Materials, China Academy of Engineering Physics. He received his BS and MS from Tianjin University in 2014 and 2017, respectively. His research direction focuses on the design and synthesis of multi-dimensional nanocomposites and their applications in novel flexible energy storage systems.

Jianli Cheng

Jianli Cheng received her PhD from Fudan University in 2009. After working at Lawrence Berkeley National Laboratory (Berkeley, USA), she became an Associate Professor at China Academy of Engineering Physics. Her research focuses on the fabrication and application of new materials for flexible energy storage/conversion systems, particularly in batteries and supercapacitors.

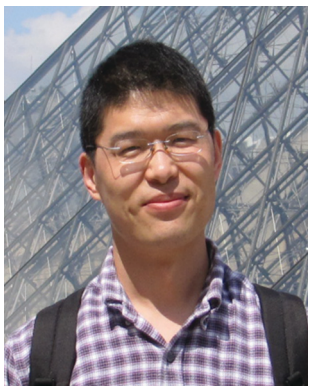

Bin Wang

Bin Wang is a Staff Scientist at the National Energy Novel Materials Center (NENMC, China) and the Institute of Chemical Materials, China Academy of Engineering Physics (ICM-CAEP). He received his PhD from Fudan University in 2009. He was a Postdoctoral Scholar at Lawrence Berkeley National Lab (LBNL, USA) during 2009–2013 and then joined the NENMC and ICM-CAEP. His research focuses on the development and applications of novel materials for flexible energy conversion and storage systems.

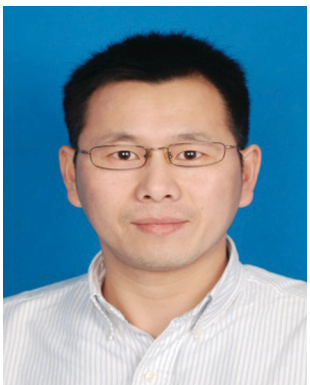

Huisheng Peng

Huisheng Peng received his PhD in Chemical Engineering from Tulane University in USA in 2006. He worked at Los Alamos National Laboratory, US Department of Energy, from 2006 to 2008. Dr Peng has been appointed as a Professor at the Department of Macromolecular Science and Laboratory of Advanced Materials at Fudan University since October 2008. He served as an Associate Chair at the Department of Macromolecular Science since 2012 and Director of the Center of Polymers and their Advanced Composite Materials since 2014. His research focuses on the development of novel energy materials and devices, particularly those based on polymers.

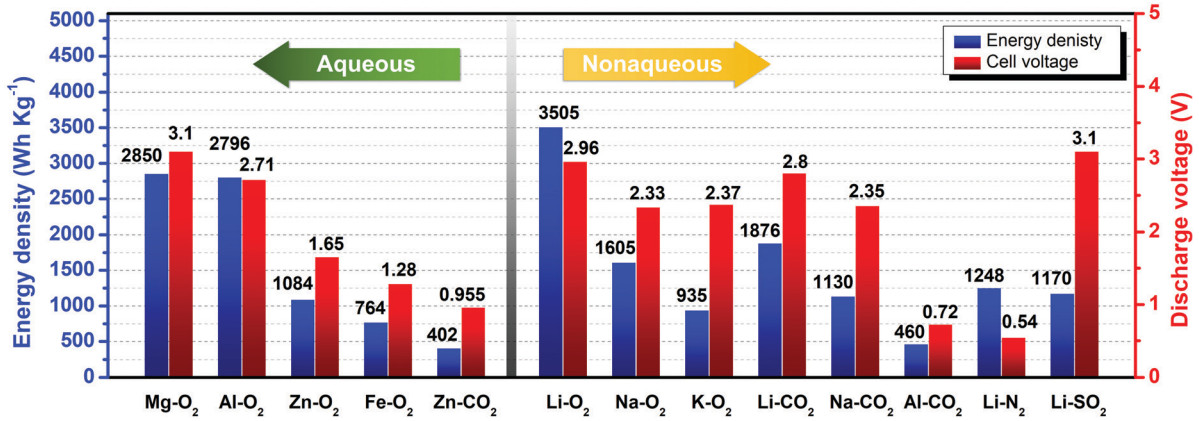

Fig. 1 Theoretical energy densities and cell working voltages for various metal–gas batteries. Data were directly obtained or calculated from the literature.[20–32] All the theoretical energy densities are given based on the total weight of the discharge products, unless specified.

energy resources are commonly available from the ambient atmosphere instead of requiring storage within the battery, which is also beneficial for achieving high energy density. In fairness, although the energy density of metal–gas batteries is closely approaching that of ideal power systems, their viability to replace LIBs for use in future EVs still currently remains unclear; this is because of problems such as sluggish gas reduction reaction rate and rapid catalysis decay, which might not meet the power/longevity criteria necessary for high-power and frequently used applications.[35,36] Meanwhile, quick charging (corresponding to gas evolution at higher rates) is more difficult to realize in currently available metal–gas batteries with relatively large overpotential,[17,34,37] leading to a long period of waiting for reuse. Further, it should be pointed out that gas storage tanks or gas depuration/transportation systems are indispensable onboard to stabilize the energy supply, which may encounter challenges with regard to safety, weight, space, reliability, and replacement.

Jun Lu

Jun Lu is a Chemist at the Argonne National Laboratory. His research interests focus on the electrochemical energy storage and conversion technology. He received his PhD from the Department of Metallurgical Engineering at the University of Utah in 2009 with a major in the research on metal hydrides for reversible hydrogen storage applications. He serves as the Associate Editor of ACS Applied Materials and Interfaces. He was elected as the Associate President and Board Committee Member of the International Academy of Electrochemical Energy Science (IAOEES). He has authored/coauthored more than 350 peer-reviewed research articles, published in Nature, Nature Energy, Nature Nanotechnology, etc.

However, in spite of the above dilemmas, we are inspired by the fact that metal–gas batteries have revealed promising potential for becoming advanced novel energy storage systems for consumer electronic products, particularly appropriate for wearable electronics with the characteristics of long-term and low-power operation on the basis of current research findings,[38–40] which have been rapidly accumulating in the last five years (Fig. 2a). Firstly, their outstanding energy storage capability enables the functional components to become more durable after the recharge process as compared to that with conventional LIB-based devices with a similar size or weight. It is a pronounced advantage that is urgent for consumer markets. Secondly, the reversible capacity delivered by metal–gas batteries originates from the electrocatalytic gas reduction/oxidation reactions in an open system such that a relatively small quantity of cathode catalysts together with easier encapsulation is necessary, which significantly lowers the fabrication cost of batteries, thereby making them widely affordable to customers. Thirdly, based on the discharge capacity and cycling behavior of current lab-scale metal–gas batteries, their service life allows them to maintain pace with the generational change (about every 2–3 years) in portable and wearable electronics. The moderate total energy storage of lab-scale devices indicates that the way to promote their electrochemical performance toward use in industrial products for consumer electronics is fairly promising.[41–43]

Nevertheless, the aforementioned favorable viewpoints do not imply that there are no bottlenecks for metal–gas batteries becoming the next-generation power accessories of wearable electronics. On one hand, a metal–gas battery comprises a metal anode, separator/electrolyte, and air cathode, which is similar to the configuration of a half-cell LIB.[7,18,33] The main structural difference between these two kinds of batteries lies in the cathode, namely, active materials are coated on aluminum foil for LIBs; however, for metal–gas batteries, catalysts need to be sprayed onto a well interconnected and porous current collector to permit sufficient gas diffusion from the ambient environment to the cathode, such as carbon paper, nickel foam, or stainless steel mesh. Owing to the introduction of gas diffusion layers, most metal–gas batteries have a rigid

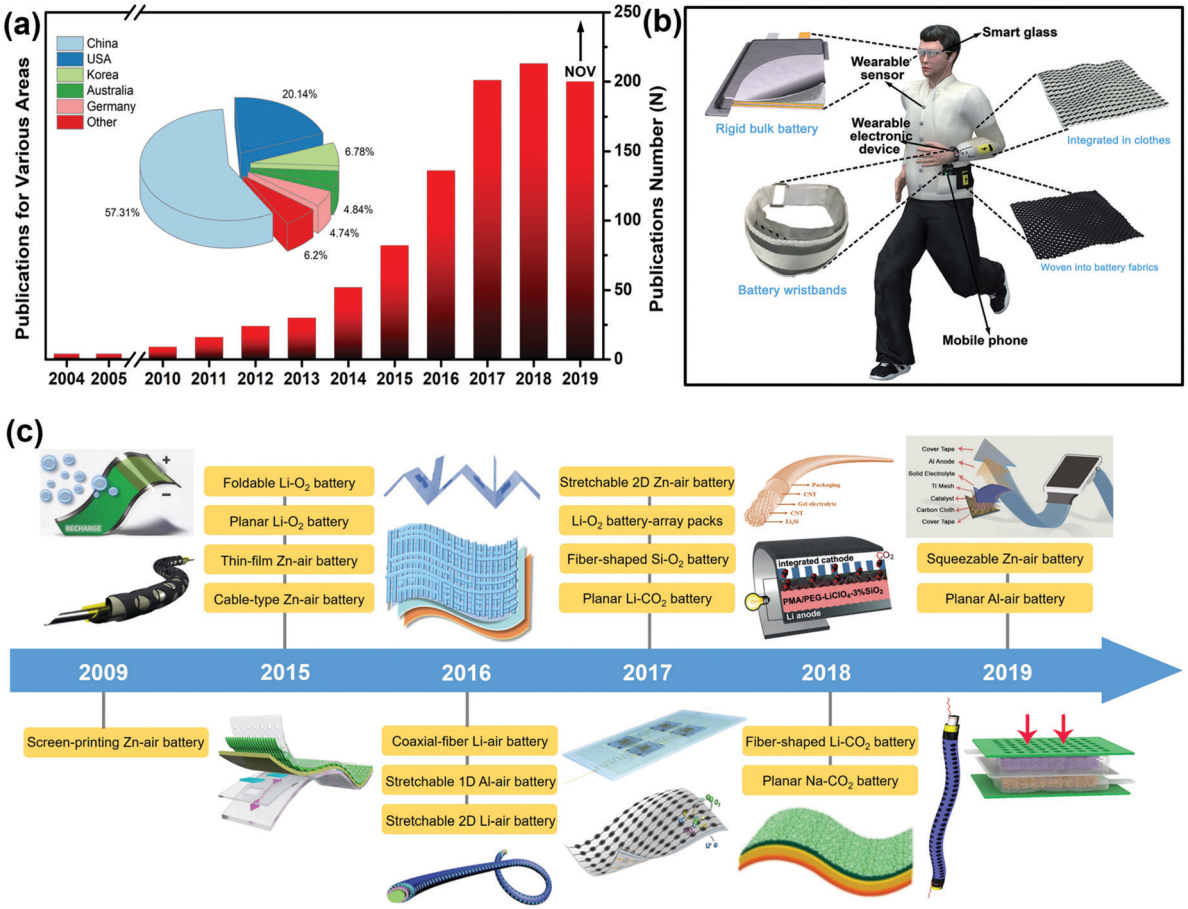

Fig. 2 (a) Number of publications that include "flexible metal–gas batteries" according to the Web of Science (as on November 2019). (b) Potential applications of flexible metal–gas batteries in wearable electronics. Reproduced with permission. Copyright 2017, Wiley-VCH.[93] (c) Timeline of the developments of flexible metal–gas batteries. Metal–gas batteries that have achieved flexibility till now are Zn–air, Li–O_2/air, Al–air, Si–O_2, Li–CO_2, and Na–CO_2 batteries.[21,29,55,59–70]

bulk structure. The lack of flexibility means that electronic devices require additional space to accommodate the power accessories in a manner that the volume and weight of the devices are not unnecessarily increased. Simultaneously, the general consensus is that batteries with a rigid structure are detrimental to the construction of flexible devices, particularly for wearable electronics that are designed to come into direct contact with the human body (Fig. 2b). Many high-tech smart electronic devices have to compromise on operational performance due to the non-deformability of batteries, *e.g.*, Huawei Mate X (5G) with a foldable screen, Apple Watch, and Google Glass.[38,43–45] It has been recognized that flexibility should be an indispensable factor of metal–gas batteries that are adaptable for use in wearable electronics. Of course, while resolving the problem of flexibility, other factors such as comfort, water/fire resistance, stretchability, and mechanical strength should also be taken into consideration in actual service conditions.[38,41,42,46–48]

On the other hand, apart from device functionality, current studies involving metal–gas batteries have also concentrated upon optimizing the electrochemical performance of catalysts. Irreversible discharge products can gradually accumulate on the cathodes as the discharge/charge cycle proceeds owing to the limited catalysis of traditional carbon-nanophases-based catalysts, which induces continuous catalytic activity decay and remarkable decrease in reaction kinetics, thereby aggrandizing the overpotential as well as resulting in unexpected electrolyte decomposition. This is the dominant reason why most of the currently available metal–gas batteries show unsatisfactory long-term cycling stability at higher rates.[18,34,37,49] Furthermore, it is equally important that all the used gases (*e.g.*, O_2, CO_2, and N_2), which can diffuse through the separator/liquid electrolyte, would result in obvious corrosion to alkali metal anodes; meanwhile, an inhomogeneous solid–electrolyte interphase (SEI) with low ionic conductivity and poor interfacial compatibility also enables the growth of dendrites and "dead" metal aggregation that may puncture the separator and cause a short circuit. These two detrimental factors reduce the electrochemical performance and even become a potential threat to battery safety.[29,50] In addition, it should be considered that liquid electrolytes suffer from a higher risk of leakage if used in metal–gas batteries with open holes in the encapsulated cathode. This is another inevitable problem that needs to be urgently addressed before discussing the possibility of applying metal–gas batteries as practical power accessories for wearable electronics.

Otherwise, the ensuing health and safety problems caused by electrolyte leakage will not be tolerated and accepted by industrial councils or customers.[18,37,42,51]

Aimed to resolve the abovementioned issues, a fair number of efforts have been made, among which three main strategies have been employed, namely, cathode catalyst microstructure/component design, metal anode modification, and novel electrolyte synthesis.[22,29,52–54] Of course, it is a fact that when compared with the long history of metal–gas electrochemistry, the concept of flexibility for metal–gas batteries has emerged only within the last decade because of the increasing demand of flexible electronic devices and the fact that relevant studies are still at a premature stage.[34,55–58] However, these efforts do push forward the development of flexible metal–gas batteries toward large-scale industrial deployment, particularly in the field of wearable electronics. For convenience, a brief chronology illustrating the development of new families of flexible metal–gas batteries—to the best of our knowledge—is shown in Fig. 2c.[21,29,55,59–70]

In this paper, we do not intend to have a comprehensive overview of previously reported metal–gas battery catalysts or electrolytes. Instead, we will focus on recent technical advances together with major dilemmas facing the currently available flexible metal–gas battery devices, highlighting how flexible cathodes with various catalyst microstructures and components affect the electrochemical performance of different categories of metal–gas batteries. Meanwhile, some impressive studies related to flexible metal anodes and (quasi-) solid-state gel polymer electrolytes (GPEs) have also been introduced for a better understanding of the construction of solid-state flexible metal–gas batteries. Flexible Zn–air batteries (ZABs) and Li–O_2/air batteries are mainly discussed. Moreover, an emerging new type of flexible Li–CO_2 battery has been briefly overviewed to elucidate the promising potential of novel metal–gas batteries. In the end, critical technical hurdles and future research directions are discussed that involve rechargeable and flexible metal–gas batteries for wearable applications.

2. Flexible metal–air batteries

2.1 Working principles and development history

Out of the many available options for metal–gas couples, gaseous O_2 has been primarily utilized to explore metal–O_2 electrochemistry because of its high activity and abundance in the ambient atmosphere.[18,56,71] Eventually, metal–O_2 couples should be used to fabricate batteries that can directly work in air; therefore, metal–O_2 batteries are also known as metal–air batteries. In these battery systems, metal anodes have a wide range of selection, such as alkali metals (Li, Na, and K), alkaline earth metals (*e.g.*, Mg and Al), and first-row transition metals (*e.g.*, Fe and Zn).[34,72] According to the different properties of metal anodes, currently available metal–air batteries can be divided into two categories: aqueous and nonaqueous, as shown in Fig. 3. The former, which relies on air-stable metals (such as Zn, Fe, Mg, *etc.*), commonly use OH^--based aqueous electrolytes, while the latter employing alkali metals (Li^+, Na^+, and K^+) choose to use aprotic organic ether-based electrolytes owing to their high chemical activity toward moisture.[34,73] On basis of the above features, metal–O_2 couples using air-stable metals/aqueous electrolytes and operating in the ambient atmosphere can be called "real metal–air batteries" (represented by ZABs), but the more precise terminology for batteries using alkali metals/organic electrolytes and operating in dry and pure O_2 gas (in most cases) without other special structural protection is metal–O_2 batteries (represented by Li–O_2 batteries). Of course, the electrochemical mechanisms for aqueous and nonaqueous systems differ considerably. For aqueous metal–air batteries, metal anodes are initially passivated in alkaline circumstances, forming a corresponding oxide or hydroxide protective layer, which only permits the migration of metal ions, thereby enabling a compatible interface with aqueous electrolytes. During the discharge process, the metal is oxidized into metal ions, while gaseous O_2 is reduced into hydroxy radicals with the assistance of catalysts on the porous air cathode. The general mechanism can be illustrated by the following equations:[73,74]

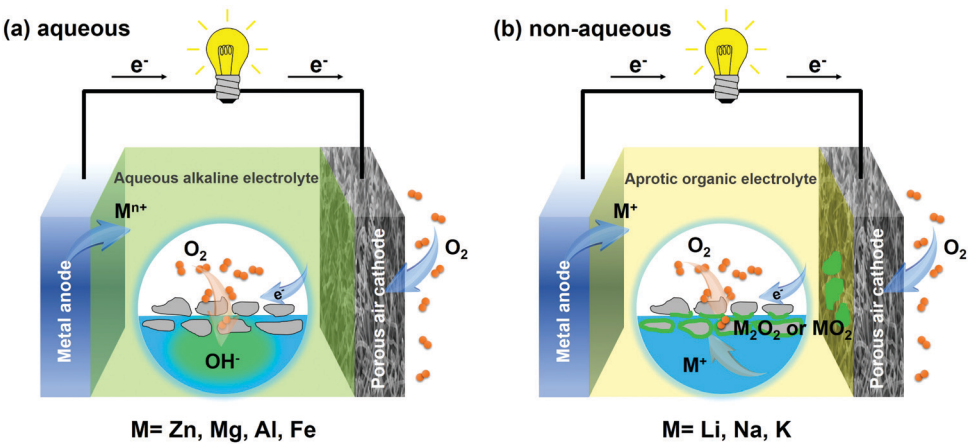

Fig. 3 Schematic configurations and working principles of (a) aqueous and (b) nonaqueous metal–O_2/air batteries. Insets show the different ORRs occurring on the porous air cathodes.

Anode:

$$M \rightleftharpoons M^+ + e^-$$

Cathode:

$$O_2 + 2H_2O + ne^- \rightleftharpoons 4OH^-$$

where M represents different kinds of metals and n is the stable oxidation number of metal ions. The aforementioned electrochemistry is reversible during charging, with metal deposition on the anode and O_2 evolution from the cathode.

Notably, the situation is much different in nonaqueous metal–air batteries. Upon discharge, the highly sensitive alkali metal anode (Li, Na, and K) is similarly oxidized into metal ions, followed by the formation of solvation clusters with organic electrolyte molecules and diffusion into the cathode. Meanwhile, cathodic reactions result in the initial one-electron reduction of O_2 to form superoxide radicals, namely, O_2^-. Desolvated metal cations can react with them to generate M_mO_2, which accumulate on the cathode. According to the hard–soft acid–base theory,[17,18,34] larger-sized Na^+ and K^+ can effectively help stabilize the superoxide metal species (NaO_2 and KO_2), while in the case of Li^+, intermediate LiO_2 cannot stably exist. In particular, this disproportionation leads to the formation of Li_2O_2 as the discharge product in Li–O_2 batteries. The oxygen reduction reaction (ORR) and oxygen evolution reaction (OER) mechanisms for nonaqueous metal–gas batteries can be explained as follows:[75–77]

Anode:

$$M \rightleftharpoons M^+ + e^-$$

Cathode:

$$mM + O_2 + me^- \rightleftharpoons M_mO_2 \quad (m = 1 \text{ or } 2)$$

Because of the low solubility in organic electrolytes, superoxides or peroxides can accumulate on the surface of air cathodes, gradually blocking the gas diffusion and ion transportation channels toward the interior of the catalyst, eventually shutting off the battery. Hence, aimed at promoting the storage capacity, most developed catalysts for use in nonaqueous metal–gas batteries are highly porous such that they can provide more space to accommodate the discharge products.[78–80] In spite of these efforts, attempts made on nonaqueous metal–gas batteries are still in their infancy. In fact, the origin of aqueous metal–gas batteries has taken place much earlier than their nonaqueous counterparts. In 1878, a primary ZAB was designed by Maiche, and the corresponding commercial products started to enter the market after about 50 years.[81] Subsequently, Fe–air, Al–air, and Mg–air batteries have been successively developed since 1960.[82–84] However, until 1996, a rechargeable nonaqueous Li–air battery using carbonate-based electrolytes was initially introduced by Abraham *et al.*[85] More recently, Na–O_2 and K–O_2 couples have attracted research interest from scientists due to the abundance of metallic Na and K in the earth as well as their lower overpotential.[26,77]

Based on different mechanisms, recent progresses and challenges involving flexible metal–air batteries will be mainly exemplified using zinc–air and Li–O_2/air batteries as the representatives for aqueous and nonaqueous systems, respectively, in the subsequent discussions.

2.2 Flexible ZABs

Due to their inexpensive, earth-abundant, highly safe, and biofriendly features, ZABs have been utilized in hearing aids, which is the only commercialized example of the use of metal–gas batteries until now.[17,18,56] ZABs can work in the ambient atmosphere because the other air components, such as N_2 and CO_2, are much more difficult to be reduced at the cathode in an aqueous system as compared to O_2 (which has high activity).[72,86] The basic working principle of ZABs can be elaborated as follows. During discharging, zinc metal initially loses two electrons and gets oxidized into Zn^{2+}, which accumulates at the anode, while atmospheric O_2 molecules are catalytically reduced to OH^- at the triple-phase boundaries among the air cathode, gas, and electrolyte. The generated OH^- on the cathode dissolves in the electrolyte, migrates to the surface of the zinc anode, and reacts with Zn^{2+} to form $Zn(OH)_4^{2-}$, which is further decomposed into insoluble ZnO. Finally, the accumulation of ZnO and the shuttle effect of Zn^{2+} block the migration channels of Zn^{2+} and degrade the active catalytic sites for ORR, thereby giving rise to increase in polarization and the eventual collapse of the battery. The overall reactions can be illustrated by the following equations, where the theoretical energy density and equilibrium potential are determined to be 1084 W h kg^{-1} and 1.65 V, respectively.[87–89]

Cathode:

$$O_2 + 4H_2O + 4e^- \rightleftharpoons 4OH^-$$

Anode:

$$Zn + 4OH^- \rightleftharpoons Zn(OH)_4^{2-} + 2e^-$$

$$Zn(OH)_4^{2-} \rightleftharpoons ZnO + H_2O + 2OH^-$$

Overall:

$$2Zn + O_2 \rightleftharpoons 2ZnO \quad (E^\theta = 1.65 \text{ V})$$

When a ZAB is charged, zinc is reversibly deposited at the metal anode and O_2 is released from the air cathode *via* the OER process. Notably, ORR active sites are vulnerable as compared to OER sites. Their low tolerance against reduplicative reductive–oxidative operations leads to the poor cycling stability of ZABs.[90–92] Meanwhile, in spite of the presence of cost-effective zinc metal together with aqueous alkaline electrolytes enables ZABs to breach into commercial applications, they are still produced having a conventionally rigid stack-type structure. Hence, employing ZABs as the power supply for wearable electronic devices still remains a challenge.

2.2.1 Flexible air cathodes. The first obstacle for flexible ZABs is to realize the flexibility of air cathodes. In this regard,

a bendable and tough substrate (*e.g.*, carbon nanotube (CNT) paper, carbon nanofiber (CNF) cloth, porous graphene (G) film, and nickel foam) is necessary for catalyst loading.[56,93–96] Generally speaking, currently available flexible air cathodes have been prepared *via* two main strategies: spraying catalyst ink onto flexible porous current collectors (spraying technique) and *in situ* construction of a catalyst/current collector integrated into free-standing electrodes (*in situ* construction).

Further, it is noteworthy to reconsider the bottleneck with regard to the sluggish ORR/OER kinetics and electrocatalytic durability of cathode catalysts, resulting in fairly limited energy conversion efficiency, low output power efficiency, and unsatisfactory cycling performance.[92,97] Although platinum (Pt) and its alloys are currently regarded as the best electrocatalysts for use in aqueous ORR, the high cost and remarkably declined activity hinder their larger utilization.[17,34] To resolve this dilemma, substantial efforts have been directed toward exploiting flexible cathodes that can anchor catalysts with higher efficiency and better durability, such as carbon nanophases, nonnoble metals and their derivatives, and rare-metal-based hybrids. They are expected to achieve satisfactory electrochemistry even when the ZABs are subjected to complex and repetitive deformations. Some typical works related to flexible ZAB cathodes are shown in Fig. 4, where the potential differences (Fig. 4a) between the half-wave potential of ORR and overpotential at 10 mA cm^{-2} of OER (tested in aqueous alkaline solutions using a three-electrode system) are compared and the electrochemical properties of the corresponding flexible ZABs (Fig. 4b) are provided.[22,59,93,94,98–108]

2.2.1.1 Flexible cathodes prepared by the spraying technique. The spraying technique is almost a universal strategy for fabricating flexible cathodes loaded with the target catalysts as long as the catalyst powder can be synthesized. There are a fair number of impressive works related to this technique.

Firstly, cost-effective and durable carbon nanophases have been widely used to fabricate flexible cathodes by spraying them onto porous current collectors. For example, Xia *et al.* synthesized a N-doped CNT/reduced graphene oxide (rGO) hybrid by pyrolyzing metal–organic frameworks grown on rGO nanosheets (Fig. 5a and b).[109] This composite demonstrated a higher onset voltage of 0.92 V and half-wave potential of 0.85 V, which were comparable to those of commercial Pt/C catalysts. After being loaded onto carbon cloth, this N-CNT/rGO hybrid could be utilized to fabricate an excellent bifunctional flexible air electrode for use in flexible ZABs.

In spite of the fact that the catalysis of carbon materials is relatively stable and durable, their electrocatalytic activity is far from satisfactory. To reduce the discharge/charge overpotential, metal-based composites have been introduced into the design and preparation of flexible cathodes for use in ZABs. Peng *et al.* used cross-stacked aligned CNT sheets dipped with RuO_2-based catalyst ink to prepare a flexible and porous air cathode for ZABs.[103] An air cathode comprising 30 layers of CNT sheets and a cross-stacking angle of 90° demonstrated the best rate performance due to sufficient O_2 diffusion and lower resistance. This cathode could maintain the discharge voltage at around 1.0 V for 30 cycles at 1 A g^{-1}. Besides rare-metal oxides, certain transition metals and their derivatives have also been studied as efficient catalysts for flexible ZAB cathodes. Cathode catalysts comprising atomically dispersed metals in carbon matrices have attracted increased interest in the recent years on account of their superior catalytic efficiency. Peng *et al.* prepared Co atoms that were well dispersed in coordination polymers (2,3,6,7,10,11-hexaiminotriphenylene) by varying the ratio of the employed metal and polymer precursors.[110] The unpaired 3d electrons of the as-obtained samples could enhance the ORR activity and selectivity of cathodes owing to the reduced coplanarity but increased radical characteristics. Chen *et al.* utilized $ZnCl_2$ crystals to create abundant defects in three-dimensional (3D) interconnected carbon networks, allowing more C–N_4 sites to accommodate single Fe atoms.[111] The formed FeN_4 active sites significantly promoted the ORR activity, thereby boosting the electrochemical performance of the corresponding flexible air cathodes. Wang *et al.* prepared single Co atoms anchored in porous N-doped carbon through the pyrolysis of two-dimensional (2D) ZIF-67 formed in a solution with water as the solvent (Fig. 5c).[112] After acid pickling, single Co atoms were effectively dispersed in N-doped carbon

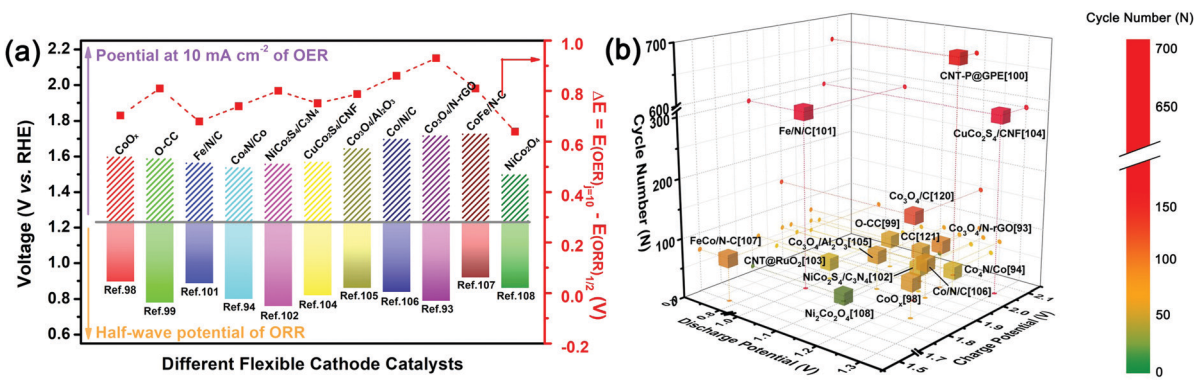

Fig. 4 Comparisons of (a) potential difference between the half-wave potential of ORR and overpotential at 10 mA cm^{-2} of OER for typical bifunctional flexible air cathodes reported earlier, and (b) discharge voltage, charge voltage, and cycling performance of flexible ZABs using different kinds of flexible air cathodes.[22,59,93,94,98–108]

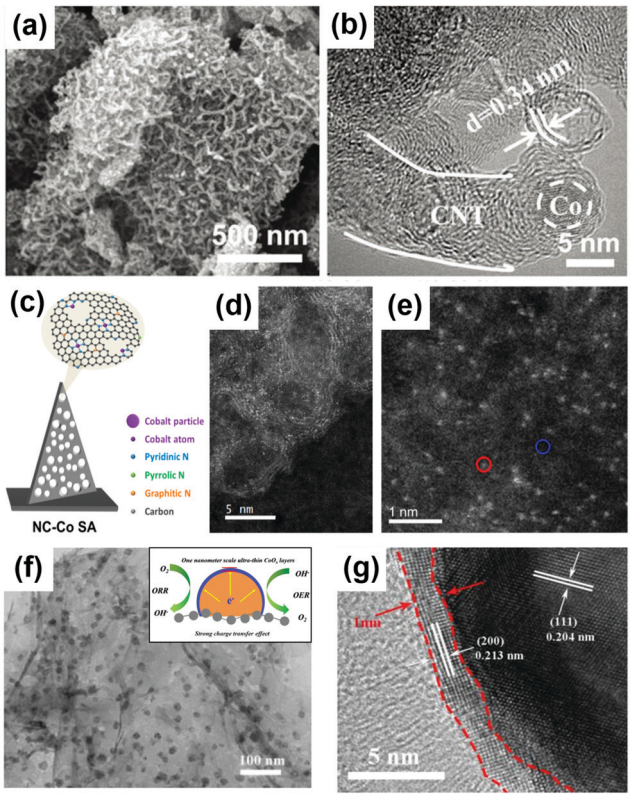

Fig. 5 (a) SEM and (b) TEM images of 2D N-doped CNTs/G hybrids. Reproduced with permission. Copyright 2019, Wiley-VCH.[109] (c) Schematic illustration of the microstructure and the (d) STEM and (e) HAADF-STEM images of Co atoms distributed across the N-doped carbonaceous support. Reproduced with permission. Copyright 2018, American Chemical Society.[112] (f and g) TEM and HRTEM images of 1 nm CoO_x layer on the metallic substrate of Co/N-rGO. Reproduced with permission. Copyright 2019, Wiley-VCH.[98]

nanosheets and tightly pinned at the N–C sites, as shown in Fig. 5d and e. This single-atom-based catalyst demonstrated an obviously larger saturation current of 10.38 mA cm^{-2} at 0.60 V in contrast to those of Co nanoparticles loaded onto carbon nanosheets and commercial Pt/C catalysts. Meanwhile, the lower overpotential for the OER process indicated that single Co atoms also facilitated the kinetics of OH^- decomposition. As a result, the assembled flexible ZABs using single-Co-atoms-based cathodes delivered lower discharge/charge overpotential and more stable cycling behavior.

Apart from single metal atoms, metals and their derivative clusters have also received equal attention due to their more facile preparation. Simultaneously, when compared with single metal atoms that have much higher utilization efficiency of the materials, metal and their derivative clusters commonly possess stronger tolerability to structural damage during repetitive ORR and OER processes, but the specific capacity decreases. The easier preparation conditions enable this type of catalysts to ensure the presence of more choices during material design. Wu *et al.* synthesized 1 nm-scale ultrathin cobalt oxide (CoO_x) layers that were highly dispersed on Co/N codoped rGO *via* solution adsorption and a subsequent high-temperature calcination process, as shown in Fig. 5f.[98] The CoO_x layers not only facilitated electron transfer, but also provided more active sites. Simultaneously, the Schottky barrier that was formed between the CoO_x layer and metallic Co sites doped in graphene promoted charge separation, thereby enhancing both ORR and OER kinetics (Fig. 5g). The air cathode was prepared by coating hydrophobic carbon cloth with CoO_x/Co–N–graphene catalyst ink. It exhibited a certain amount of flexibility and decent electrochemical performance, namely, relatively stable discharge/charge profiles were recorded even when the cathode was bent from 0° to 180°. In addition, after recovery from the bent state, the cathode showed negligible voltage change during the subsequent cycling behavior for 10 h. In the subsequent optimizations, Deng *et al.* reported a modified CoO_x-based hybrid that comprised atomically thin mesoporous Co_3O_4 layers strongly coupled with N-doped reduced graphene oxide (N-rGO) nanosheets as a highly active and durable bifunctional catalyst for use in both ORR and OER, yielding low Tafel slopes of 54 and 101 mV $decade^{-1}$, respectively.[93] Interestingly, they constructed a continuous production line to spray catalyst ink onto a bundle of carbon fibers to fabricate a length-controllable fiber-shaped air electrode, which was subsequently directly wrapped onto the remaining configuration of the battery. The as-obtained battery yielded high discharge potential of 1.2 V and low charge potential of 2.0 V. Apart from cobalt-based materials, other earth-abundant and low-cost metals, such as Fe and Mn, have already been introduced into the family of ORR and OER catalysts.[59,101,107] Cho *et al.* prepared a Fe_3C/Fe/N-doped carbon catalyst derived from the pyrolysis of iron acetylacetonate and commercial silk fibroin.[59] The flexible cathode was obtained by casting Fe_3C/Fe/N-doped carbon catalyst suspension onto a tailor-made gas diffusion layer composed of activated charcoal and polytetrafluoroethylene (PTFE) binder. Notably, this Fe-based catalyst loaded on the air electrode delivered a flat discharge voltage plateau at nearly 0.90 V for 10 h at 0.1 mA cm^{-2}. Furthermore, bimetallic catalysts were also employed as catalysts for use in ZABs. For example, a bimetal–carbon hybrid catalyst was developed by Ma *et al.*,[107] where alloyed FeCo nanoparticles embedded in bamboo-like N-doped graphitic carbon nanotubes (N-GCNT/FeCo) were synthesized by a method involving pyrolysis and catalytic growth at ~500–800 °C. After a similar spraying process, a N-GCNT/FeCo-based flexible cathode was obtained, which demonstrated outstanding long-term cycling stability of 240 cycles for 40 h and discharge/charge potential for the gas was only 0.26 V. The corresponding energy density and peak power density could reach 653.2 W h kg^{-1} and 89.3 mW cm^{-2}, respectively, based on the weight of the catalysts. Some other categories of catalyst powders such as metal phosphides and metal chalcogenides have also been used for fabricating flexible air cathodes for use in ZABs.

In general, catalytic sites from metal-based species exhibit better electrocatalytic activity than those obtained from their carbon-based counterparts, and catalysts with smaller size (*e.g.*, single atoms, few layers, or defects) and homogeneous distribution are more likely to possess faster reaction kinetics, but they might have more vulnerable structures; this can yield

lower overpotential but weaker cycling stability during discharge/charge processes in contrast to those observed in large-sized nanoparticles, nanotubes, or nanosheets. On the other hand, the flexibility of air cathodes prepared by spraying techniques highly depends on the flexibility of the original substrates. Commonly, as they have lower thickness and larger crosslinked microstructures, CNT and G cloths are capable of advantageous deformability when compared with CNF cloth and nickel foam. Further, it should be pointed out that despite the higher feasibility to fabricate flexible cathodes loaded with any target catalyst, it is difficult to ensure intimate interfacial bonding between the active catalyst and current collector using the spraying method, which is critical to further promote the cycling stability as well as rate capability. Further, it enhances the total weight and unnecessarily reduces the energy density of the battery.

2.2.1.2 Flexible cathodes prepared by in situ construction. Finding another preparation strategy that can simultaneously maintain sufficient interfacial bonding and flexibility has hindered the applicability of flexible ZABs. The *in situ* synthesis of free-standing catalyst cathodes has been proposed to address the above problems inherent in spraying methods. Comparatively speaking, the synthesis process for integrated free-standing catalyst cathodes commonly requires meticulous design and relatively tedious posttreatments. As per the current technology status, certain free-standing catalysts with specific microstructures and components can be prepared mainly through three ways or their combinations: hydrothermal/solvothermal growth, electrostatic spinning, and floating-catalyst chemical vapor deposition (FCCVD).[22,94,102,106,108] These as-obtained integrated free-standing catalyst cathodes are highly flexible and demonstrate better electrochemical performance even under various deformation conditions.

Flexible carbon substrates themselves can demonstrate certain electrocatalytic activity after suitable surface modifications. For example, a flexible carbon cloth cathode with abundant oxygen-rich functional groups and nanoporous surfaces was manufactured by Zhao *et al. via* acid oxidation treatment followed by air calcination.[99] The facile oxidation steps activated the commercial carbon cloth to produce an efficient flexible metal-free cathode for ZABs, out of which the oxygen electrocatalytic performance outperformed the oxygen-doped carbon materials that have been reported until now. Only the low overpotential of 360 mV at 10 mA cm^{-2} for OER was realized by this cathode, which was among the best performances among those of other metal-free catalysts. When used in ZABs, this cathode showed excellent cycling stability during the initial 1000 min. Choi *et al.* reported a composite consisting of graphene hydrogel/B-doped graphene quantum dots that was prepared *via* the self-assembly of rGO during a hydrothermal process.[114] The obtained composite exhibited 3D interconnected architecture with high porosity and large specific surface area. B-Doped graphene quantum dots were highly dispersed in the skeleton of the rGO, allowing abundant and stable active sites for long-term cycling (94% of the initial current density was retained after 25 h of operation). Chen *et al.* reported an ordered multidimensional array assembled by one-dimensional (1D) CNTs and 2D carbon nanoridges on nickel foam that prevented the internal blockage of the electrode in the ORR process (Fig. 6a).[113] Numerous CNTs were grown on the outer walls of the ordered carbon nanoridges such that a sufficient number of voids remained between the adjacent CNTs/nanoridges sheets, providing abundant gas diffusion channels for the interior active sites (Fig. 6b–d). Consequently, this flexible air cathode showed a current density of 0.8 V for ORR and potential of 300 mV at 10 mA cm^{-1} for OER, as shown in Fig. 6e. The assembled flexible ZABs using this cathode demonstrated an impressive energy density of 946 W h kg^{-1}.

However, issues related to limited electrocatalytic activity also occurred in integrated free-standing air electrodes. Hence, metal-based components have been similarly introduced into free-standing composites, similar to that discussed in the section of the spraying method. Deng *et al.* designed an integrated free-standing electrode based on $NiCo_2S_4$/graphitic carbon nitride/CNT hybrid ($NiCo_2S_4$@g-C_3N_4–CNT, Fig. 6f).[102] They took advantage of the self-assembly effect of C_3N_4 nanosheets to interconnect all the components together during *in situ* hydrothermal growth, as proved by the TEM images shown in Fig. 6g and h. The synergistic effect of bimetallic Ni/Co sites and pyridinic-N site in g-C_3N_4 considerably facilitated the electron transfer and reaction kinetics, while the entangled CNTs ensured the high electronic conductivity of the entire electrode. Benefitting from these favorable features, $NiCo_2S_4$@g-C_3N_4–CNT exhibited considerable potential as a flexible cathode for use in ZABs. It exhibited higher onset potential of 0.87 V and larger limited current density of 4.8 mA cm^{-2}. Simultaneously, the Tafel slope of $NiCo_2S_4$@g-C_3N_4–CNT was 74 mV $decade^{-1}$, closely approaching the value of 69 mV $decade^{-1}$ for Pt/C—the best ORR catalyst. The LSV curves shown in Fig. 6i reveal the much improved OER activity as compared to those of the control samples. The further modification of the $NiCo_2S_4$ catalysts was implemented by Chen *et al.*[115] They adopted electrophoretic deposition to anchor defect-enriched N-doped graphene quantum dots (N-QDGs) on needle-like $NiCo_2S_4$ arrays grown on carbon cloth. Bifunctional active sites and synergistic coupling enabled this N-QGDs/$NiCo_2S_4$ catalyst to deliver enhanced OER and ORR capabilities and excellent cycling stability of 200 h. Meanwhile, its mechanical bendability was efficiently maintained.

Several modifications of CoO_x-based integrated free-standing catalysts have been attempted by Lu *et al. via* the *in situ* hydrothermal growth of Co(OH)F nanowire arrays on carbon cloth and the subsequent N-dopant reaction.[22] These as-synthesized flexible air cathodes of N-doped Co_3O_4 mesoporous nanowire arrays anchored on carbon cloth exhibited high ORR kinetics, namely, a high open-circuit voltage of 0.94 V could be achieved and maintained at this level during the discharge process for 10 h. Impressively, outstanding volumetric capacities of 98.1 mA h cm^{-3} at 2.5 mA cm^{-3} and 84 mA h cm^{-3} at 25 mA cm^{-3} could be achieved, indicating its decent high-rate capability. It is also noteworthy that the peak power density could reach 32.0 mW cm^{-3} at 90 mA cm^{-3}, facilitating the prospect of practical applications. Another impressive

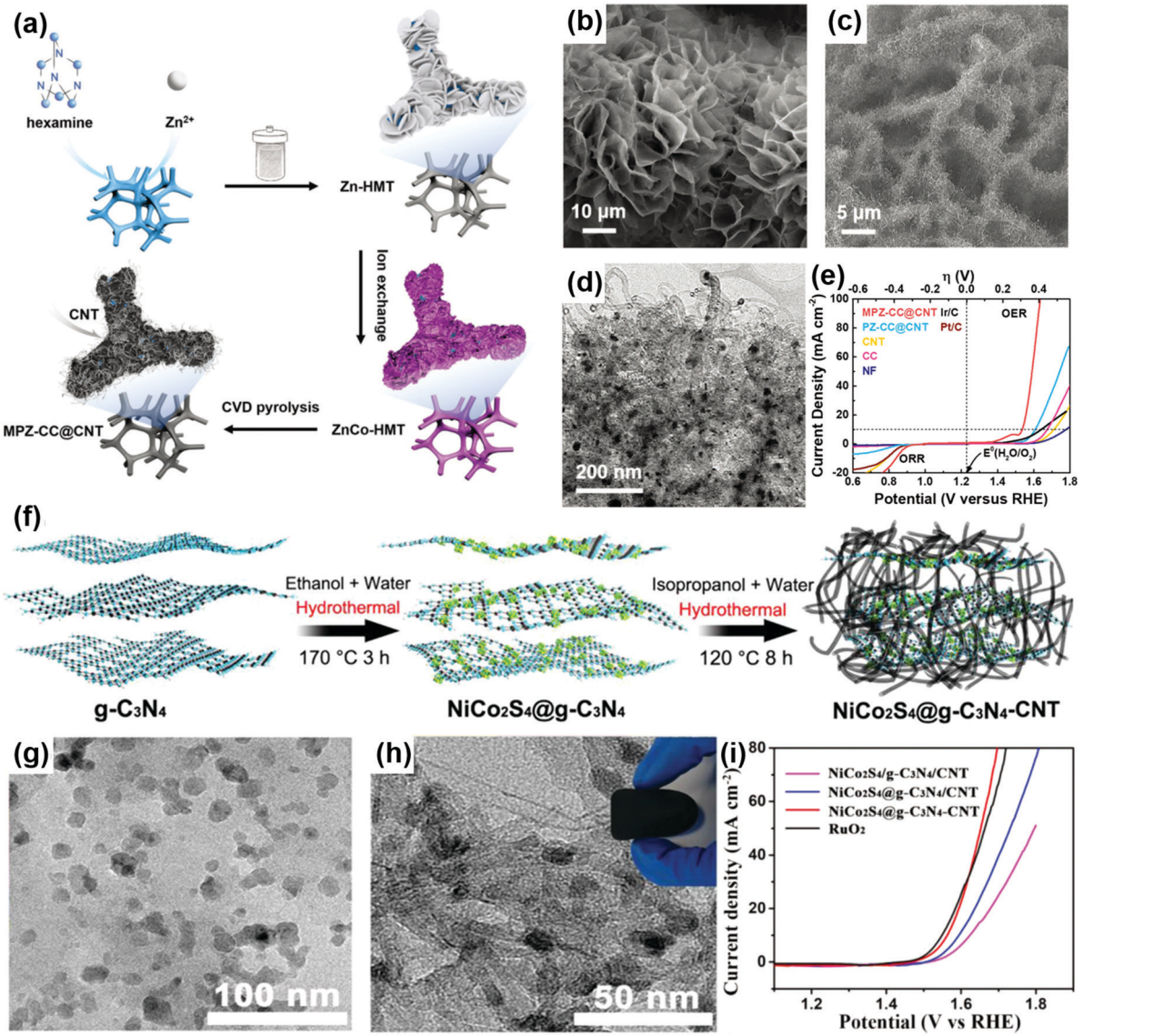

Fig. 6 (a) Schematic of the synthesis of MPZ-CC@CNT on nickel foam. SEM images of (b) ZnCo-hexamine and (c) MPZ-CC@CNT. (d) TEM image and (e) ORR/OER polarization curves of MPZ-CC@CNT. Reproduced with permission. Copyright 2019, Wiley-VCH.[113] (f) Fabrication procedures of $NiCo_2S_4$@g-C_3N_4-CNT. TEM images of (g) $NiCo_2S_4$@g-C_3N_4 and (h) $NiCo_2S_4$@g-C_3N_4-CNT. (i) OER activities of different $NiCo_2S_4$/g-C_3N_4/CNT samples. Reproduced with permission. Copyright 2019, Wiley-VCH.[102]

work involving the construction of Co_3O_4-based nano/micro arrays on carbon cloth was reported by Li *et al.*[116] ZIF-67 nanopolyhedrons were formed on the surface of ZIF-67 microsheets *via* two-step growth successively in water and methanol. After calcination, the unique nano/micro arrays were effectively maintained on the carbon cloth. This hierarchical structure guaranteed sufficient catalyst loading, abundant active sites, and fast reaction kinetics. The lower overpotential of 310 mV at 10 mA cm^{-2} and Tafel slope of 58 mV $decade^{-1}$ were recorded, illustrating their superior electrocatalytic capabilities toward ideal ORR and OER. The excellent electrochemical performance of the corresponding flexible ZABs under different deformation conditions further evidenced the promising potential of this Co_3O_4-based cathode.

Apart from an individual preparation strategy (*e.g.*, hydrothermal growth/assembly, high-temperature calcination, *etc.*), a combination of various technologies endows the integrated free-standing catalyst design with more choices with regard to complex microstructure and species range. Here, three typical cases related to Co-based free-standing catalysts have been discussed to better elucidate the above statement. As expected, the optimization of the microstructure of cobalt-based catalysts has been further implemented by Lu *et al.*[105] They employed the atomic layer deposition (ALD) technique to generate Al_2O_3 as both confinement and protective nanolayers to grasp volatile carbon and alleviate the aggregation of metal oxides during ZIF pyrolysis, yielding an electrode comprising Al_2O_3-nanolayer-coated Co_3O_4/N-doped carbon hollow microcubes (Co-NC@Al_2O_3)

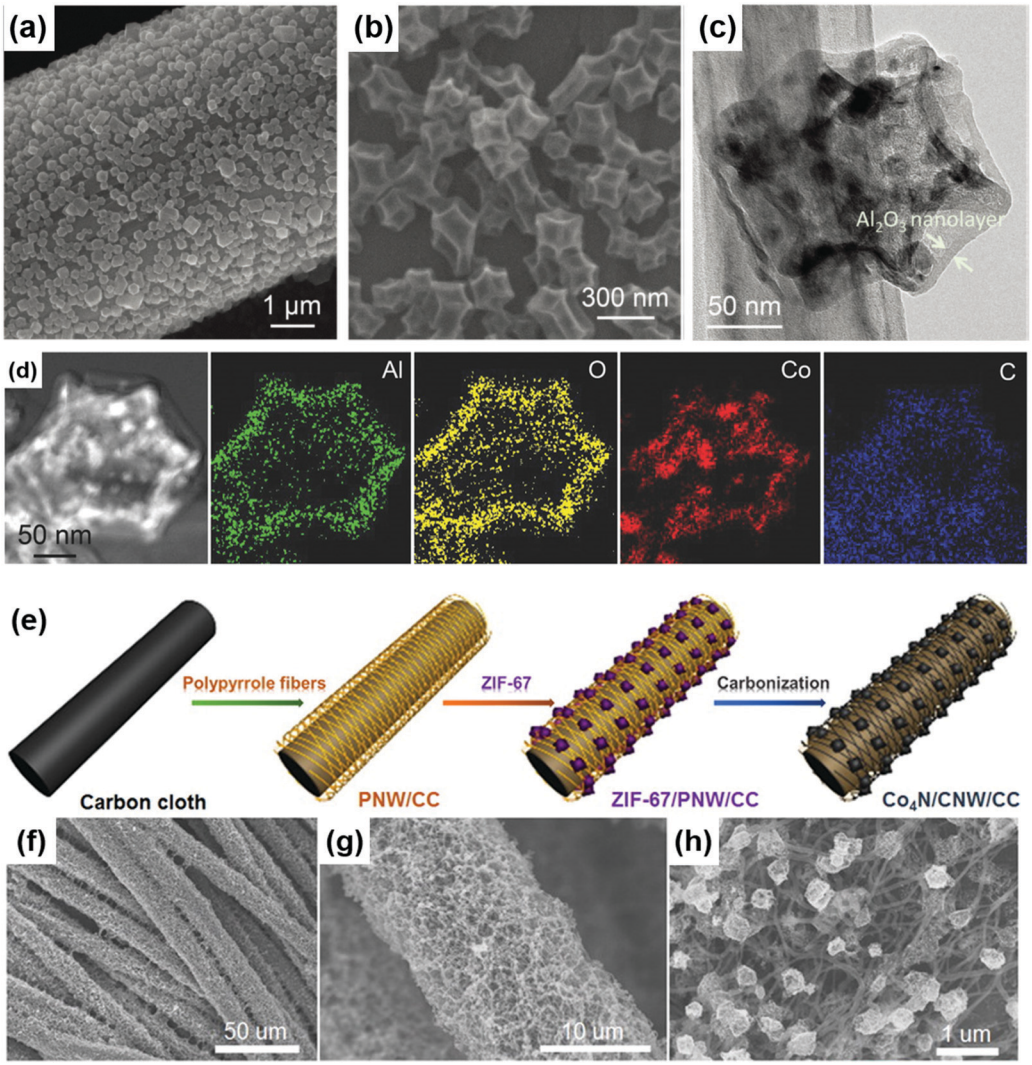

Fig. 7 SEM images of (a) Zn/Co-ZIFs and (b) Co-NC@Al_2O_3 grown on carbon cloth. (c) TEM image and (d) elemental mappings of Co-NC@Al_2O_3 particles. Reproduced with permission. Copyright 2018, Wiley-VCH.[105] (e) Schematic illustrating the synthesis procedure and (f–h) SEM images of Co_4N/CNW/CC. Reproduced with permission. Copyright 2016, American Chemical Society.[94]

on carbon cloth as bifunctional catalysts for use in ZABs (Fig. 7a–d). The electrode demonstrated half-wave potential of 0.86 V for ORR and a low Tafel slope of 47.8 mV decade^{-1} for OER, exhibiting decent durability with no remarkable activity degradation after running oxygen electrocatalytic reactions for 10 h. A potential difference of 787 mV between the half-wave potential of ORR and the overpotential at 10 mA cm^{-2} of OER (an indicator of the bifunctionality of catalysts) was achieved by this cathode. Notably, the excellent flexibility of this air cathode has been identified by similar galvanostatic discharge/charge profiles under different deformation conditions. Zhang *et al.* utilized the electrospinning technique to root 3D intertwined polypyrrole (PPY) nanofiber networks on the carbon cloth, followed by the *in situ* growth of pearl-like ZIF-67 strung on these nanofibers *via* the solvothermal method, as shown in Fig. 7e.[94] After calcination in an inert atmosphere, porous N-doped carbon species anchored on noble-metal-free Co_4N nanoparticles and Co–N–C active sites were formed on the interconnected N-doped CNFs, as shown in Fig. 7f–h. The superior OER activity of Co_4N coupled with the high ORR activity of Co–N–C coordination sites enabled this specially designed free-standing electrode to form bifunctional electrocatalysts for use in ZABs. Meanwhile, benefitting from the enhanced structural stability of the intertwined N-doped CNF networks, this cathode not only exhibited low overpotential of 310 mV at 10 mA cm^{-2} for OER and high half-wave potential of 0.8 V for ORR, but it could steadily operate for over 20 h. When evaluated as a ZAB cathode, it displayed a low discharge/charge difference of 1.09 V at 50 mA cm^{-2} and superior longevity of up to 408 cycles. Li *et al.* used a mixed solution of ethyl alcohol, ferrocene, and thiophene as the carbon resource and catalyst to generate a CNT film *via* the FCCVD method, followed by CV activation and hydrothermal reaction to create N/O dopants in CNT walls and electrodeposition of $NiCo_2O_4$ nanosheets on the CNT surface.[108] The obtained flexible cathode demonstrated excellent oxygen electrocatalytic activities with low Tafel slopes of 50 and 92 mV decade^{-1} for ORR and OER, respectively.

When used as a ZAB cathode, it revealed low discharge overpotential of ~0.7 V as well as relatively stable cycling behavior. More attractively, this N/O-codoped CNT/$NiCo_2O_4$ film could serve as an "all-in-one" air electrode for flexible ZABs without requiring any additional binder, current collector, and gas diffusion layer, ensuring the high conductivity of the entire electrode, as well as reducing unnecessary components used for interconnecting the active materials.

It needs to be pointed out that due to the advancements in preparation technologies and equipment, other integrated free-standing catalysts with certain unique microstructures and complex components, such as Fe/N/C–S–Fe_xC/Fe active sites embedded in microporous carbon fibers,[101] $CuCo_2S_4$ nanosheets anchored on N-doped CNFs,[104] Co nanoislands rooted on Co/N-doped carbon nanosheets supported by carbon felts,[106] and porous Co–FeCo/N–C needlelike arrays anchored on carbon cloth,[117] have also been explored as ZAB cathodes, showing comparable or better electrochemical performances and sufficient mechanical flexibility. However, according to earlier reports, air cathodes prepared by *in situ* construction seem to yield weaker mechanical strength when compared with their counterparts prepared by spraying techniques. This is possibly because the interactional surface radicals and cross-linked microstructure of soft carbon substrates would be partially damaged in the *in situ* construction process, thereby leading to lower resistance to external strain or stress. Although there are still certain obstacles, recent development in flexible air cathodes ensures that flexible ZABs can put forward a big step toward practical applications.

2.2.2 Flexible Zn metal anodes. As an indispensable component of flexible ZABs, Zn metal anodes have not been exhaustively researched as compared to catalytic cathodes until now. In fact, Zn anodes are responsible for the reversible storage of Zn^{2+}, which is also a critical factor for determining the final rate capability and cycling stability of the assembled ZABs.

In most cases, commercial zinc foils or zinc wires were directly used as flexible metal anodes.[98–108] This is possibly based on the following considerations. First, for the majority of reported works related to flexible ZABs, they commonly focused on cathode design to highlight the significance of the newly proposed catalysts to facilitate ORR and OER kinetics. Hence, flexible battery devices have been fabricated as a proof-of-concept application for cathodes by using commercial Zn products in order to simplify the procedure and lower the cost. Secondly, air-insensitive zinc foils and wires have good mechanical strength, flexibility, and processability such that they can be easily handled into the target objects in the ambient environment. Thirdly, currently used commercial products are absolutely excessive when used as ZAB anodes as compared to the real amount of Zn that is needed for reactions. Simultaneously, almost all earlier ZABs have been tested under a short-time discharging/charging roundtrip (commonly less than 30 min per cycle) to evaluate their cycling performance, during which a very small quantity of Zn participates in the deposition/extraction reactions on the anodes. As a result, the local collapse of Zn seems to have a negligible impact on the electrochemical performances of the entire battery under the currently available evaluation methods. However, the low utilization of the anode can obviously reduce the energy density of the device, and pure Zn metal is easily damaged or even broken during repeated deformations because of inherent metal fatigue. Furthermore, when the working time per cycle is increased, SEI fracture and dendritic or "dead" crystals caused by pure Zn anode can lead to serious battery performance decay. The above issues deserve comprehensive attention with regard to fabricating practical products for the consumer market.

It is believed that existing anode modification strategies in Zn-ion batteries (ZIBs) may also be effective for ZABs, considering the similar functions of their anodes. In ZIBs, four modification techniques are mainly adopted to achieve better zinc deposition on the anodes, namely, regulating the crystal orientation, adjusting the SEI components, coating nucleation-inductive layers, and constructing nanostructures confined by carbon substrates.[118–126] For example, Archer *et al.* used graphene to drive the epitaxial deposition of Zn with locked crystallographic orientation, which delivered superior reversibility over thousands of cycles even at moderate and high rates.[119] Cui *et al.* designed a ZnF_2-rich, ionically permeable SEI film on the Zn anode surface by regulating the solvation structure.[118] These artificial SEI-decorated Zn anodes showed small voltage hysteresis as well as stable cycling performance in galvanostatic Zn plating/stripping tests. Lu *et al.* constructed a 3D flexible CNT/CNF hierarchical framework as a robust scaffold for uniform Zn plating and stripping.[122] The obtained Zn/CNT/CNF anodes not only lowered the Zn nucleation overpotential, but also promoted the homogenous distribution of electric field, thereby yielding highly reversible Zn deposition without dendrites or other byproducts.

In fact, because of the higher handleability than the other three modification ways, constructing Zn nanostructures confined within carbon substrates was adopted to fabricate novel flexible Zn anodes for use in ZABs, as reported by Wang *et al.*,[69] Yang *et al.*,[22] and Zhi *et al.*;[100] they synthesized various Zn nanoarrays on N-doped carbon foam, carbon cloth, and plicated CNT film *via* electrodeposition, respectively. Nevertheless, attention has only been paid to the mechanical functions of anodes (*e.g.*, compressibility, flexibility, and stretchability), while the structural-designs-induced improvement in the electrochemical performance were not involved or ignored in their studies.[69,111] To achieve industrialization capability, metal anode modification (like dendrite-free deposition, SEI design, and gas corrosion protection) should be additionally studied included as an important part of flexible ZABs.

2.2.3 Optimization of aqueous GPEs. At present, it is a fact that the ORR and OER activities of cathode catalysts are usually measured in O_2-saturated alkaline or acidic aqueous solutions. A liquid electrolyte is obviously detrimental to the construction of flexible ZABs for wearable electronics, considering the safety and health problems associated with the potential leakage

of electrolytes.[40,73,127,128] Therefore, several efforts have been directed toward the development of quasi- or solid-state electrolytes, among which GPEs have received the highest attention and have been widely used in flexible ZABs, owing to their advantages such as good interfacial compatibility, relatively high chemical stability, and facile preparation. Of course, continuous optimization has been further conducted to synthesize some multifunctional GPEs with higher ionic conductivity as the ''blood'' of flexible ZABs. A comparison on different kinds of GPEs for use in solid-state flexible ZABs has been summarized in Table 1,[12,54,100,113,116,117,129–137] including parameters such as matrices, components, ionic conductivity, merits, and weaknesses.

In brief, polyvinyl alcohol (PVA), polyethylene oxide (PEO), polyacrylonitrile (PAN), polyacrylic acid (PAA), and polyacrylamide (PAM) have been commonly selected as the host polymer substrates for current GPEs used in ZABs, and numerous additives have been introduced into such polymer matrices to enhance their mechanical and electrochemical performances.[138,139] Several recent impressive works will be introduced in this section. In most cases, PVA was employed. For example, Hu *et al.* reported a porous PVA-based GPE composite that was synthesized by mixing PVA and PEG solutions, followed by adding 5 wt% SiO_2 nanoparticles as ceramic fillers to improve electrolyte retention and ion diffusion, as shown in Fig. 8a.[129] After crosslinking and imbibing 6 M KOH solution, the GPE membrane was obtained. It exhibited good ionic conductivity of 57.3 mS cm^{-1} (Fig. 8b) and ensured the assembled ZABs could steadily work for over 48 h. Chen *et al.* fabricated a PVA-gel-based electrolyte membrane by utilizing glutaraldehyde (GA) and HCl to crosslink freeze-dried PVA membranes.[133] After sufficiently soaking in KOH/PVA solution, the GPE membrane (ionic conductivity: 15 mS cm^{-1}) could be used in ZABs. The GPE could support the assembled flexible ZABs to work normally even at bending angles of up to 180°. Benefitting from the simple preparation process, this membrane could be produced on a large scale, which laid the foundation for industrial-scale ZABs.

Next, the structure and components of this type of membrane were optimized by Qiao *et al.*[130] Similarly, they also employed PVA as the matrix to accommodate guar hydroxypropyltrimonium chloride (GG), but it was achieved *via* a binary crosslinking strategy using glutaraldehyde and pyrrole-2-carboxaldehyde (PCL) as the crosslinking agents. It is noteworthy that this membrane demonstrated an interconnected porous structure originating from the trapped GG chains in the PVA network, providing abundant channels for ion migration. Therefore, the resultant membrane showed superior OH^- ionic conductivity of 123 mS cm^{-1} at room temperature. Moreover, the fabricated hybrid membrane exhibited excellent tensile strength of 90 MPa and high thermal degradation onset temperature of up to 230 °C, which was much better than those of its commercial counterpart (A201) and most of the earlier polymer electrolyte membranes. Hence, ZABs that used this hybrid GPE membrane exhibited enhanced capacity, improved cycling stability, and stable electrochemical performance within the temperature range from 0 to 120 °C. Moreover, biomass-like bacterial cellulose (BC) can be introduced into a PVA substrate to increase the mechanical strength of the GPE. Chen *et al.* prepared a flexible PVA/BC/KOH/$Zn(CH_3COO)_2$ composite hydrogel electrolyte through a mixed solution combined with freeze-drying methods.[132] The GPE was composed of dual networks of PVA and BC, exhibiting an intertwined and microporous structure. Because of the unique load-bearing dual networks, this composite membrane exhibited a high tensile strength of 0.951 MPa, while the ionic conductivity could still reach 80.8 mS cm^{-1}. ZABs using this type of GPE delivered better rechargeability, too.

Some other types of GPEs based on dimethyloctadecyl-[3-(trimethoxysilyl)propyl]ammonium chloride (DMOAP),[131] PAM,[54] or cellulose[132] were also obtained by UV irradiation

Table 1 Comparison of different kinds of GPEs for use in solid-state flexible ZABs

Polymer matrix	Solutes	Additives	Ionic conductivity (mS cm^{-1})	Advantages	Limitations
PVA	KOH	—[116]	—	General compatibility/moderate ionic conductivity	Viscous fluid/poor processability
	KOH	SiO_2[129]	57.3		
	KOH	GA/HCl[133]	15		
	KOH	Cellulose (NFC) hydrogel[134]	75		
	OH^-	GG/GA/PCL[130]	123		
	KOH/$Zn(Ac)_2$	—[113]	—		
	KOH/$Zn(Ac)_2$	Bacterial cellulose[132]	80.8		
	KOH/NH_4Cl/$ZnCl_2$ (neutral)	—[135]	71.4		
PVA–PEO	KOH	Glass fibers[12]	10	Good mechanical strength	Low ionic conductivity
PVA–PAA	Nafion/OH^-	—[136]	6.6	Thin film/low crossover of $Zn(OH)_4^{2-}$	Low ionic conductivity
PAA	KOH	NFC hydrogel/APS/gelatin[137]	96.9	Moderate ionic conductivity	Low mechanical strength
	KOH/ZnO/$(NH_4)_2S_2O_8$	*N*,*N*′-MBA[117]	—		
PAM	KOH	MBAa/APS[54]	330	High ionic conductivity/UV-induced fast polymerization	Low mechanical resistance to alkaline solution
DMOAP	OH^-	Cellulose nanofibers[131]	21.2	Thin film	Low ionic conductivity
PANa	KOH	Cellulose/MBAA[100]	280	High ionic conductivity/super stretchability	Tedious preparation

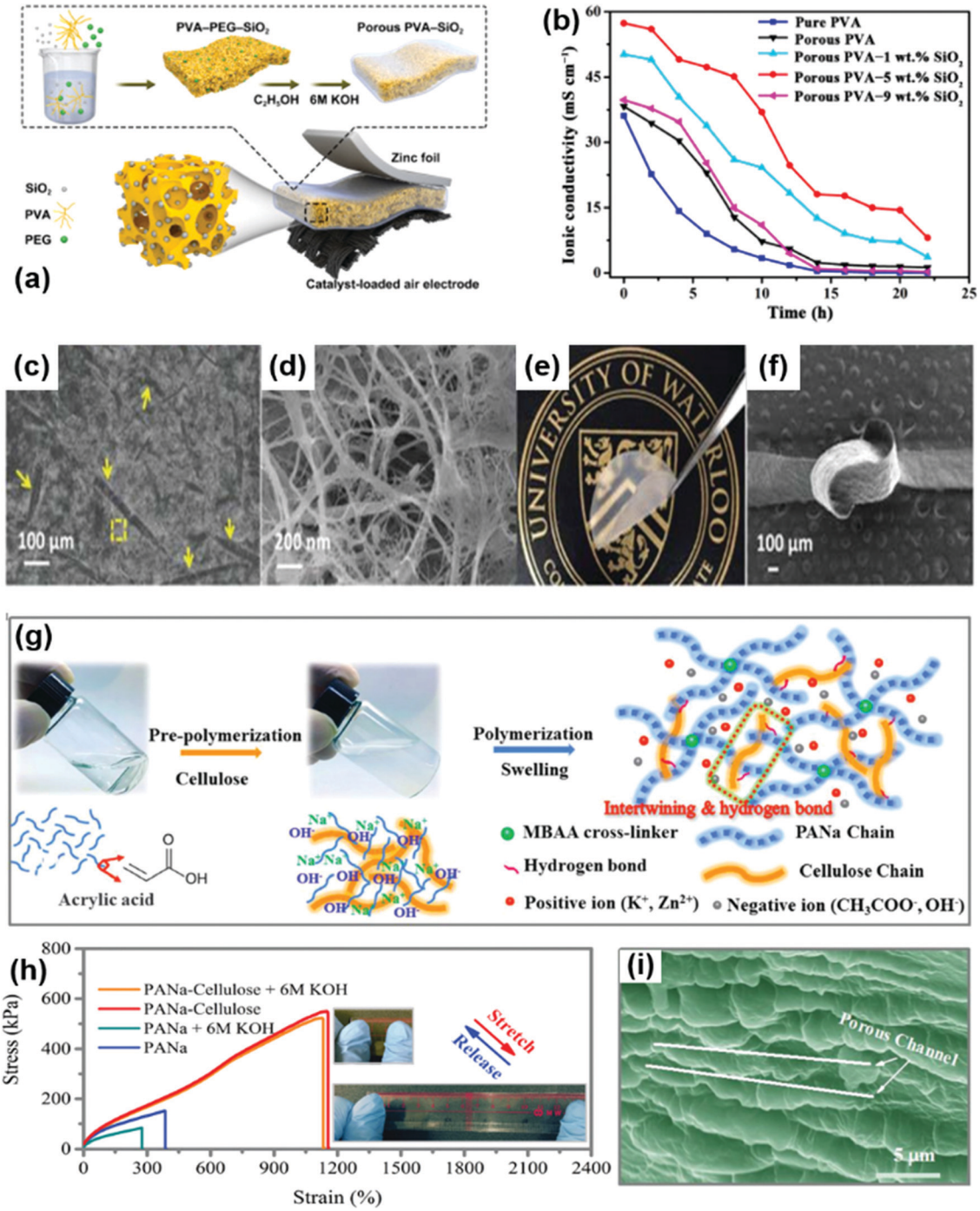

Fig. 8 (a) Schematic diagram of PVA-based GPE. (b) Ionic conductivity of porous PVA–1, 5, 9 wt% SiO_2 nanocomposite GPEs at 25 °C and 50% RH. Reproduced with permission. Copyright 2018, Elsevier.[129] (c, d and f) SEM images (surface view) and (e) photograph of the 2-QAFC membrane. Reproduced with permission. Copyright 2016, The Royal Society of Chemistry.[131] (g) Synthesis procedure, (h) stress–strain curves, and (i) SEM image (cross-section view) of the PANa-cellulose hydrogel electrolyte. Reproduced with permission. Copyright 2019, Wiley-VCH.[100]

or temperature-induced chemical crosslinking. As shown in Fig. 8c–f, Chen *et al.* reported a nanoporous DMOAP-functionalized cellulose nanofiber film as a solid-state electrolyte for use in ZABs; the film was obtained by a method involving a simple mixed solution and vacuum filtration.[131] The as-obtained electrolyte film was transparent, highly flexible, and processable, with an ionic conductivity of 21.2 mS cm^{-1}. A special work reported by Zhi *et al.* is noteworthy here.[100] Until now, PVA-based GPEs have faced a formidable challenge because of their poor stretchability and fairly limited ion transport capability. In contrast, although hydrogels, such as PAA and PAM, possess stronger water retention capabilities, they lose their mechanical robustness when the alkaline KOH electrolyte is incorporated. Aimed at the absence of GPEs with both high

stretchability and ion transport capability, Zhi *et al.* developed a super-stretchable dual-network hydrogel electrolyte where sodium polyacrylate (PANa) chains played the role of soft domains and carboxyl/hydroxyl groups coupled with cellulose served as the KOH stabilizer (Fig. 8g–i). The GPE exhibited ionic conductivity of 280 mS cm^{-1} and could be easily stretched to 1200%. Flat ZABs using this GPE maintained their normal functionality (with stable discharge voltage of ~1.2 V and charge voltage of ~2.1 V) even after being stretched to 800%. These enhanced mechanical properties can be attributed to the physical entanglements of these chains and chemical crosslinking, as well as the presence of hydrogen bonds in the polymer networks. The dynamic recombination of the broken intermolecular hydrogen bonds during the deformation process also contributed toward the superior stretchability.

2.2.4 Different battery configurations. Until now, planar and fiber-shaped configurations have been dominant in flexible ZABs. Comparatively speaking, the present technology is relatively mature to fabricate batteries with 2D stack-type structures and a few attempts have been further devoted toward achieving multifunctions while retaining the flexibility of ZABs.

Noteworthily, before discussing the details of the representative works, a confusing evaluation has been initially proposed for readers as they peruse the subsequent discussion. Currently, there is a lack of widely accepted criteria that can be used to evaluate the flexibility of batteries. Researchers commonly made a judgment based on their own subjective ideas instead of objective indexes; therefore, almost all the reported works promoted the flexibility of their devices regardless of the types of deformations tolerated by the batteries. In addition, flexibility is indeed closely related to the size of the devices and test standards. It is unfair to judge which battery has better flexibility if they are not subjected to the same test conditions. For example, when conducting a bending test, after fixing the length/thickness of the devices and the curvature radius/applied stress, the maximum bending angle is a reasonable and convincing index to evaluate flexibility. Therefore, it is assumed that more attention should be paid to this research direction, and relevant test criteria should be established as soon as possible.

2.2.4.1 Flexible planar configurations. The procedures for assembling planar flexible ZABs are similar to those used for fabricating coin-type ZABs; however, flexible electrodes, quasi- or solid-state electrolytes, and flexible encapsulating materials are used here for protection (*e.g.*, polydimethylsiloxane (PDMS), polyethylene terephthalate (PET), Al-plastic film, and shrinkable tube). Typically, Han *et al.* fabricated such a planar flexible ZAB by using free-standing bimetallic Ni/Co catalysts as the cathode, Zn foil as the metal anode, PVA/KOH-based GPE as the electrolyte and separator, and Al-plastic film with through holes for encapsulation (Fig. 9a–c).[102] This solid-state ZAB exhibited high specific capacity of 480.7 mA h g^{-1} based on the weight of the consumed Zn, corresponding to an energy density of 530.5 W h kg^{-1}, which rivaled that of liquid ZABs. Meanwhile, this battery also exhibited superior rechargeability as it could last for more than 42 cycles (14 h) without recognizable discharge/charge voltage changes. Similar discharge voltage platforms at different bending angles of 0°, 90°, and 180° with various applied current densities confirmed the considerable flexibility of this battery. Notably, the assembled solid-state flexible ZABs could work in a wristband and provide electricity for a watch with a light-emitting diode (LED) screen, further confirming their promising potential for use in flexible and wearable electronics.

2.2.4.2 Flexible fiber-shaped configurations. As compared to their 2D planar counterparts, 1D flexible fiber-shaped energy storage devices have significantly advantageous geometrical conformability to irregular surfaces (*e.g.*, the human body), which enables them to be more attractive in wearable electronics applications.[15,41,45,48,140,141] Therefore, attempts to make 1D flexible fiber-shaped ZABs have increased in the recent years.[59,93,94,103] It has been recognized that 1D flexible batteries have higher requirements with regard to battery configuration design as well as flexibility and catalytic activity of the cathode.

Based on the flexible degrees of cathodes, either Zn spring/spiral Zn foil or Zn wire can be used as the fiber-shaped anode to adjust the curvature of the wrapping cathode. As shown in Fig. 9d and e, Park *et al.* used spiral zinc foil and carbon-cloth-loaded catalysts to fabricate an all-solid-state cable-type ZAB,[59] which showed almost unchanged discharge voltages at different bending angles. Meng *et al.* adopted a similar strategy to design another cable-type ZAB using zinc spring as the anode.[94] After encapsulating into shrinkable tubes with through holes, the ZAB could be bent, twisted, or even knotted without any collapse in the electrochemical functions. However, the diameter of 1D ZABs prepared by this method was relatively large, thereby leading to unsatisfactory flexibility of the obtained battery. Employing highly flexible carbon fiber bundles or CNT paper as the cathode substrate could effectively prevent this problem. Zeng *et al.* directly wrapped CNT paper band on a GPE-coated Zn wire, affording ultralong fiber-shaped ZABs (length: >50 cm),[108] which exhibited considerable flexibility and it could tolerate pattern-like deformations such as that by a cotton wire. Li *et al.* obtained fiber-shaped ZABs with a high aspect ratio and a coaxial structure by wrapping catalysts-containing carbon fiber bundles on a GPE-coated Zn wire.[93] This fiber-shaped ZAB (volumetric energy density: 36.1 mW h cm^{-3}) could be easily woven into the fabric to produce a self-powering textile material that could drive electronic watches, LED screens, and smartphones (Fig. 9f–h), revealing the promising applications of these flexible ZABs in a wide variety of wearable electronics.

2.2.4.3 Flexible configurations with multifunctions. In the process of fabricating ideal flexible ZABs, the stretchable characteristic can be further achieved by the strain-accommodating engineering of the device structure. For example, Zhong *et al.* connected four flexible anode/GPE/cathode units by serpentine-shaped Cu conductors to fabricate a planar ZAB prototype.[70] All the active components were encapsulated in highly elastic Ecoflex substrates. Benefitting from the elastic properties of

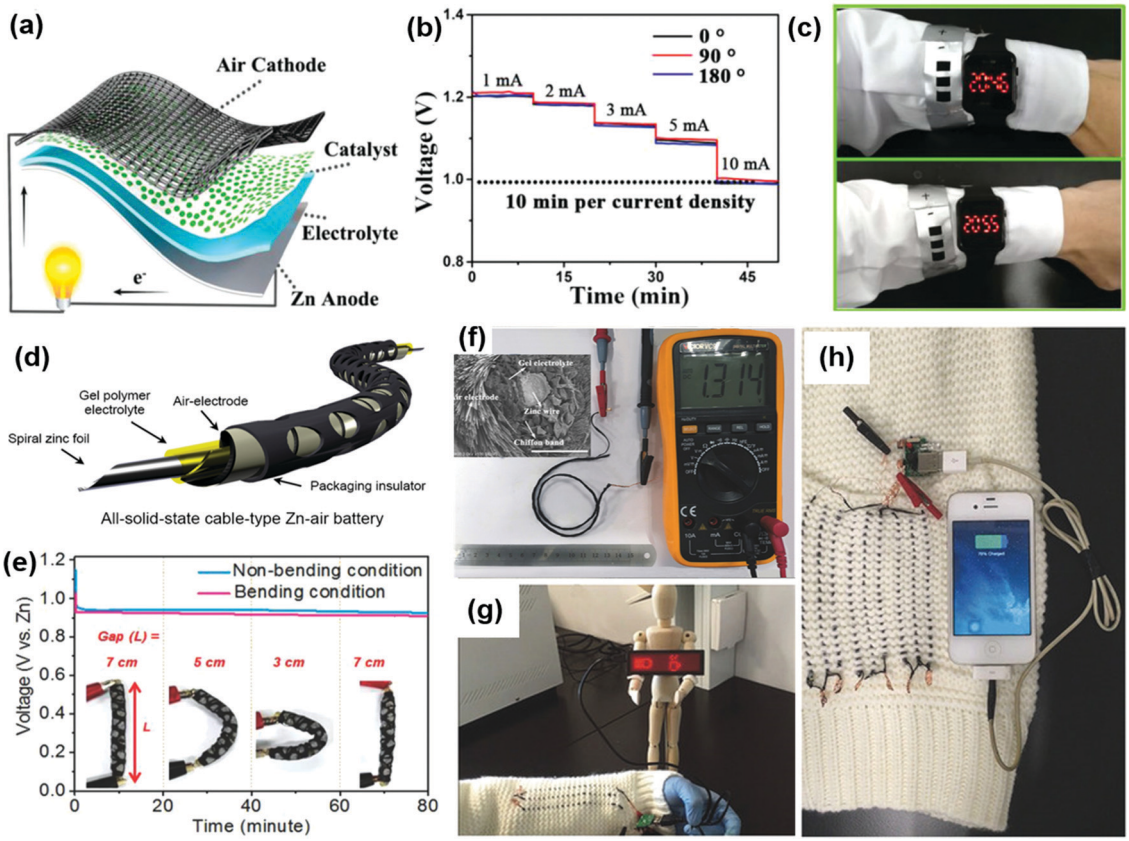

Fig. 9 (a) Schematic illustration of a typical planar flexible ZAB. (b) Rate performance of planar flexible solid-state ZABs based on $NiCo_2S_4$@g-C_3N_4-CNT electrodes. (c) Two solid-state ZABs in series powering a LED watch. Reproduced with permission. Copyright 2019, Wiley-VCH.[102] (d) Schematic diagram of the all-solid-state cable-type flexible ZAB. (e) Discharge curves of cable-type ZABs under different bending angles. Reproduced with permission. Copyright 2014, Wiley-VCH.[59] (f) Cross-sectional SEM image and OCP demonstration of a fiber-shaped ZAB using catalysts-loading carbon fiber bundles as the wrapping cathode. (g and h) Potential applications of self-powered textile knitted with three ZABs in series. Reproduced with permission. Copyright 2017, Wiley-VCH.[93]

serpentine-shaped conductors and encapsulation materials, this 2D ZAB prototype could simultaneously achieve flexibility and stretchability. The electrochemical performance could be retained at an acceptable level even if the flexible device was subjected to 125% strain. As a proof of concept, this flexible and stretchable ZAB prototype was attached onto a fabric worn on the human elbow. It could facilely bend, stretch, and shrink in consonance with bodily movements. Similarly, Xu *et al.* used a zinc spring as the metal anode and spinnable aligned CNT arrays as the flexible cathode to prepare fiber-shaped ZABs, but the recoverable distortion was less than 10%.[103]

Stretchability could also be incorporated into flexible ZABs as an intrinsic feature by fabricating both stretchable electrodes and GPEs. Ma *et al.* reported 800% stretchable flat ZABs by using plicated catalyst-loaded CNT paper, Zn-deposited CNT paper, and 1200% stretchable GPE.[100] Unexpectedly, the electrochemical performance improved even further after the battery was stretched up to 800%. Simultaneously, this type of flexible ZAB exhibited certain waterproof capability owing to the hydrophobicity of the cathode, demonstrating the excellent environmental adaptability of these batteries (Fig. 10a–d). In addition, the compressible property can also be realized by electrode design. In particular, a planar squeezable ZAB was recently reported by Wang *et al.*[69] Melamine sponges have been utilized to fabricate 3D nitrogen-doped carbon foam (NCF). The corresponding anodes and cathodes were obtained by electroplating Zn nanosheets and Fe–Co_3O_4 nanowires in highly porous NCF skeletons. After the impregnation of GPEs into electrode sponges, they were assembled together with a separator set in the middle. The assembled ZABs resulted in negligible changes in the discharge/charge voltage during the compressing (up to 60% strain) and releasing processes, and almost 95% of their power density could be retained after 500 deformation cycles.

Nevertheless, in spite of these remarkable progresses made by current studies, flexible ZABs are still facing numerous questions that need to be resolved for their use as practical power accessories in flexible devices, namely, cathode catalysts with high efficiency and low cost, metal anodes with superior Zn^{2+} plating/stripping and durable flexibility, GPE with high safety and ionic conductivity, interfacial bonding between GPE and electrodes, encapsulating materials, packaging technique, integration processes, eligibility criteria, and reliability.

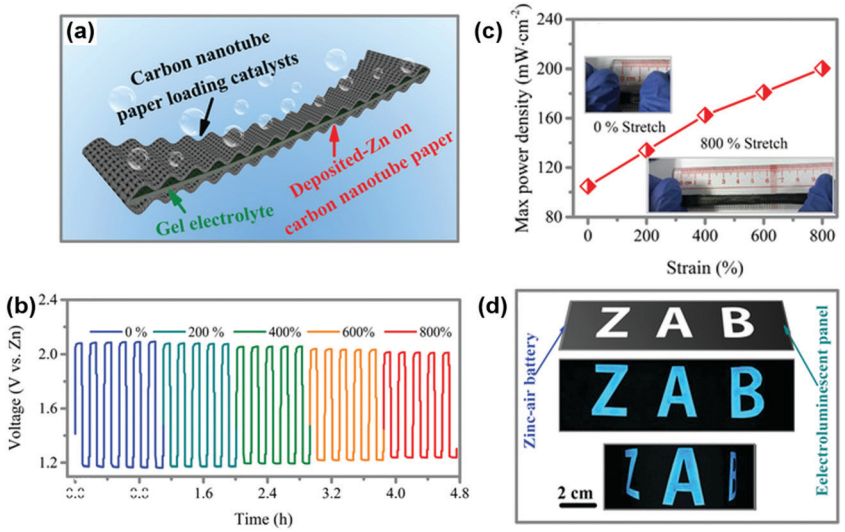

Fig. 10 (a) Schematic illustration of 800% stretchable flat-shape ZAB. (b) Galvanostatic discharge/charge cycling curves, (c) maximum power density as a function of tensile strain, and (d) application of the stretchable flat ZABs. Reproduced with permission. Copyright 2019, Wiley-VCH.[100]

2.3 Flexible Li–O_2/air batteries

As compared to aqueous ZABs, nonaqueous Li–O_2/air batteries (Li–O_2 batteries operate in pure O_2 and Li–air batteries operate in ambient air) have a much higher theoretical energy density of $\sim$3500 W h kg^{-1} with regard to the ORR process.[75,76,142] Due to this merit, Li–O_2/air batteries have been attracting tremendous attention over the past decade. For example, in 2009, IBM first proposed the "Battery 500" project, followed by active correspondence or participation from several famous research organizations all over the world. They ambitiously proposed to develop practical Li–air battery packs that could ensure a driving range of 500 mi (800 km) for EVs.[17,18] However, the development progress of Li–air batteries has been proven to be distinctly more complicated than initially thought; therefore, no Li–air battery technology has been able to satisfy the above target until now. Comparatively speaking, the ORR process of Li–O_2/air batteries proceeds in aprotic organic ether-based electrolytes *via* a mechanism that is drastically different from that observed in aqueous alkaline solutions for ZABs. (It needs to be mentioned that some studies discuss constructing aqueous Li–O_2/air batteries, but the corresponding energy density is absolutely not comparable to that of nonaqueous counterparts.[33,35,36] Hence, they do not belong to the discussion scope of this paper.) Unlike common electrocatalytic reactions in aqueous solutions, Li^+ plays a definite role in ORR and OER processes of Li–O_2 batteries, which, in turn, puts forward stricter requirements with regard to ionic conductivity, ion transport number, chemical stability, and volatility of the electrolyte. The general reaction steps of nonaqueous Li–O_2 batteries can be understood by means of the following equations.[76,78,143]

Cathode:

$$O_2 + e^- \rightarrow O_2^-$$

$$O_2^- + Li^+ \rightarrow LiO_2$$

$$LiO_2 + Li^+ + e^- \rightarrow Li_2O_2$$

$$2LiO_2 \rightarrow Li_2O_2 + O_2$$

Anode:

$$Li \rightarrow Li^+ + e^-$$

Overall:

$$2Li + O_2 \leftrightarrow Li_2O_2 \quad (E^\theta = 2.96\ V)$$

During the discharge process (ORR), O_2 is initially reduced to super oxide radicals, which then combine with desolvated Li^+, generating intermediate LiO_2 on the cathode. Due to the inherent thermodynamic instability of LiO_2, it spontaneously converts into Li_2O_2 through further lithiation or disproportionation. As the final discharge product, Li_2O_2 has strong oxidability, which can easily inflict structural damage to air electrodes and electrolytes, thereby resulting in performance decay of the batteries. Upon charging, Li_2O_2 is decomposed into Li^+ and O_2 under the assistance of the OER sites.

Notably, on account of the high sensitivity of Li metal to air, moisture, and organic electrolytes, the fabrication processes of Li–O_2 batteries are more complicated and rigorous. All the assembling processes should be operated in Ar-protected glove boxes with strict requirements regarding the H_2O and O_2 contents (commonly less than 1 ppm). Furthermore, considering the formation of lithium superoxides or lithium peroxides, most Li–O_2 batteries have to be evaluated under dry and pure O_2 atmospheres.[142,144] Otherwise, CO_2, NO_2, H_2O, and other components of air can easily react with the discharge products, leading to a faster decay of the cycling performance or even the sudden shutting down of the battery.[145] Despite these harsh preparation and working conditions, Li–O_2 batteries

are still sufficiently captivating for both academia and industry because of their unique electrochemistry and convenient O_2-harvesting ability from the ambient environment. This is the reason why studies involving flexible Li–O_2 batteries have been increasing in the recent years, although Li–O_2 batteries face more complex scientific and industrial problems. More encouragingly, through coupling multifunctional catalyst components as well as designing a gas protective layer, Li–O_2 batteries have recently embarked on the way to becoming real Li–air batteries.[76,78]

2.3.1 Flexible gas cathodes for different battery configurations. By constructing specially structured catalysts, preparing novel electrolytes, and redesigning battery configurations, multifunctional flexible Li–O_2 batteries with better electrochemical performances have been gradually developed. Nevertheless, certain issues need to be additionally specified. On one hand, the performance of cathode catalysts for Li–O_2 batteries cannot be measured by conventional electrocatalysis evaluation methods (*e.g.*, LSV and Tafel slopes) because Li^+ is intrinsically involved in the cathode redox reactions in organic electrolytes.[146,147] Although the role of Li^+ is not very clear until now, it is still much different from the common electrocatalytic processes in aqueous alkaline or acidic solutions used in ZABs (Zn^{2+} does not participate in the ORR and OER reactions on cathodes). Hence, the ORR and OER activities of the cathode catalysts are directly reflected by the electrochemical performances of the assembled full Li–O_2 batteries, instead of using the three-electrode system in aqueous solution to separately evaluate these two indexes ($E_{(ORR)1/2}$ and $E_{(OER)j=10}$, similar to those in ZAB-related studies). On the other hand, when compared with flexible ZABs, studies regarding flexible Li–O_2/air batteries began much later; therefore, they are still in their infancy. Fortunately, existing design strategies and knowledge accumulated from flexible ZABs can be used in studies regarding flexible Li–O_2 batteries. As a result, most of the currently available flexible Li–O_2 cathodes integrate free-standing catalysts and they are carefully designed to accommodate the special configurations of the proposed flexible batteries.

Hence, for a better and more comprehensive understanding, typical battery configurations together with their specially designed flexible cathodes will be simultaneously introduced in the subsequent discussion. First, representative works were compared, as shown in Fig. 11,[50,53,55,60–62,64,148–160] in terms of their discharge/charge voltage, discharge capacity, and cycling behavior. Obviously, different microstructures and components of the cathode catalysts result in significant disparity in the electrochemical properties of Li–O_2/air batteries. On average, flexible cathodes with active components of metals and their derivatives outperform those with pure carbon nanophases with regard to reaction kinetics, but it is difficult to formulate a generic regulation between rare metals and metal carbides/oxides/sulfides on the basis of the currently available limited experimental results.[60–62,64,148–160] This is possibly because the microstructure and configuration design could effectively promote the ORR and OER capabilities of different kinds of catalysts.

2.3.1.1 Flexible planar configurations. After a systematical investigation, it has been found that planar configurations based on 2D flexible electrodes still dominate the currently available flexible Li–O_2/air batteries. Representatively, Zhang *et al.* performed some impressive works in this field.

For example, a flexible, free-standing, and recoverable cathode was successfully fabricated by growing hierarchical rutile TiO_2 nanowire arrays onto carbon textiles (TiO_2 NAs/CT) (Fig. 12a).[60] This hybrid cathode showed better catalytic activities than those of pristine carbon textiles. A cell with a TiO_2 NAs/CT cathode delivered a larger discharge capacity of 3000 mA h g^{-1} (*vs.* 770 mA h g^{-1} for carbon textiles) (Fig. 12b) and could last for over 356 cycles, which is nearly 30 times higher than that obtainable with untreated carbon textiles. More importantly, the TiO_2 NAs/CT cathode exhibited decent mechanical rechargeability. After washing, the collapsed cathode could return to its normal status and keep cycling again (up to 1000 cycles). Moreover, the worthwhile performance retention under harsh bending and twisting illustrated its potential applications in advanced flexible Li–O_2 batteries (Fig. 12c). Further, they formulated an

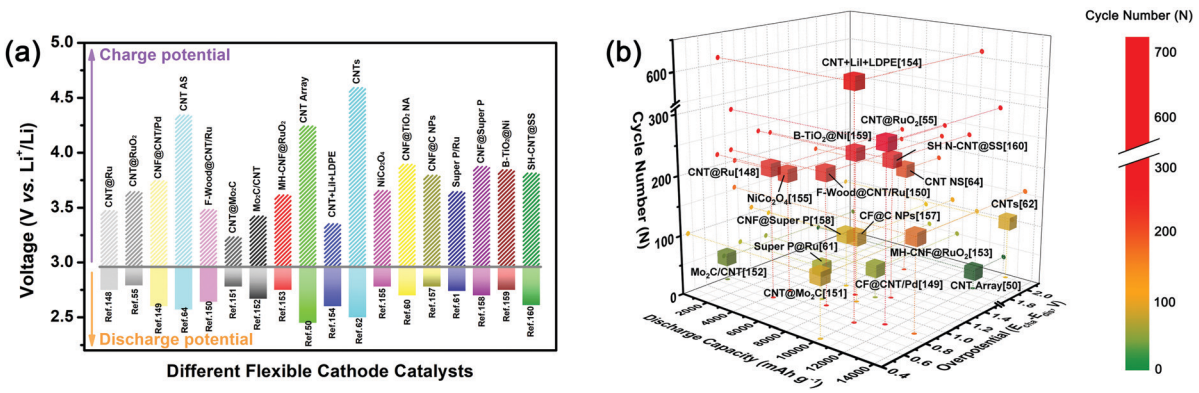

Fig. 11 Comparisons of (a) potential differences between the charge and discharge voltages of typical bifunctional flexible air cathodes used in Li–O_2 batteries reported earlier and (b) discharge capacity, overpotential, and cycling performance of those flexible Li–O_2 batteries using different types of flexible air cathodes.[50,53,55,60–62,64,148–160]

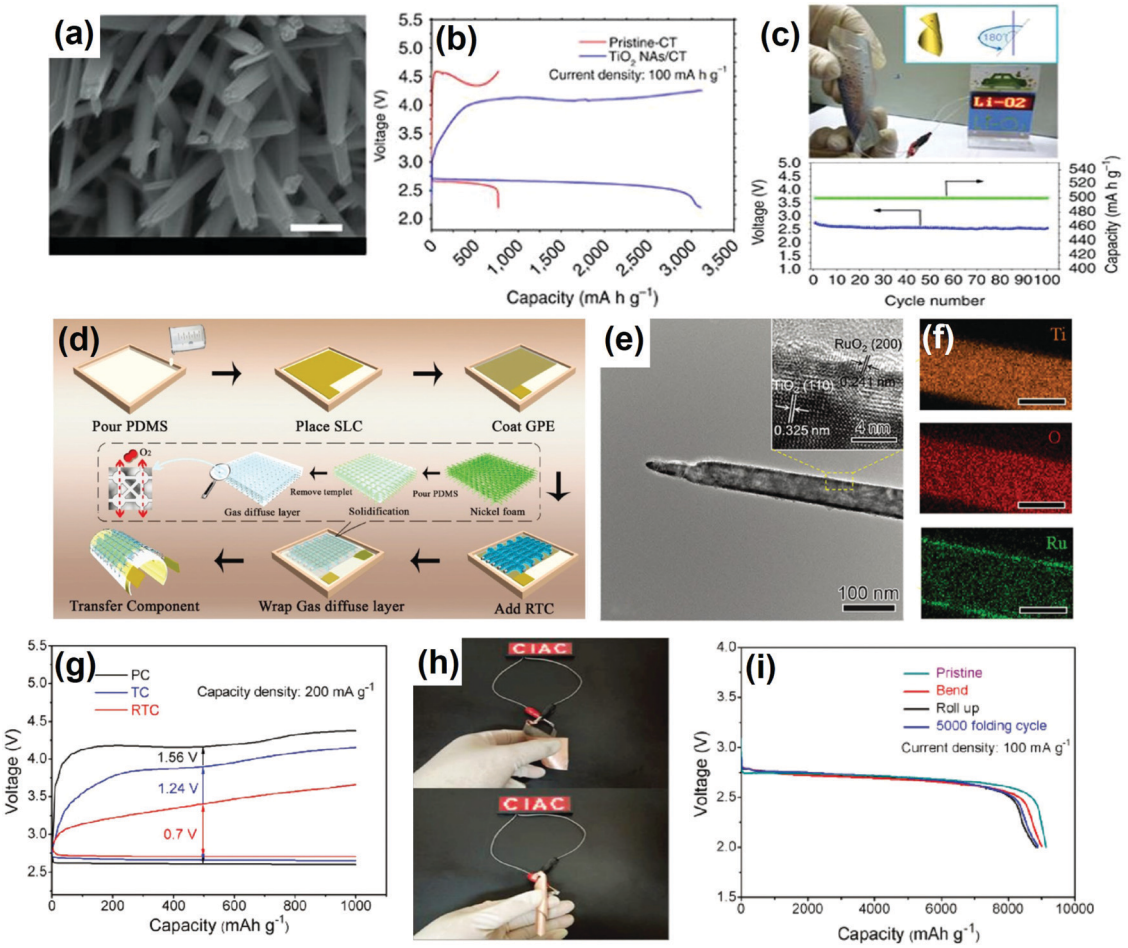

Fig. 12 (a) SEM image of a TiO_2 NAs/CT cathode. (b) Full discharge/charge profiles and (c) bending properties at 180° of a planar flexible Li–O_2 cell. Reproduced with permission. Copyright 2015, Nature Publishing Group.[60] (d) Schematic depicting the fabrication of an integrated, flexible Li–O_2 battery. (e) TEM and HRTEM (inset) images, (f) elemental mappings, and (g) first discharge/charge curves of RuO_2/TiO_2 NWs. (h) Integrated flexible Li–O_2 battery powering a LED screen under various bending and twisting conditions and (i) their corresponding discharge profiles. Reproduced with permission. Copyright 2017, Wiley-VCH.[161]

integrated self-package flexible Li–O_2 battery with low thickness and high deformability, which is shown in Fig. 12d.[161] On one hand, in a flexible cathode, ultrathin RuO_2 nanoparticles were electrodeposited on TiO_2 arrays grown on carbon cloth to further reduce the energy barriers of ORR and OER (Fig. 12e and f). Not only was the discharge/charge voltage difference reduced from 1.56 V (pure carbon cloth) to 0.7 V (Fig. 12g), but also the full discharge capacity ($\sim$9000 mA h g^{-1}), rate capability, and lifespan (210 cycles) were significantly improved. On the other hand, because a specially designed elastic PDMS sheet with interconnected open pores acted as both the gas diffusion layer and encapsulation material, the entire configuration of this Li–O_2 battery was made to be sufficiently compact. This intimate and thin structure enabled the battery to have higher flexibility, which could be largely bent, folded, rolled, or even twisted without any obvious capacity decay (Fig. 12h and i). Such high deformability is fairly impressive among the reported 2D flexible Li–O_2 batteries until now. Moreover, motivated by the special shape and structure of golden toad eggs, Zhang *et al.* synthesized a self-standing, lightweight N-doped CNF cloth with hierarchical macropores *via* a hard-template-assisted electrospinning method.[153] After the precursor was subjected to preoxidation, carbonization, and detemplating, the obtained CNF cloth was decorated with homogenously distributed ultrafine RuO_2 nanoparticles by solution impregnation. This RuO_2-N-doped carbon-hybrid flexible cathode reached a high full-discharge specific capacity of 13 290 mA h g^{-1} even at a large current density of 1 A g^{-1}. Simultaneously, it also exhibited excellent rate performance and cycling behavior of above 150 cycles.

Of course, there are still some other special free-standing catalysts with various microstructures and components that have been successfully synthesized to fabricate traditional 2D flexible Li–O_2 batteries, such as brush-like CoN_4-anchored CNF membranes,[162] free-standing 3D $CuCo_2S_4$ nanosheet arrays grown on nickel foam,[163] and hierarchical porous $NiCo_2O_4$ nanoneedle arrays on carbon cloth.[155] All of them demonstrated obviously enhanced electrochemical performances while maintaining their flexibility when compared with pristine flexible substrates.

Designing ion/gas diffusion pathways in flexible cathodes is another research hotspot in this field, which is fairly

meaningful for improving the electrode structure as well as the electrochemical performance of flexible Li–O_2/air batteries toward industrial levels. Hu *et al.* pioneered the design and preparation of gas cathodes possessing high-speed pathways for gas diffusion and ion migration.[149,150] They proposed two kinds of cathodes with decoupled ion transport and gas diffusion channels for high-performance flexible Li–O_2 batteries. The former was cotton-fibers-knitted textile coated with single CNT and Pd nanoparticles, where the hierarchical structure of the conductive textile networks provided separate pathways for ion/gas diffusion.[149] The electrolyte could diffuse along the cotton fiber bundles, while O_2 gas could permeate through the woven gaps. Benefitting from the noncompetitive transportation channels, the cathode revealed a high area specific capacity of 8.6 mA h cm^{-1}, low discharge/charge voltage difference of 1.15 V, and good cycling duration of 50 cycles for an optimized amount of electrolyte. In contrast, the latter came could be attributed to a nature-inspired wood structure that had abundant hierarchical channels for multiphase transport (gas diffusion, ion migration, and discharge product deposition). Similar to the artificial textile-based multichannel cathode described above, natural wood could retain these favorable features after the delignification treatment.[150] Cellulose nanofibers have sufficient amount of nanopores that can facilitate fast Li^+ ion transportation, while unperturbed wood lumina functioned as a diffusion channel for gas permeation (Fig. 13a–f). After loading with CNT/Ru catalysts, the cathode showed a record areal capacity of 67.2 mA h cm^{-2}, low overpotential of 0.85 V, and decent life duration of 220 cycles because of the noncompetitive triple pathways design. These electrochemical indexes are much better than those of the cathodes with densified or flooded structures (Fig. 13g). Further, it should be pointed out that the assembled Li–O_2 battery based on wood-derived cathode exhibited both high mechanical strength and superior flexibility.

2.3.1.2 Flexible fiber-shaped configurations. As specified in the section on "flexible ZABs", 1D flexible devices have advantageous adaptability to irregular geometric surfaces. This is also very effective for flexible Li–O_2 batteries.

In particular, Peng *et al.* pioneered 1D energy storage devices based on a cable-type structure. In 2016, a new family of flexible Li–air batteries was reported by them, namely, a fiber-shaped flexible Li–air battery with a coaxial fiber architecture.[62] They produced this battery by wrapping aligned CNT sheets on a GPE-coated lithium wire, followed by encapsulating the entire device inside a shrinkable tube with numerous ventholes. The aligned CNT arrays endowed the cathode with a certain elastic property, thereby ensuring sufficient electroconductivity and preventing mechanical failure during bending. The battery exhibited a discharge capacity of 12 470 mA h g^{-1} and could be normally discharged/charged for 100 cycles even in ambient air instead of a pure O_2 atmosphere. Notably, the obtained fiber-shaped batteries were easily woven into the fabric, and the self-powered textile prototype could be used for powering a commercial LED display screen, confirming the promising potential of this fiber-shaped Li–air battery for wearable consumer electronics. To alleviate the negative effects of moisture and greenhouse gases present in ambient air on the electrochemical performance, they further improved the configuration and active components of the fiber-shaped "real" Li–air batteries (Fig. 14a–c).[154] A low-density polyethylene (LDPE) film

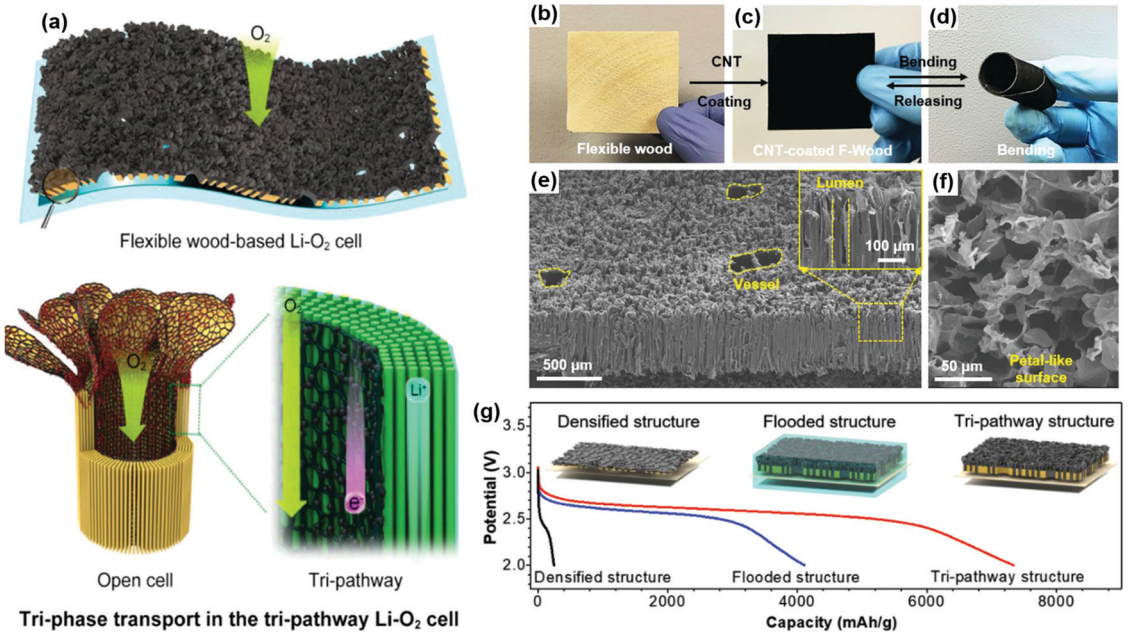

Fig. 13 (a) Schematic elucidating the tree-inspired tri-pathway design for flexible Li–O_2 cells. (b–f) Morphology of the flexible CNT-coated F-Wood membrane. (g) Discharge curves for the CNT/Ru-coated F-Wood electrodes with moderate (tri-pathway structure) or excess (flooded structure) amounts of electrolyte, and the densified electrode (densified structure). Reproduced with permission. Copyright 2019, Wiley-VCH.[150]

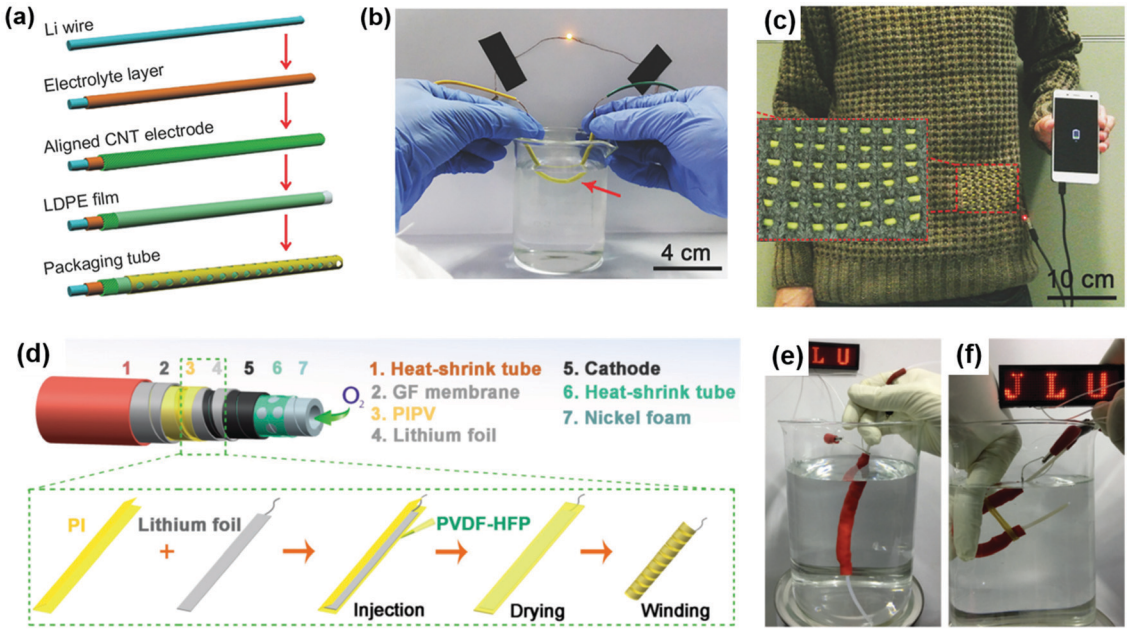

Fig. 14 (a) Schematic of the fabrication process. (b) Waterproof property of the flexible fiber-shaped Li–air battery with a LDPE layer. (c) Potential applications of Li–air batteries woven into a fabric to charge a portable phone. Reproduced with permission. Copyright 2017, Wiley-VCH.[154] (d) Schematic depicting the architecture and (e and f) waterproof property of the trans-structured SFLO battery. Reproduced with permission. Copyright 2017, Wiley-VCH.[148]

was placed between the aligned CNT array cathode and porous shrinkable tube as the protective layer to suppress the permeation of H_2O into the cathode while retaining high O_2 permeability. After optimizing the battery configuration, the fabricated fiber-shaped Li–air battery could actually operate in the ambient atmosphere instead of requiring dry and pure O_2 gas, and the cycling life of the battery was extended to a surprising value of 610 cycles. In addition, because of the flexible components and moisture-resistant LDPE protective layer, this fiber-shaped Li–air battery could not only be woven into the fabric to constitute wearable self-powered textiles as the power supply for portable electronics, but also retain its normal functions even in water, extending the adaptability of Li–air batteries toward practical working conditions.

To extend the usability, Yan *et al.* further redesigned the structure of common fiber-shaped Li–O_2 batteries, as shown in Fig. 14d.[148] This unique "trans-structure" enabled the provision of O_2 gas from the inner channels, while the outer walls of the device were protected by complete shrinkable tubes without pores. Benefitting from the combination of the advantages of the trans-structure and fire/water resistance of the GPE, this special Li–O_2 battery could work even when the entire device was completely immersed in water (Fig. 14e and f), and it was fairly fire-resistant as compared to common fiber-shaped Li–O_2 batteries with holes on the encapsulations that allow gas diffusion from the ambient atmosphere. This work provided newer design thoughts for future flexible fiber-shaped Li–O_2/air batteries.

Undoubtedly, several other researchers have also performed impressive works involving 1D flexible Li–O_2 batteries. For example, Liu *et al.* sprayed Super P, a commercial carbon material, and polymer binders onto flexible carbon textiles in order to fabricate a simple carbon-based cathode for use in Li–O_2 batteries by means of a cost-effective strategy.[158] The fabricated flexible fiber-shaped Li–O_2 battery delivered worthwhile life duration of more than 90 cycles at a discharge terminal voltage of above 2.0 V. Unexpectedly, the battery also demonstrated a certain water-survivable capability, which could still light up a red LED even though a portion of the battery was immersed in water. Yang *et al.* synthesized a blood-capillary-like free-standing, flexible, and low-cost cathode, where superhydrophobic N-doped CNT forests were grown *in situ* on stainless steel mesh (N-CNT@SS) through a facile and scalable FCCVD method.[160] The N-CNT@SS cathode exhibited a high discharge capacity of 9299 mA h g^{-1} and stable cycling behavior for up to 232 cycles. With regard to the fiber-shaped devices, strong mechanical properties and superior moisture resistibility could be simultaneously achieved.

2.3.1.3 Unique configurations with multifunctions. On the way to constructing practical flexible Li–O_2/air batteries, several unique configurations have also been proposed to achieve multi-functions besides flexibility, which are worth emphasizing here.

Zhang *et al.* exploited a large-scale flexible cathode fabrication method by employing a brush to coat catalyst ink on commonly used paper in various patterns.[61] The low cost of paper and ink together with the facile and effective electrode synthesis approach are fairly attractive for industrial-scale production. More interestingly, inspired by the unique characteristics of this paper–ink cathode, a foldable Li–O_2 battery pack was prepared for the first time. The unique foldable structure of

the battery played the critical role of a power switch, which enabled this Li–air battery to provide electricity under a compression state that could automatically stop after the external force was released (Fig. 15a–c). Further, it should be noted that the low weight (~1.93 g) of the device was beneficial for improving its whole gravimetric/volume energy density. Similarly, to achieve these low weight, robust, and wearable features, Zhang *et al.* designed a novel segmented Li–O_2 battery pack, where the overall air electrode was broken up into an array of disks without the necessity of gas diffusion layers (Fig. 15d).[55] The active catalytic component in the cathode was RuO_2 nanoparticles dispersed on CNTs (RuO_2@CNTs). Because of its low weight (0.637 g) and ultrathin configuration (0.474 mm), this fabricated wearable Li–O_2 battery delivered a fairly high gravimetric energy density of 294.68 W h kg^{-1} (based on the total weight of the device) and reached a large volumetric energy

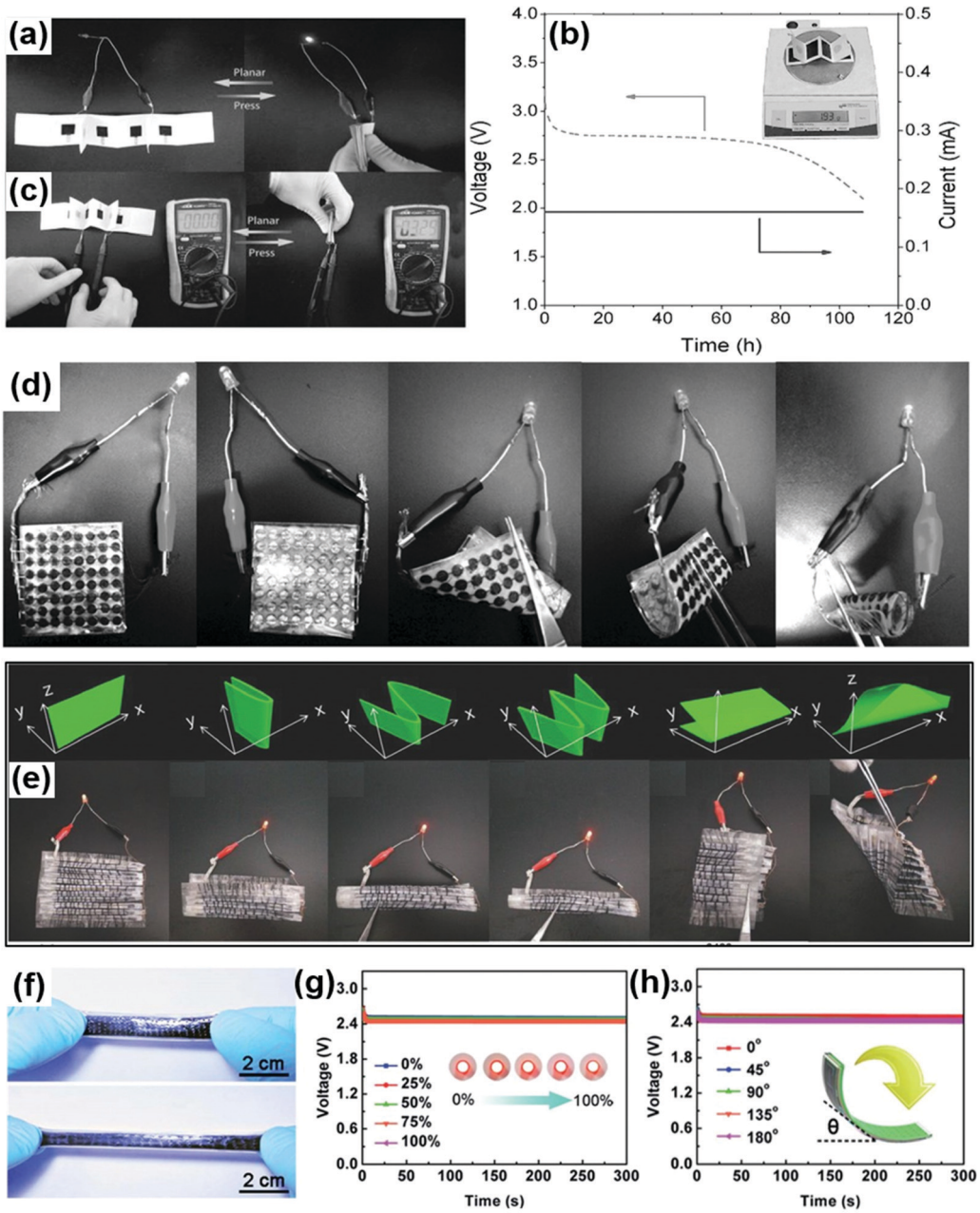

Fig. 15 (a–c) Working mechanism of a foldable Li–O_2 battery pack and its corresponding electrochemical performance. Reproduced with permission. Copyright 2015, Wiley-VCH.[61] (d) Ultrathin, lightweight, and wearable segmented Li–O_2 prototype powering a LED under bending conditions. Reproduced with permission. Copyright 2016, Wiley-VCH.[55] (e) Bamboo-slips-like structured Li–O_2 battery powering a LED under various deformation conditions. Reproduced with permission. Copyright 2016, Wiley-VCH.[157] (f) Stretchable Li–air battery before and after stretching. Discharge curves of the stretchable Li–air battery under increasing strains (g) and different bending angles (h). Reproduced with permission. Copyright 2016, The Royal Society of Chemistry.[64]

density of 274.06 W h L^{-1}. The two values were obviously higher than those obtainable from conventional coin-type, cable-type, and soft-package-type Li–O_2 batteries. Impressively, even after 10 000 cycles of folding or stretching, the discharge/charge profiles still overlapped, further elucidating that this specially designed battery configuration was highly flexible.

Not limited to this, other efforts involving novel cathode catalysts and practical assembly configurations for high-performance and flexible Li–O_2 batteries have been carried out. Typically, a distinct flexible Li–O_2 battery configuration was reported by Liu *et al.*, which seemed to be inspired by Chinese bamboo slips (Fig. 15e).[157] A commonly used conductive additive, Super P, was coated on the surface of a carbon wire to constitute an air electrode, without any remarkably negative influence on flexibility. After being matched with GPE-coated lithium metal anode, a bamboo-slips-like Li–O_2 battery was obtained. It could be easily attached onto clothes worn on the human body and could tolerate intricate deformations. Moreover, Peng *et al.* successfully fabricated a flexible and stretchable Li–air battery for the first time by combining rippled CNT sheets and Cu-springs-connected lithium metal sheets, as shown in Fig. 15f.[64] Even when the battery experienced 1000 stretching cycles under strain of 100%, the electrical resistance was only increased by less than 4%. Moreover, the discharge voltage plateau of this as-prepared battery could be effectively maintained under the stretched state (Fig. 15g and h). This work presented a new and generic function of flexible Li–O_2 batteries that should be taken into consideration in future studies.

Combining flexible Li–O_2/air batteries with other energy systems to construct flexible integrated devices with multifunctions is also a very meaningful research direction that deserves our attention, although only a few relevant reports have been published. An illumination-assisted flexible self-powered energy system based on a Li–O_2 battery as reported by Zhang *et al.* is noteworthy in this case.[164] They grew porous TiN/TiO_2 nanowires on carbon cloth as bifunctional cathodes for use in flexible Li–O_2 batteries. Due to the photocatalytic activity of TiN/TiO_2 composites, the overpotential of the battery could be reduced to 0.19 V with the aid of solar energy (Fig. 16a and b). Inspired by this particular physicochemical property, a flexible self-powered energy system was constructed by attaching a flexible 2D solar cell onto the anode side of the Li–O_2 battery, as shown in Fig. 16c. By rational circuit design, the Li–O_2 battery could utilize the electricity provided by the solar cell to recharge itself under low overpotential when there was sufficient illumination while powering other electronics in the external circuit when the environment became dark (Fig. 16d and e). Simultaneously, due to the integrated configuration, this self-powered energy system was capable of sufficient deformability, suggesting its promising potential as an ideal uninterruptible power supply for wearable electronics.

Generally speaking, these attempts on designing or optimizing the electrode structure and battery configuration have had a positive impact on promoting the development of "real" flexible Li–air batteries toward ideal power suppliers under practical service conditions. Enhancing the total energy storage capability of battery packs while maintaining sufficient flexibility and multifunctionality is one of the most important concerns at the present stage.

2.3.2 Flexible Li metal anodes. Similar to flexible ZABs, lithium foils or lithium sticks/wires have been widely utilized in currently available flexible Li–O_2/air batteries, which can be used to better highlight the advantages of newly proposed cathode catalysts or electrolytes.[148–160] Fortunately, lithium anode modification has been extensively investigated as compared to its Zn counterpart because of the academic prosperity of lithium-ion-based energy storage systems. Air-/moisture-sensitive properties and easier dendrite growth ensure that

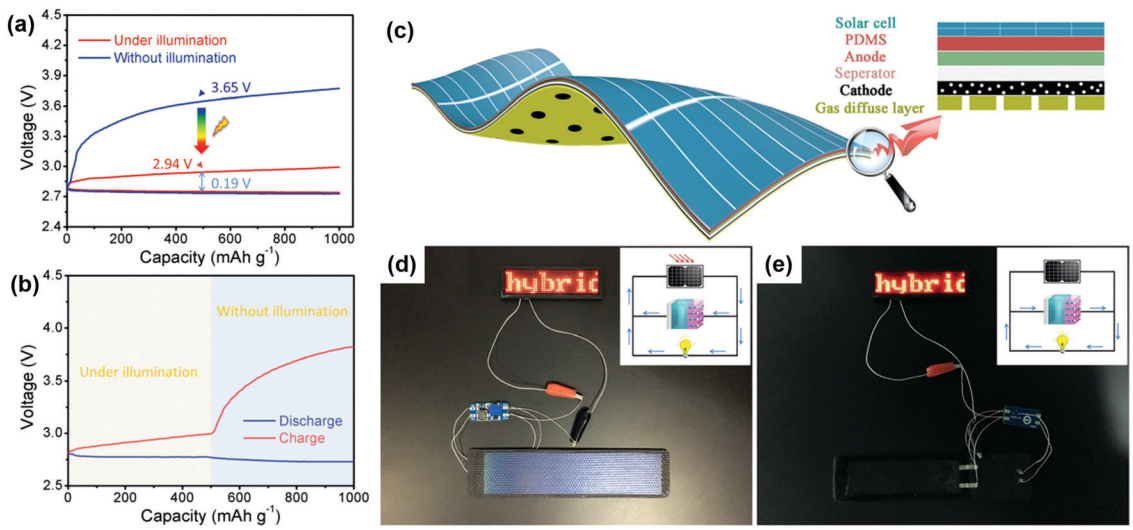

Fig. 16 (a) Discharge/charge profiles and (b) dynamic light response discharge/charge voltages of the CC@TiN/TiO_2 NW cathodes with or without illumination. (c) Illustration of the structure of the self-powered energy system. (d and e) Digital photographs of the assembled self-powered energy system working with or without light. Reproduced with permission. Copyright 2019, Wiley-VCH.[164]

lithium anodes have a rapid performance response to structural/component modifications regardless of its use in secondary-metal-ion batteries or metal–gas batteries.[165–169]

Resolving dendrite-based issues is the most important priority for Li anode studies, which underlines the foundation of battery safety. In preliminary studies, porous metal frameworks have been employed as host scaffolds to accommodate Li through melting–impregnation or electrodeposition methods on account of the worthwhile wettability between different metals.[166] Nickel foam, porous Cu, Cu nanotube arrays, *etc.* have usually been selected as the soft substrates for Li deposition. Highly conductive 3D pathways provided by metal substrates are beneficial for electric field distribution, inducing the first deposition of Li^+ along the surface of metal scaffolds until all the voids are filled instead of dendrite formation. However, Li anodes prepared by this strategy exhibit poor flexibility due to the limited flexibility of the original metal substrates and intrinsic metal fatigue. As a result, most of them can only tolerate a small bending angle ($<90^\circ$) at a large curvature radius. In addition, their volume mass is remarkably enlarged, which reduces the energy density of the device. Aimed to resolve the above problem, carbon nanophases have been utilized as Li host materials, for example, free-standing GO film,[168] CNF clothes,[165] CNT arrays/films,[167] and bioderived porous carbon.[169] Similarly, a large specific surface area and abundant defects of carbon nanophases offer uniform nucleation sites and action channels for Li^+ plating/stripping such that dendritic and "dead" Li can be largely suppressed in these Li/C hybrid anodes even at higher rates. However, the decline in flexibility cannot be completely avoided because of the existence of Li–C interfaces and LiC_x phases. Although ideal flexible anodes for Li–O_2/air batteries have not been developed, a recent research outcome may provide some inspiration for future designs. Li *et al.* fabricated a Li anode by infusing a suitable amount of molten Li into the CNT fibers modified with ZnO nanowire arrays.[170] Because ZnO is lithiophilic, Li prefers to deposit on it as a film coating rather than getting combined with the CNT fibers. Hence, the obtained hybrid Li anode inherited the superior flexibility of pristine CNT fibers and it can be wrapped on an elastic wire to achieve stretchability. It is hoped that these modified Li anodes can be quickly designed and evaluated, accelerating the advance of Li anodes toward particularly appropriate examples for flexible Li–O_2/air batteries.

Moreover, we consider that constructing artificial SEI on Li anodes may be another promising solution, considering the fact that pretreated SEI can effectively alleviate dendrite growth and gas corrosion in some rigid Li–O_2 cells that have been reported earlier,[171–174] but enhancing the integrity and preventing the breakage of the SEI layer during deformation seems to be a Gordian knot.

2.3.3 Optimization of aprotic GPEs. In comparison to electrode design and modification, it is noteworthy that electrolytes that are adaptable for use in flexible Li–O_2 batteries have already become another focus point of research. Admittedly, the health and safety problem is the most important factor for the possible commercial applications of flexible Li–O_2 batteries (particularly those purposed at wearable electronics that necessitate direct contact with human skin) when taking into account the poisonousness and dangerousness of the used organic electrolyte; therefore, problems such as electrolyte leakage, flammable property, dendrite formation, atmospheric sensitivity, and mechanical failure should be avoided as much as possible. It is considered that advance in GPE technology is a critical step toward addressing the aforementioned dilemmas and underlines the development of flexible Li–O_2/air batteries toward commercialization.

Some efforts related to this have been recently made. In contrast to ZABs, the polymer host of the GPE that is used in flexible Li–O_2/air batteries is relatively fixed because well-known polymer frameworks can hardly satisfy the comprehensive requirements of Li–O_2/air batteries.[172,182] For example, PEO-based GPE exhibited a narrow potential window and poor room-temperature ionic conductivity. PAN-based GPE only showed unsatisfactory interfacial compatibility with Li metal anode, while PMMA-based GPE suffered from weak mechanical properties and poor flexibility. Among them, poly(vinylidene fluoride-*co*-hexafluoropropylene) (PVDF-HFP) has been commonly used as the primary polymer matrix for the GPE of Li–O_2/air batteries due to its low crystallinity, abundant ionic migration channels, stable chemical property, good processability, and fire resistance. Besides PVDF-HFP, a few other polymers, such as polyimide (PI), poly(methyl methacrylate-*co*-styrene) (PMS), ethylenediamine (EDA), polyethylene glycol dimethyl ether (PEGDME), and thermoplastic polyurethane (TPU), have also been investigated, which have demonstrated advantageous features in certain aspects. Typical earlier works involving GPE for use in flexible Li–O_2/air batteries are listed in Table 2,[50,53,148,154,156,175–181] illustrating their basic structural and electrochemical features as well as unique merits and weaknesses.

We selected several typical works among them to discuss in detail here. Wang *et al.* prepared an integrated quasi-solid-state electrolyte by infusing PVDF-HFP/super hydrophobic nano-fumed silica (SH-SiO_2) ceramic homogeneous solution into cellulose paper (denoted as PS-QSE),[53] which took advantage of component interaction to realize high ionic conductivity (0.93 mS cm^{-1}), chemical stability (a stable voltage range of up to 3.63 V), mechanical strength, and flexibility. This synthesized PS-QSE could effectively prohibit the growth of dendrites during cycling and suppress lithium metal anode corrosion caused by O_2 and H_2O in air. Therefore, the overpotential of a Li–air battery fabricated using PS-QSE was much lower than that of the one fabricated using conventional liquid electrolytes under ambient air. Benefitting from the high safety and flexibility of PS-QSE, the assembled flexible Li–air battery was deformable and tailorable according to desired shapes. Aimed to resolve the issue posed by the high charge overpotential of the traditional Li^+/tetraglyme (TEGDME)-based electrolyte, Peng *et al.* added the redox mediator LiI into TEGDME/lithium difluorosulfimide (LiSFI)/PVDF-based GPE prepared by subjecting the mixed precursor solution to UV radiation.[154] LiI could effectively play the role of a ferry to boost electron transport between the discharge product and electrolyte/electrode, thereby

Table 2 Comparison of typical aprotic GPEs reported earlier for use in flexible Li–O_2/air batteries

Polymer matrix	Electrolyte	Additives	Ionic conductivity (mS cm^{-1})	Voltage window (V)	Advantages	Limitations
PVDF–HFP	LiTFSI–TEGDME	SH-SiO_2/cellulose fiber[53]	0.93	4.75	Water-resistance	
	$LiClO_4$/$LiNO_3$–TEGDME	MnOOH@Al_2O_3 film[175]	1.04	4.5	Moderate mechanical strength	Complex components
	$LiCF_3SO_3$–TEGDME	HMPP/TMPET/LiI[154]	2.52	<3.75	High ionic conductivity/UV-induced fast polymerization	Weak mechanical strength
	BMPy–TFSI/LiTFSI	—[50]	0.335 (25 °C) 1.16 (100 °C)	4.5	Work in high temperature	High cost
	$LiClO_4$–DMSO	SiO_2/TTF[176]	—	4.75	Mediate Li_2O_2 oxidation reaction	Unhealthy/volatilization
	LiTFSI–TEGDME	HMPP/TMPET/LiI/SiO_2[177]	1.01	4.5	Mediate Li_2O_2 oxidation reaction/UV-induced fast polymerization	Weak mechanical strength
PVDF–BBP–PVB	$BF_4Li/Li_{1+x}A_xGe_{2-x}(PO_4)_3$	—[178]	0.003	—		Low ionic conductivity/unstable
PVDF–HFP/PI	$LiCF_3SO_3$–TEGDME	—[148]	0.025	4.5	Fire-resistance	Low ionic conductivity
PMS	$Li_{1.6}Al_{0.5}Ge_{1.5}(PO_4)_3$/LiTSFI–TEGDME	PE separator/SiO_2[179]	0.32	5.2	High voltage window	High cost/tedious preparation
EDA	Li^+–TEGDME	—[180]	—	5.5	High voltage window/resistance to moisture	Poor processibility
PEGDME	LiTSFI	SiO_2[181]	—	4.6	Easy preparation	Weak mechanical strength
TPU	LiTFSI–TEGDME	SiO_2/nonwoven fabric[156]	1.02	5.0	High mechanical strength/water-resistance	Limited flexibility

facilitating the reversible formation and decomposition of Li_2O_2. As a result, the GPE modified with LiI reduced the charge potential to around 3.5 V, which was distinctly lower than that of the original GPE. At the same time, the cycling stability was enhanced because of the lowered decomposition of the electrolyte during the low-voltage charge processes. Attractively, Yan *et al.* designed a PVDF-HFP/PI membrane as a composite multifunctional separator (PIPV) with high electrolyte uptake, as shown in Fig. 17a–d.[148] Although the obtained PIPV film revealed abundant pores in their framework, it still exhibited higher mechanical strength coupled with improved flexibility inherited from PI. Owing to the hydrophobicity of both these components, this composite film could largely prevent moisture corrosion of the Li anode. However, it only showed fairly limited ionic conductivity of 0.025 mS cm^{-1}.

Besides PVDF-HFP, a few other polymers have also been used as novel host polymers. Two examples are briefly introduced here. Ding *et al.* reported that GPE induced with TEGDME (also known as G4) was formed *in situ via* the crosslinking reaction between liquid G4 and lithium ethylenediamine (LiEDA) on the surface of a Li anode (Fig. 17e–g).[180] This G4 GPE showed a surprising voltage window of up to 5.5 V, which was among the highest in all the reported GPEs that have been used in Li–O_2 batteries until now. Li–air batteries employing this G4 GPE also showed significantly enhanced cycling stability. Nevertheless, such a preparation strategy exposed a shortcoming that the G4 GPE film was absolutely not processible and it was easily damaged during deformation on account of the low thickness of the *in situ* reaction layer. Shao *et al.* employed a similar strategy to fabricate a highly crosslinked quasi-solid electrolyte (FST-GPE) consisting of thermoplastic polyurethane (TPU), aerogel SiO_2, and nonwoven cotton fabric, which were plasticized by conventional lithium bis(trifluoromethylsulfonimide) (LiTFSI)/TEGDME liquid electrolyte.[156] The resulting flexible Li–O_2/air battery could achieve up to 250 discharge/charge cycles with an operation time of over 1000 h in O_2 gas and maintain its normal working for over 20 days under extreme bending conditions in ambient air.

Furthermore, ionic liquid gel electrolytes, as emerging GPEs for use in Li–O_2 batteries, have started to recently receive interests from researchers. For example, Sun *et al.* developed a novel category of ionic liquid gel electrolyte on account of the fact that it could offer a wider electrochemical window and lower volatility.[50] The ionic liquid gel electrolyte was prepared by mixing the ionic liquid of 1-*n*-butyl-1-methylpyrrolidinium bis(trifluoromethylsulfonyl)imide (BMPy-TFSI), LiTFSI, and PVDF-HFP (Fig. 17h). Consequently, the obtained fiber-shaped Li–air battery could stably work over a large range of temperatures from 25 to 140 °C. In particular, it could demonstrate a high full discharge capacity of ~12 000 mA h g^{-1} at 100 °C and excellent long-term cycling stability of 380 cycles at a high rate of 10 A g^{-1} at 140 °C (Fig. 17i and j). On account of the inevitable heat accumulation when the battery is working or recharging, this work promoted the high-temperature performance and safety protection of flexible Li–O_2/air batteries into a higher research level.

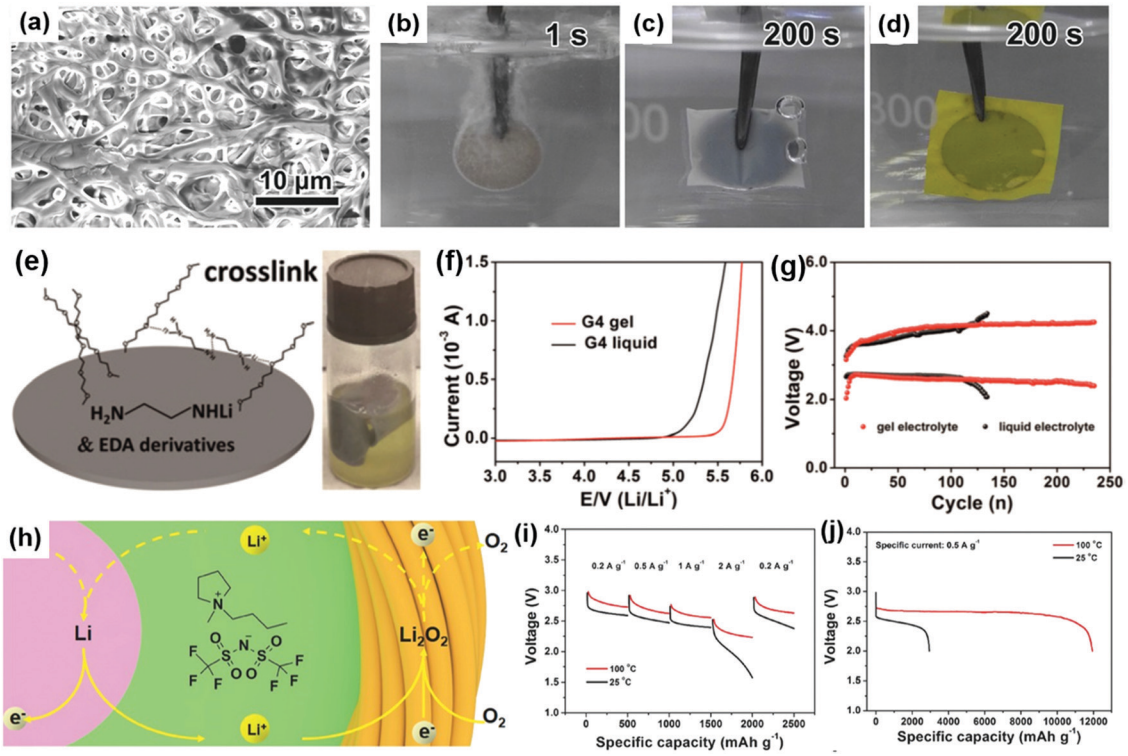

Fig. 17 (a) SEM image of PI. Photographs of (b) pristine lithium sheet, lithium coated with (c) PP and (d) PIPV immersed in water. Reproduced with permission. Copyright 2017, Wiley-VCH.[148] (e) Schematic and photographic illustration of the formation process of G4 GPE on Li foil. (f) LSV of G4 gel and liquid with 0.5 M $LiClO_4$. (d) Cycling performances of flexible Li–air batteries using G4 GPE and liquid electrolyte. Reproduced with permission. Copyright 2018, Wiley-VCH.[180] (h) Working mechanism and (i and j) electrochemical performances of ionic-liquid-based GPE in ambient and high-temperature environments. Reproduced with permission. Copyright 2017, Wiley-VCH.[50]

Although several progresses regarding flexible Li–O_2/air batteries have been achieved *via* continuous electrode/electrolyte/configuration optimizations until now,[183,184] three main components, namely, efficient catalytic cathodes, stable and highly ion-conductive (quasi-) solid-state electrolyte, and dendrite-free flexible lithium metal anodes (few studies have been recently published), still need special considerations for use in flexible systems.

2.4 Other advanced metal–O_2/air batteries

Apart from ZABs and Li–O_2/air batteries, their alkaline counterparts (*e.g.*, Na, K, Mg, Fe, Al, Si, *etc.*)[20,21,23,26,27,63,65,77,84,185–187] have also been investigated for use in metal–O_2/air batteries. Their general working principles coupled with other electrochemical indexes are listed in Table 3 for convenience. Among them, some novel kinds of metal–O_2/air batteries have already been used to fabricate flexible devices or flexible components successfully, while the remaining still need tremendous efforts to overcome the challenges faced by them.

Herein, certain representative works on these potential novel flexible metal–gas batteries have been briefly introduced. Zhang *et al.* prepared a binder-free N-doped CNF embedded and coated with homogeneously dispersed Co nanoparticles by a scalable electrospinning strategy for fabricating cathodes for use in Na–O_2 batteries.[188] This electrospun and carbonated core–shell nanofiber cathode afforded an enhanced discharge capacity of 6102 mA h g^{-1}, lower charge voltage plateau (3.4 V), and longer cycling life of up to 112 cycles when compared with those obtainable from N-doped CNFs. Zhou *et al.* directly used benzene/ferrocene-catalyzed CNT paper as the flexible cathodes for Na–O_2 batteries,[185] which exhibited the full discharge and charge capacities of 7530 and 3300 mA h g^{-1}, respectively, and a small overpotential gap of 0.2 V during cycles. Wu *et al.* reported a K–O_2 battery for which the discharge product was stable KO_2 instead of hyperoxide species observed in Li–O_2 batteries.[27] KO_2 could be reversibly formed and decomposed during the discharge/charge processes in 0.5 M KPF_6/dimethoxyethane (DME) electrolyte without the utilization of catalysts, resulting in a fairly low discharge/charge potential difference of less than 0.05 V. This is the lowest overpotential value ever reported for metal–O_2 batteries. Du *et al.* synthesized a PdSn/CNT nanocomposite catalyst for Mg–air batteries that was obtained by means of a facile chemical reduction method.[20] This hybrid catalyst revealed remarkable ORR activity in an alkaline solution, enabling the assembled Mg–air battery to have a flat discharge voltage plateau of around 1.25 V within 13 h as well as the highest power density of 112.4 mW cm^{-2}. Fascinatingly, Peng *et al.* created two new kinds of all-solid-state fiber-shaped metal–O_2 batteries (Al–O_2 and Si–O_2 batteries) for the first time.[63,65] Fiber-shaped Al–O_2 batteries not only demonstrated a specific capacity of 935 mA h g^{-1} and an energy density of 1168 W h kg^{-1}, but also could be

Table 3 Theoretical voltage, capacity, energy density, chemical reaction mechanism, and progress with regard to flexibility of other categories of metal–O_2/air batteries

Battery type	Chemical reaction mechanism (electrolyte categories)	Theoretical voltage (V)	Theoretical capacity (mA h g^{-1})	Theoretical energy density (W h kg^{-1})	Progress on flexibility
Fe–O_2[23]	$3Fe + 2O_2 \rightleftharpoons Fe_3O_4$ (alkaline aqueous electrolyte)	1.28	597	764	Catalyst powder
Mg–O_2[20]	$2Mg + O_2 + H_2O \rightleftharpoons 2Mg(OH)_2$ (alkaline aqueous electrolyte)	3.1	919	2850	Catalyst powder
Na–O_2[26]	$2Na + O_2 \rightleftharpoons Na_2O_2$	2.33	688	1605	Catalyst powder
	$Na + O_2 \rightleftharpoons NaO_2$ (organic electrolyte)	2.27	487	1105	
K–O_2[27]	$K + O_2 \rightleftharpoons KO_2$ (organic electrolyte)	2.37	394	935	Catalyst powder
Si–O_2[65]	$2LixSi + xO_2 \rightleftharpoons xLi_2O_2 + 2Si$ (organic electrolyte)	~2.5	—	—	Flexible 1D device
Al–O_2[63]	$4Al + 3O_2 + 6H_2O \Rightarrow 4Al(OH)_3$ (alkaline aqueous electrolyte)	2.71	1031	2796	Flexible 1D/2D devices

integrated into fabric-based wristbands and provide electricity to a LED watch.[63] Si–O_2 batteries were designed with highly flexible coaxial architecture, which ensured its effective operation after bending for 20 000 cycles.[65] Further, this battery produced at a continuous scale demonstrated the capability of being woven with textile fibers to constitute a real self-powering fabric, suggesting its promising potential for commercial applications. Generally, despite the fact that all these novel metal–gas batteries are in their infancy, they do provide alternatives as future power accessories for wearable electronics.

3. Flexible metal–CO_2 batteries

The proposed metal–CO_2 batteries have been considered to be the ideal candidate for next-generation high-performance energy storage and conversion systems for use in portable electronics and even (hybrid) EVs. They not only demonstrate a high theoretical energy density, but also provide a novel and facile strategy to achieve CO_2 capture without the necessity of extra energy consumption, which is inevitably demanded in traditional CO_2 fixation methods. Consequently, this environmentally friendly property is beneficial for alleviating the greenhouse effect and endowing metal–CO_2 batteries with a promising significance in the progress of sustainable development.

3.1 Working principles

Until now, the feasibilities of Li–CO_2,[189] K–CO_2,[190] Na–CO_2,[191] Al–CO_2,[30] and Zn–CO_2[24] systems have been successfully verified by coupling various groups of electrodes and electrolytes. Li–/Na–CO_2 batteries, which possess relatively high theoretical energy densities, comprise ether-based organic electrolytes, while Al–CO_2 batteries employ an ionic liquid as the electrolyte. In contrast, two different kinds of Zn–CO_2 batteries have been constructed in the mode of two cells using an aqueous solution. General information regarding the abovementioned four metal–CO_2 batteries is listed in Table 4.

Among the various kinds of metal–CO_2 batteries, a Li–CO_2 battery is one of the most attractive representatives because it possesses a high working voltage (~2.8 V) and high energy density (~1875 W h kg^{-1}) because of the four-electron transfer reaction. Its theoretical energy density is the largest among all known metal–CO_2 batteries, which is comparable to that of Li–O_2 batteries.[192,193] Hence, more studies related to Li–CO_2 batteries have been reported as compared to their counterparts. Despite the fact that some efforts have been directed toward the exploration of the detailed energy storage mechanism of Li–CO_2 batteries, it cannot reach an agreement at the current stage. One possible reaction procedure is presented here for ref. 37 and 194–196.

Cathode:

$$2CO_2 + 2e^- \rightarrow C_2O_4^{2-}$$

$$C_2O_4^{2-} \rightarrow CO_2^{2-} + 2CO_2$$

$$CO_2^{2-} + C_2O_4^{2-} \rightarrow 2CO_3^{2-} + C$$

$$2Li^+ + CO_3^{2-} \rightarrow 2Li_2CO_3$$

Anode:

$$Li \rightarrow Li^+ + e^-$$

Table 4 Theoretical voltage, capacity, energy density, and chemical reaction mechanism of other categories of metal–CO_2 batteries known to date

Battery type	Chemical reaction mechanism (electrolyte categories)	Cathode catalyst	Theoretical voltage (V)	Theoretical capacity (mA h g^{-1})	Theoretical energy density (W h kg^{-1})
Li–CO_2[189]	$4Li + 3CO_2 \rightleftharpoons 2Li_2CO_3 + C$ (organic LiTFSI/TEGDME)	CNT/graphene	2.80	670	1876
Na–CO_2[191]	$4Na + 3CO_2 \rightleftharpoons 2Na_2CO_3 + C$ (organic $NaClO_4$/TEGDME)	Activated MCNT	2.35	480	1130
K–CO_2[190]	$4K + 3CO_2 \rightleftharpoons 2K_2CO_3 + C$ (organic KTFSI/TEGDME)	N-CNT–rGO	2.48	372	922
Al–CO_2[30]	$4Al + 9CO_2 \rightleftharpoons 2Al_2(CO_3)_3 + 3C$ (ionic liquid $AlCl_3$/[EMIm]Cl)	Au@Pd	~0.72	638	~460
Zn–CO_2 (1)[24]	$Zn + CO_2 + H_2O \rightleftharpoons ZnO + HCOOH$ (aqueous KOH/NaCl)	3D Pd	0.955	825	788 (Zn)
		nano-sheets		420	402 (ZnO + HCOOH)
Zn–CO_2 (2)[44]	$Zn + CO_2 + H_2O + 2OH^- \Rightarrow Zn(OH)_4^{2} + CO$ (discharge)	Ir@Au	0.707	825	583 (Zn)
	$Zn(OH)_4^{2-} \Rightarrow Zn + 1/2O_2 + 2OH^- + H_2O$ (charge) (aqueous KOH/$KHCO_3$)			332	235 ($Zn(OH)_4^{2-}$ + CO)

Overall:

$$4Li + 3CO_2 \leftrightarrow 2Li_2CO_3 + C \quad (E^{\theta} = 2.80\ V)$$

On the basis of this mechanism, oxalate species form the intermediate discharge product of the CO_2 reduction reaction (CO_2RR), which can then be disproportionated into carbonate and amorphous carbon. During the charge process, active sites for CO_2 evolution reaction (CO_2ER) help facilitate Li_2CO_3 to decompose and release Li^+ and gaseous CO_2. According to the overall reaction, it offers a hopeful perspective that future commercialized flexible Li–CO_2 batteries can provide a renewable energy source for wearable, portable, or flexible electronics, as well as (hybrid) EVs. Meanwhile, a large amount of CO_2 has been fixed into these batteries, considerably alleviating the greenhouse effect on earth. More oxygen can be retained for sustaining life. The environmentally friendly property enables Li–CO_2 batteries to help reduce CO_2 emissions and contribute toward the sustainable development of human society. In addition, when compared with the discharge product of Li_2O_2 in Li–O_2 batteries, lithium carbonate species in Li–CO_2 batteries are more chemically stable and safer, making them particularly suitable for wearable consumer electronics.

3.2 Development of Li–O_2/Li–CO_2 batteries toward developing Li–CO_2 batteries

Primary studies on Li–O_2/Li–CO_2 batteries were performed to understand what happened in the ORR and OER electrochemistry of Li–O_2 batteries if ambient air (which contains contaminants such as CO_2) was utilized instead of pure O_2 gas as the gas resource.[193,197,198] It is recognized that this is a crucial step for enabling currently available Li–O_2 batteries to become real Li–air batteries.

The first exploration was conducted by Takechi *et al.*,[197] where Li–O_2/Li–CO_2 batteries demonstrated enhanced discharge capacities in mixed gases with a wide range of CO_2 ratio from 10% to 80%. Nevertheless, only Li_2CO_3 was detectable in the discharged cathode and the morphology of the discharge products was fairly different than that of Li_2O_2—the discharge product of Li–O_2 batteries. The discharge voltage plateau of Li–O_2/Li–CO_2 batteries was observed at 2.7 V, which was identical to that of Li–O_2 batteries. This enhanced performance could be attributed to the rapid capture of CO_2 to $O_2^{\cdot-}$, forming Li_2CO_3 that was slowly deposited. Later, McCloskey *et al.* studied the electrochemical behaviors of rechargeable Li–O_2 batteries when CO_2—a contaminant gas (10% volume concentration)—participated in the chemical reactions.[199] It was found that besides larger capacity, the overpotential saw an obvious upward trend in subsequent cycles. Based on the isotopic labeling measurement results using $^{18}O_2$ and $C^{18}O_2$, it was deduced that the formation of Li_2CO_3 could be attributed to the chemical reactions between Li_2O_2 and CO_2. No CO_2 was involved in the real electrochemical reduction or oxidation processes. Gradually, the content of CO_2 in the mixed O_2/CO_2 gas was increased to 50% by Kang *et al.*[193] They found that the reactions between O_2^- radical and CO_2 were favorable when using high-dielectric dimethyl sulfoxide (DMSO), while these reactions were suppressed in low-dielectric DME. Consequently, Li–O_2/(50%)CO_2 battery using a DMSO-based electrolyte could last for 20 cycles. However, sulfoxide was vulnerable to nucleophilic attacks from reduced oxygen species. In addition, Li *et al.* fabricated a rechargeable Li–O_2/Li–CO_2 battery (O_2/CO_2 = 1 : 2 in volume) using a TEGDME-based electrolyte, but there was a rapid increase in the overpotential during the discharge/charge cycles.[198] Most researchers agree that CO_2 does not influence the redox reactions in Li–O_2/Li–CO_2 batteries.

In the process of pursuing full CO_2 as the gas resource for Li–gas batteries, A. Archer and co-workers were the first to report a primary high-temperature Li–CO_2 battery with conductive carbon particles as the cathode.[189] By employing an ionic liquid electrolyte, the battery delivered enhanced capacities and discharge voltages as the ambient temperature rose from 25 to 100 °C. Next, Li *et al.* found that Super P-based cathodes could be reversibly discharged and charged in O_2/CO_2 atmospheres, and they even lasted for 7 cycles in pure CO_2 gas with 1 M $LiCF_3SO_3$ as the electrolyte in TEGDME.[198] Inspired by the possible electrochemically catalytic utilization of CO_2 in the case of transition metal carbonates for use as anode materials for LIBs, Zhou *et al.* exploited practical rechargeable Li–CO_2 batteries with moderate electrochemical performances using CNTs or graphene as the air cathodes in TEGDME-based electrolytes at room temperature.[28,200] Starting from this milestone, the research gates for Li–CO_2 batteries have been opened.

3.3 Present flexible Li–CO_2 batteries

At present, research interests in this field mainly focus on developing novel catalysts or redox mediators for Li–CO_2 batteries. Very few works related to flexibility have been reported so far. The dominant challenges for preparing high-performance flexible Li–CO_2 batteries lie in the following aspects:

(i) Conventional carbon nanophase catalysts induce the formation of thermodynamically stable Li_2CO_3, blocking the active catalytic sites and resulting in sluggish kinetics of CO_2 reduction (O═C═O cleavage) and evolution reactions (CO_2 release). The dramatically increased charge overpotential (4.2–4.5 V) leads to the rapid failure of batteries.

(ii) A majority of the present catalysts are in the powder state. They need to be sprayed onto rigid current collectors in order to fabricate air electrodes, which is obviously detrimental toward the fabrication of flexible Li–CO_2 batteries.

(iii) Traditional liquid organic electrolytes are inappropriate for the construction of flexible Li–CO_2 batteries due to the risk of electrolyte leakage and flammable properties. Several attempts have been made to resolve some of the above problems by exploring novel catalysts and (quasi-) solid-state electrolytes.

Similarly, like Li–O_2 batteries, Li–CO_2 batteries also need to operate in pure and dry CO_2 gas, and their electrochemical performance can only be evaluated in fully assembled batteries with organic electrolytes containing solvated Li^+. Therefore, we will introduce several impressive works in the subsequent discussion on gas cathodes that have been categorized according

to different geometrical shapes or functions of their corresponding flexible Li–CO_2 batteries.

3.3.1 Flexible air cathodes for planar batteries. As expected, the origin of flexible Li–CO_2 batteries traditionally focuses on constructing 2D planar flexible configurations, too. Considering that known carbon nanophase powders (*e.g.*, Super P, CNT, and graphene)[28,198,200–202] exhibit relatively limited catalytic activity in the reported rigid Li–CO_2 cells, the study of cathode catalysts for flexible Li–CO_2 batteries has employed transition/rare metals and their derivatives that exhibit higher electrochemical activities.[194,203–213] Further, the preparation methods for 2D flexible cathodes mainly lie in spraying and *in situ* integration. The former involves spraying catalyst powders onto flexible current collectors (*e.g.*, nickel foam, carbon cloth, *etc.*), while the latter involves the direct generation of active catalyst hybrids as a free-standing film *via* hydrothermal growth, electrospinning, *etc.*

For example, Wang *et al.* synthesized N-doped worm-like carbon embedded with MoFeNi and MoC nanocomposites on nickel foam as a binder-free cathode.[216] Because of the high catalytic activity of transition metals, this cathode delivered obviously lower charge potential of around 3.8 V. This Li–CO_2 battery could also run for 90 cycles with relatively stable discharge/charge plateaus. However, the flexibility of the cathode was barely satisfactory, based on our observations in the deformation test. A wood-derived flexible Ru/C-based cathode was reported by Hu *et al.*[217] This cathode not only provided decoupled transportation channels for ions and gas, but could also achieve efficient catalysis by ultrafine Ru nanoparticles decorated on CNT networks. Benefitting from the synergistic effect of the structural and component designs, this cathode exhibited outstanding cycling stability of up to 200 cycles without any obvious catalytic activity decay. As a proof of concept, a flexible Li–CO_2 punch cell was fabricated by employing this wood-derived cathode, which showed decent tolerance to bending deflections like the foldable and rollable states. They also expected that this battery could be applied in space suits for Mars exploration and powering aerospace electronic equipment.

Zhou *et al.* fabricated free-standing Ir/C nanofiber networks by electrospinning and calcination methods.[218] The porous structure together with the high activity of ultrafine Ir nanoparticles endowed the free-standing cathode with excellent CO_2RR and CO_2ER electrochemistry. In particular, it exhibited a high areal discharge capacity of 11.54 mA h cm^{-2} with a flat discharge platform of 2.8 V at 40 μA, as well as excellent cycling performance for more than 120 cycles. Similarly, Guo *et al.* synthesized Ir-based catalysts,[214] where high-density wrinkled Ir nanosheets were fully anchored on the surface of highly porous, N-doped CNFs (denoted as Ir NSs-CNFs). These ultrathin Ir nanosheets exposed sufficient accessible active sites for CO_2RR and CO_2ER (Fig. 18a–d). Li–CO_2 batteries with Ir NSs-CNFs cathode exhibited outstanding long-term cycling stability, namely, it delivered at least 400 deep discharge/charge cycles with a curtailing capacity of 1000 mA h g^{-1} at 500 mA g^{-1} (Fig. 18e), which is the best cycling performance among all the reported Li–CO_2 batteries. The operation time of this battery also could last for a surprising period of 3000 h. In a majority of the common works, the electrolytes were completely volatilized before this period, and the battery was invalidated within the initial dozens of cycles. Li *et al.* prepared conjugated cobalt polyphthalocyanine (CoPPc) powders *via* a facile microwave heating method.[215] Due to its solubility and intrinsic cross-linked elasticity, the as-obtained catalyst powder was reprocessable and could be easily cast on elastic and flexible PET substrates (Fig. 18f–h). Impressively, this cathode achieved excellent cycling behaviors of more than 50 cycles even though the curtailing capacity was set to 1.0 mA h cm^{-2}, which is much larger than that under usual test conditions ($\sim$0.05–0.2 mA h cm^{-2} as per the gravimetric unit). To verify the possibility of practical applications, a large-sized 2D pouch cell assembled by CoPPc-loaded carbon cloth and Li foil was attached to the watchband and utilized for powering the electronic device in a CO_2 atmosphere under different bending states, as shown in Fig. 18i and j.

3.3.2 Flexible air cathodes for fiber-shaped batteries. Owing to different geometrical factors, traditional preparation methods would entail a higher risk of electrolyte leakage in fiber-shaped metal–gas batteries with holes on the encapsulation materials. This might even lead to potential comfort, health, and safety issues. Meanwhile, considering the high aspect ratio of the battery, a much higher requirement is imposed on electrode conductivity. Special design strategies need to be developed for 1D configuration and electrode materials, which can make fiber-shaped devices easier, safer, and more efficient with regard to fabrication and utilization.

Inspired by earlier reported 1D devices, Wang *et al.* reported some progress in the development of fiber-shaped flexible Li–CO_2 batteries, considering their unique structural advantages as described in the section on Li–O_2/air batteries.[219] First, they fabricated a flexible hybrid fiber comprising highly wrinkled surfaces and N-doped CNTs networks anchored on Ti wires as flexible fiber-shaped cathodes (N-CNTs@Ti) exhibiting high performance and high flexibility by means of a modified FCCVD method. When compared with traditional CNT powder-based planar nondeformable cathodes, this specially designed flexible fiber-shaped N-CNTs@Ti cathode not only achieved a significantly enhanced full discharge capacity (9292.3 mA h g^{-1}), but also lowered the voltage polarizations at various current densities. It was considered that the highly wrinkled surfaces and N-6/N-Q dopants induced more efficient sites for catalytic reactions. As a proof of concept, a quasi-solid-state fiber-shaped flexible Li–CO_2 battery was fabricated to power a PDMS/CNTs-based strain sensor that was attached onto a human palm. Next, after optimizing the FCCVD process, bamboo-like N-doped CNT arrays were successfully grown on Ti wires (B-NCNT@Ti) with a larger linear mass loading density (Fig. 19a–e).[220] As expected, this modified B-NCNTs@Ti electrode exhibited outstanding long-term cycling stability of 360 cycles at 1 A g^{-1} (Fig. 19f). Moreover, it was employed to fabricate a trans-structured fiber-shaped flexible Li–CO_2 battery, where N-CNTs@Ti was placed in the center as the cathode and Li foil was wrapped on the outside as the anode and protected by an intact shrinkable tube without any gas diffusion holes. This unique configuration enabled the battery

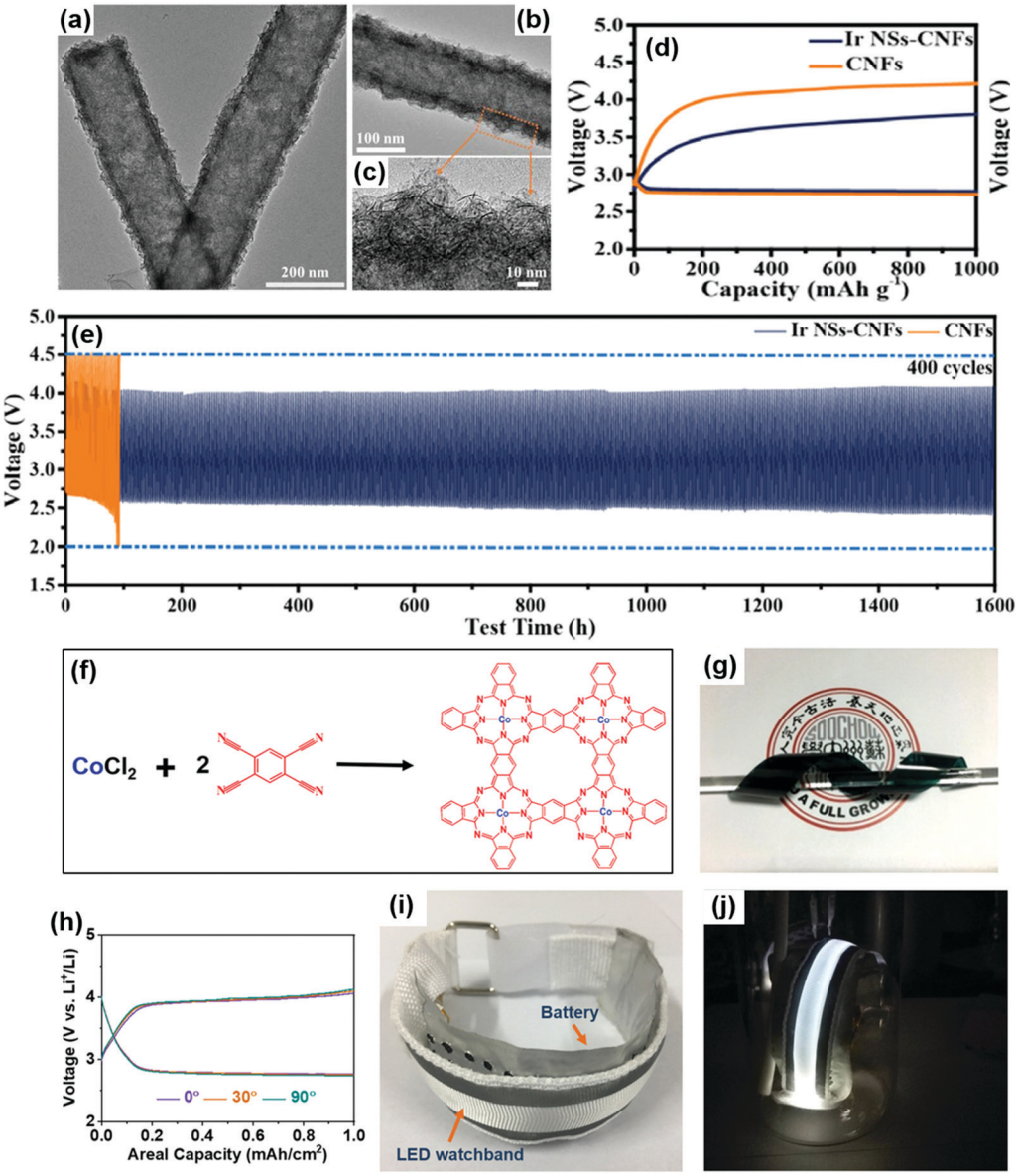

Fig. 18 (a–c) SEM images. (d) First discharge/charge profiles and (e) cycling performance of Li–CO_2 batteries with Ir NSs-CNFs and CNFs as cathodes. Reproduced with permission. Copyright 2018, Wiley-VCH.[214] (f) Preparation and structural characterizations of CoPPc. (g) CoPPc film cast on a twisted PET substrate. (h) Discharge/charge curves under various bending states and (i and j) potential applications of the flexible Li–CO_2 pouch cell. Reproduced with permission. Copyright 2018, Wiley-VCH.[215]

to prevent any negative influence from environmental moisture and electrolyte leakage. To illustrate the potential applications, the battery was incorporated into a fiber-shaped dye-sensitized solar cell using B-NCNT@Ti as the counter electrode to prepare an integrated self-powered energy system, achieving total photochemical-electric energy conversion efficiency of 4.6%. This self-powered system was further used to drive a wearable breath sensor, which sufficiently elucidated its wide adaptability to wearable electronics (Fig. 19g–i).

Subsequently, in order to resolve the issue of low energy efficiency caused by the high charge voltage of the carbon nanophase catalysts, they synthesized ultrafine Mo_2C nanoparticles anchored on CNT cloth hybrid films as free-standing and binder-free cathodes for quasi-solid-state flexible Li–CO_2 batteries with coaxial fiber architecture (Fig. 20a–h).[67] Because of the synergistic effects of the CNT substrate and Mo_2C catalyst, low charge potential of around 3.4 V, high energy efficiency of 80%, and cycling stability of 40 cycles could be achieved. The intermediate discharge product of $Li_2C_2O_4$ stabilized by Mo_2C *via* coordinate electrons transfer was considered to be responsible for the reduction in overpotential. Although the component mass was not purposely controlled, it still afforded a decent energy density of 117 Wh kg^{-1} based on the total weight of the device. Besides the excellent adaptability to irregular geometric surfaces, the fabricated Li–CO_2 battery was also fire-resistant (Fig. 20i–l) owing to the fire resistance of

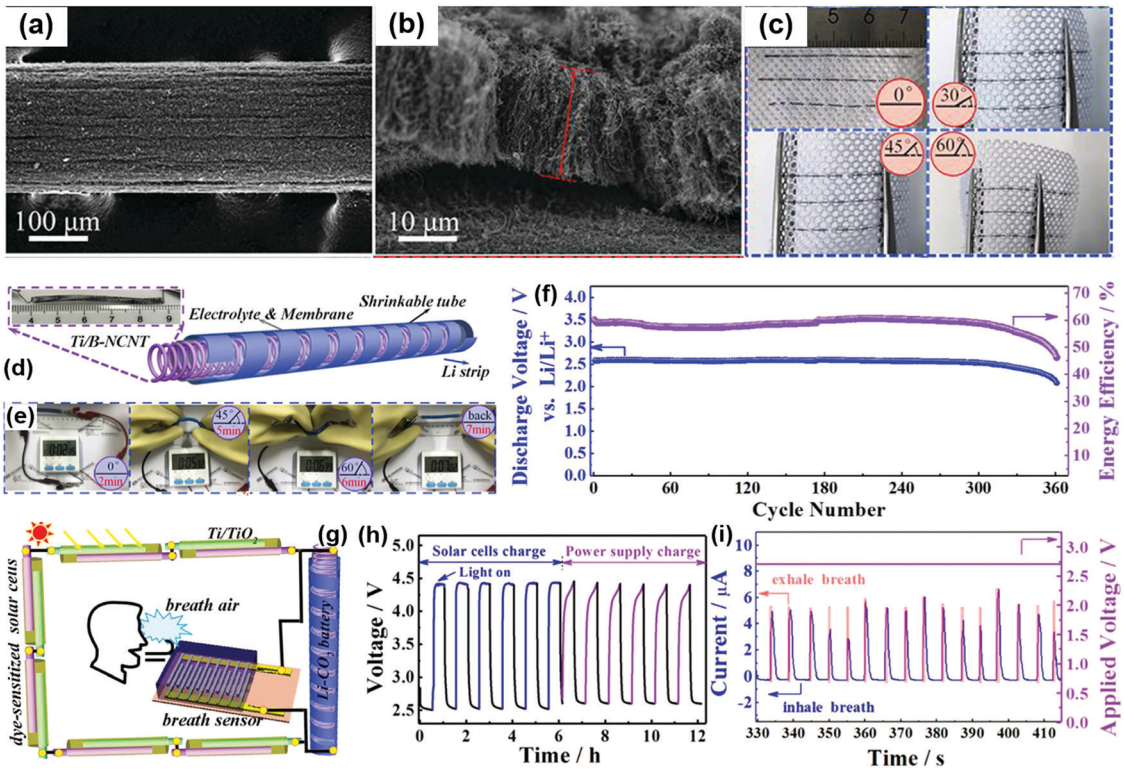

Fig. 19 (a and b) SEM images of B-NCNT grown on a Ti wire. (c) Ti/B-NCNT electrodes woven into a fabric at different bending angles. (d) Schematic diagram of FLCBs. (e) Photographs of a digital timer powered by FLCBs at different bending angles. (f) Cycling performance of FLCBs. (g) Schematic illustration of a self-powered breath monitor consisting of an energy harvester (FDSSCs), energy storage (FLCBs), and response device. Electrochemical responses of (h) self-powered FLCBs photocharged by FDSSCs or galvanostatic power supply and (i) breath monitor. Reproduced with permission. Copyright 2019, Wiley-VCH.[220]

the GPE used. Accordingly, this Li–CO_2 battery was considered to possess several factors of ideal energy accessories for use in wearable electronics.

Apart from Li–CO_2 batteries, other typical alkaline metals have also been explored to fabricate metal–CO_2 batteries, including Na–CO_2,[29,221] K–CO_2,[190] Al–CO_2,[30] and aqueous Zn–CO_2 batteries.[24,44] Some of them have already achieved flexibility, while some of them are still in the primary stage of principle investigation. These explorations on metal–CO_2 batteries are also very attractive for use in aerospace exploration; for example, this may be a possible energy system that can provide electricity on Mars where the atmosphere consists of 96% CO_2 gas. More importantly, the further understanding of the reversible Li–CO_2 reaction mechanism can facilitate to address the predicaments facing present Li–air batteries, where CO_2 in the ambient atmosphere can result in the formation of thermodynamically stable lithium carbonates as discharge products, which can rapidly decrease the cycling performance. Of course, it is believed that by persistent efforts, more advanced flexible metal–CO_2 batteries with improved safety and high performance can be constructed in the near future, yielding energy storage systems for use in portable and wearable electronics to step forward to the next revolution.

3.3.3 GPE development and optimization. To avoid the possible leakage of liquid electrolytes and improving safety, exploiting adaptable GPEs is fairly meaningful for preparing highly safe and comfortable (quasi-) solid-state flexible Li–CO_2 batteries, particularly those which can be employed in wearable electronics. However, studies on GPE began a little later than those on gas cathodes. They are still at a very nascent stage.[222,223] At present, few GPEs for Li–CO_2 batteries have been reported and they usually originate from the inheritance and modification of electrolytes or membranes for Li–air batteries, solar cells, and fuel cells.[66,224,225]

Typically, Li *et al.* synthesized a novel kind of GPE, which was composed of a PVDF matrix filled with a TEGDME-based liquid electrolyte for use in Li–CO_2 batteries.[225] When compared with individual LiTFSI/TEGDME liquid electrolytes, the battery cells with GPE demonstrated enhanced discharge capacity, better rate performance, and improved cycling stability (up to 60 cycles). The discharge products of GPE-based Li–CO_2 showed an amorphous film-like morphology, which was fairly different from the nanoparticles-like morphology of the battery using liquid electrolytes. Importantly, the synthesized GPE also demonstrated certain flexibility, laying the foundation for the construction of flexible solid-state Li–CO_2 batteries. Wang *et al.* added binuclear cobalt phthalocyanine (Bi-CoPc) into the above GPE as a redox mediator to boost the decomposition of the discharge products at lower charge overpotential.[224] Expectedly, the discharge and charge voltage difference for the cells with

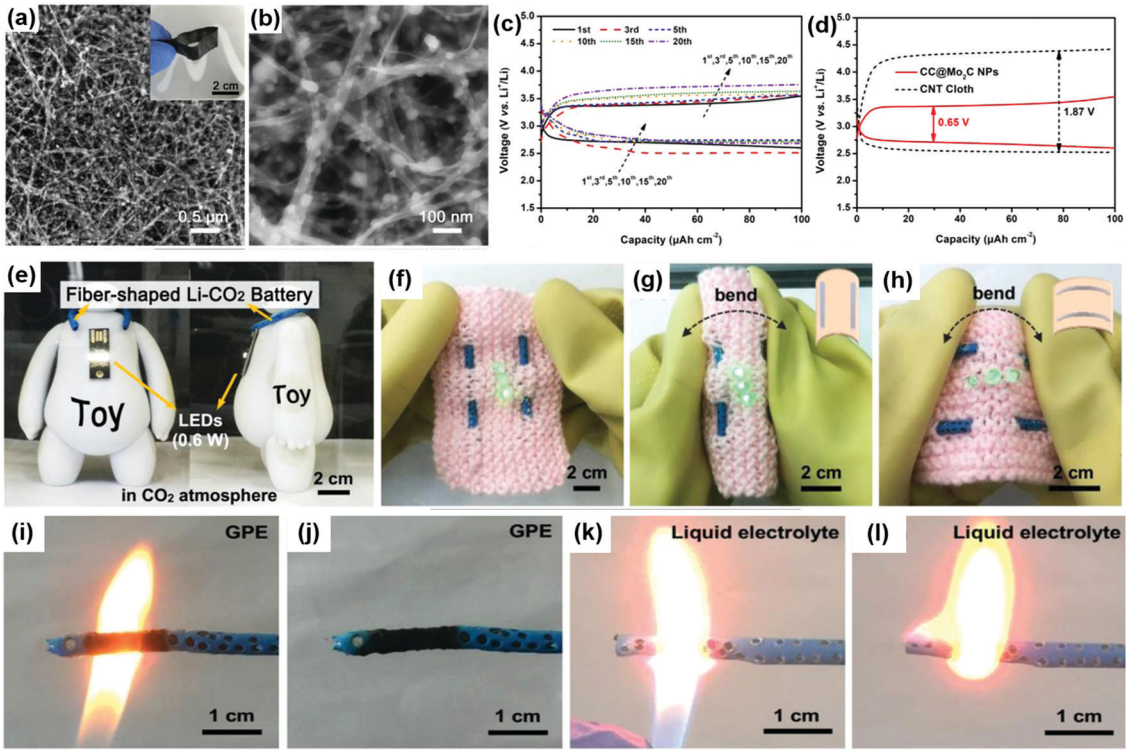

Fig. 20 (a and b) SEM images and (c and d) electrochemical performances of CC@Mo_2C NPs film. (e–h) Flexibility and potential applications of this quasi-solid-state fiber-shaped Li–CO_2 battery using CC@Mo_2C NPs cathode. (i–l) Comparison of the fire resistance of Li–CO_2 batteries with GPE and traditional liquid electrolytes. Reproduced with permission. Copyright 2018, Wiley-VCH.[67]

Bi-CoPc-based GPE was reduced to 1.14 V, which was distinctly lower than 1.90 V of the cells with pristine GPE. Moreover, the cycling life was also extended to 120 cycles and the flexibility was effectively maintained. Chen *et al.* created a new family of composite polymer electrolytes (CPEs) that consisted of PMA/PEG–$LiClO_4$–3 wt% SiO_2 ceramic fillers for use in Li–CO_2 batteries.[66] The CPE had high ionic conductivity of 7.14×10^{-2} mS cm^{-1} at 55 °C. Multiwalled CNTs were coated on a thin CPE to constitute an incorporated CPE@CNTs cathode. More importantly, a lightweight, flexible, all-solid-state planar Li–CO_2 battery was fabricated using the CPE@CNTs-integrated cathode, nickel foam (air diffusion layer), and lithium foil anode. It could be reversibly discharged and charged for 100 cycles with a curtailing capacity of 1000 mA h g^{-1} at 55 °C. Furthermore, the flexible liquid-free pouch-type battery demonstrated a lab-scale high full discharge capacity of 993 mA h corresponding to the high energy density of 521 W h kg^{-1} based on the total weight of the battery. This study provided details of the fundamental and technological progresses made in flexible Li–CO_2 batteries having practical-scale energy density and satisfactory flexibility.

4. Novel flexible metal–gas battery candidates

Besides metal–O_2/air and metal–CO_2 batteries, there are still a few innovative investigations on possible metal–gas batteries, such as Li–N_2,[31,226] Li–O_2/H_2O,[227] Li–O_2/HCl,[228] and Li–SO_2[32] batteries. All of them employed a nonaqueous electrolyte. For convenient reading, the general reaction mechanisms coupled with the theoretical electrochemical indexes corresponding to every novel metal–gas battery are summarized in Table 5.

Herein, we will provide a brief introduction for these cutting-edge metal–gas batteries that might become the potential candidates for use in advanced flexible metal–gas for commercialization. Zhang *et al.* proposed a new concept of reversible nitrogen fixation based on a rechargeable Li–N_2 battery.[226] By employing common carbon cloth as the cathode and $LiCF_3SO_3$/TEGDME as the electrolyte, a Li–N_2 cell prototype realized reversible N_2/Li_3N electrochemistry for 40 cycles. The faradaic efficiency toward N_2 fixation for this Li–N_2 battery was 59%, without any extra energy support from the external environment. Since carbon cloth was chosen as the cathode, the first challenge to construct flexible Li–N_2 batteries (namely, flexible electrodes) has already been conquered. Hybrid and aqueous Li–air batteries have also been primarily studied. Andrei *et al.* reported a Li–O_2/H_2O hybrid energy system, where an organic electrolyte was used at the anode and aqueous electrolyte at the cathode.[227] The energy density coupled with specific capacity was positively affected by the increased solubility and diffusion rate of O_2 in the cathode. The power density of the system was relatively low due to the limited O_2 diffusion and large interfacial resistance. However, it is noteworthy that such hybrid Li–O_2/H_2O battery possesses an ultrahigh energy

Table 5 Theoretical voltage, capacity, energy density, and chemical reaction mechanism of other categories of metal–gas batteries known to date

Battery type	Chemical reaction mechanism (electrons transfer number)	Theoretical voltage (V)	Theoretical capacity (mA h g^{-1})	Theoretical energy density (W h kg^{-1})	Progress on flexibility
Li–N_2[226]	$6Li + N_2 \rightleftharpoons 2Li_3N$ ($6e^-$)	0.54	2311	1248	Flexible cathode
Li–O_2/H_2O[227]	$4Li + O_2 + 2H_2O \rightleftharpoons 4LiOH$ ($4e^-$)	3.4	1119	3804	Catalyst powder
Li–O_2/HCl[228]	$4Li + O_2 + 4HCl \rightleftharpoons 4LiOH + 2H_2O$ ($4e^-$)	4.3	521.4	2242	Catalyst powder
Li–SO_2[32]	$2Li + 2SO_2 \rightleftharpoons Li_2S_2O_4$ ($2e^-$)	3.1	377	1170	Catalyst powder

density of 3804 W h kg^{-1} as well as a stable working voltage of 3.4 V. Similarly, the electrochemistry of a hybrid Li–O_2/HCl battery has also been investigated.[228] Based on the reaction $4Li + O_2 + 4HCl \rightleftharpoons 4LiCl + 2H_2O$, this hybrid energy system demonstrated the highest discharge voltage of 4.3 V among all the reported metal–gas batteries, thereby resulting in a high energy density of 2242 W h kg^{-1}. It should be admitted that the detailed principles of the above hybrid Li–O_2 batteries are still not very clear. Moreover, a novel rechargeable system based on Li–SO_2 batteries was demonstrated by Kang and co-workers for the first time.[32] This Li–SO_2 battery could store and release electricity by the reversible formation and decomposition, respectively, of the discharge product $Li_2S_2O_4$. The rechargeable Li–SO_2 battery demonstrated a moderate discharge capacity of 5400 mA h g^{-1} at around 3.1 V; this performance is marginally better than that of a Li–O_2 battery. Importantly, with the assistance of redox mediators, Li–SO_2 batteries could only show small discharge/charge voltage polarization of less than 0.3 V, which is one of the highest energy efficiencies recorded by Li–gas batteries.

5. Summary and prospective

Metal–gas batteries, which employ gases as the energy resources to generate electricity, have practical significance in functioning as next-generation high-performance energy storage systems for portable and wearable electronics, considering their ultrahigh theoretical energy density and convenient gas-harvesting capability from the ambient environment. Recent progresses in flexible metal–gas batteries have been summarized in this review. Encouragingly, flexible and rechargeable ZABs, Li–O_2/air batteries, Li–CO_2 batteries, and so on can be generally fabricated for use at ambient temperatures. However, there are still tremendous obstacles that hinder the progress of flexible metal–gas batteries into commercial applications. These difficulties mainly lie in the sluggish electrochemical reactions at the air cathode, low ionic conductivity, instability, risk of electrolyte leakage, metal anodic corrosion, and dendrite growth, which result in limited discharge capacity, weak rate capability, and poor cycling stability of these batteries. To conquer these challenges, numerous efforts have been devoted toward the aspects of cathode catalyst, electrolyte, and metal anode, as discussed in this article. It needs to be admitted that although these efforts have had a certain positive impact, there are still considerable scientific and technological difficulties that need to be overcome. To look for newer opportunities and technologies to break through the bottleneck dilemmas of current flexible metal–gas batteries, subsequent research directions may deserve more academic attention from the perspective of practical applications:

(i) Perform additional *in situ* characterizations and theoretical computations to better understand the detailed reaction mechanisms of metal–gas batteries. Different from electrocatalysis, the roles played by metal ions in the gas/solid redox reactions are still unclear, especially for metal–CO_2 or metal–N_2 batteries.

(ii) Develop newer types of quasi- or solid-state electrolytes with high ionic conductivity, low volatility, stable chemical stability, and fire-resistant property. The desirable electrolyte for use in flexible metal–gas batteries should firstly prevent electrolyte leakage and any potential health and safety problems and then pursue the ideal ionic conductivity and ion migration number approaching those of liquid electrolytes. In addition, easy encapsulation is another necessary factor that deserves important consideration for use of GPEs in engineering production.

(iii) Fabrication technologies of flexible cathodes need more investigations, focusing on exploiting novel, cost-effective, eco-friendly, and efficient free-standing catalysts at an acceptable level of practical energy storage. The cycling stability of cathodes under half or even full discharge/charge states (instead of 500 or 1000 mA h g^{-1} as the curtailing capacity) is urgent to overcome. This is the main bottleneck to enable flexible metal–gas batteries to become practicable and rechargeable next-generation energy storage devices with much higher energy density. Moreover, how to maintain good balance between mechanical strength and structural voids in the cathodes also deserves considerable attention. This determines whether the assembled flexible batteries can maintain their electrochemical performance and flexibility during long-term deformation.

(iv) Considering that currently available metal–gas batteries are commonly operated in a pure gas atmosphere (especially Li–O_2 batteries), developing multifunctional catalysts and finding effective battery management systems to allow metal–gas batteries to work in mixed-gas atmospheres containing O_2, CO_2, N_2, *etc.* are fairly meaningful to promote metal–gas batteries toward forming "real" metal–air batteries that can directly harvest gas resources conveniently from the ambient atmosphere.

(v) Devote more efforts into the exploitation of flexible metal anodes. The use of flexible metal anodes can be avoided in other flexible energy storage systems such as supercapacitors and secondary-metal-ion batteries, but they are an indispensable part of metal–gas batteries. Fewer concerns have been focused on anodes at current lab-scale devices. However, dendritic or "dead" crystals that cause performance decay cannot be ignored,

particularly when the curtailing capacity or working time is increased in practical products for the consumer market. In addition, durable deformability, gas corrosion protection, and utilization efficiency are also noteworthy for future designs.

(vi) Simplify and standardize the assembly processes together with test procedures of flexible metal–gas batteries. Configurations coupled with encapsulation problems are both noteworthy in engineering approaches. Meanwhile, suitable measurement criteria involving electrochemical performance, flexibility, mechanical strength, and other comfort-/safety-related features should be formulated as soon as possible. In particular, it is more appropriate to evaluate the electrochemical performance of flexible cathodes in the assembled flexible devices instead of that in coin-type cells.

(vii) Explore other advanced metal–gas batteries. Employing earth-abundant, air-stable, and highly safe metals, such as Mg, Al, Zn, and so on, to fabricate metal–CO_2/metal–N_2 batteries is also very interesting due to their hopeful prospective of energy utilization and environmental conservation.

It is believed that after a general understanding and addressing the inherent scientific issues existing in present flexible metal–gas batteries, more practical and appropriate flexible devices can be constructed, which, in turn, can promote the integral development of flexible metal–gas batteries to become a cost-effective, safe, environmentally friendly, and advanced energy storage system for portable and wearable consumer electronics in the future.

Conflicts of interest

There are no conflicts to declare.

Acknowledgements

The authors acknowledge the financial support from the National Natural Science Foundation of China (Grant No. 21875226), the Science Foundation for Distinguished Young Scholars of Sichuan Province (Grant No. 2017JQ0036 and 2016JQ0025), the Chengdu Rongpiao Talent Plan, the ''QianYingBaiTuan'' Plan of China Science City, the Tianfu Wanren Plan, and the ''Global Experts'' program. The work at Argonne National Laboratory was supported from the U.S. Department of Energy (DOE), Office of Energy Efficiency and Renewable Energy, Vehicle Technologies Office. Argonne National Laboratory is operated for DOE Office of Science by UChicago Argonne, LLC, under Contract number DE-AC02-06CH11357.

Notes and references

1 M. Li, J. Lu, Z. Chen and K. Amine, *Adv. Mater.*, 2018, **30**, 1800561.
2 B. Kang and G. Ceder, *Nature*, 2009, **458**, 190.
3 Y. Xue, Q. Zhang, W. Wang, H. Cao, Q. Yang and L. Fu, *Adv. Energy Mater.*, 2017, **7**, 1602684.
4 Z. Wang, J. Cheng, Q. Guan, H. Huang, Y. Li, J. Zhou, W. Ni, B. Wang, S. He and H. Peng, *Nano Energy*, 2018, **45**, 210.
5 A. Mauger, H. Xie and C. M. Julien, *AIMS Mater. Sci.*, 2016, **3**, 1054.
6 Y. Lu, L. Yu and X. W. Lou, *Chem*, 2018, **4**, 972.
7 F. Cheng, J. Liang, Z. Tao and J. Chen, *Adv. Mater.*, 2011, **23**, 1695.
8 G. Zubi, R. Dufo-López, M. Carvalho and G. Pasaoglu, *Renewable Sustainable Energy Rev.*, 2018, **89**, 292.
9 L. Zhou, K. Zhang, Z. Hu, Z. Tao, L. Mai, Y.-M. Kang, S.-L. Chou and J. Chen, *Adv. Energy Mater.*, 2018, **8**, 1701415.
10 X. Li, X. Li, J. Cheng, D. Yuan, W. Ni, Q. Guan, L. Gao and B. Wang, *Nano Energy*, 2016, **21**, 228.
11 J. Zhou, J. Qin, N. Zhao, C. Shi, E.-Z. Liu, F. He, J. Li and C. He, *J. Mater. Chem. A*, 2016, **4**, 8734.
12 C. Yang and S.-J. Lin, *J. Power Sources*, 2002, **112**, 497.
13 C. He, S. Wu, N. Zhao, C. Shi, E. Liu and J. Li, *ACS Nano*, 2013, **7**, 4459.
14 J. Qin, C. He, N. Zhao, Z. Wang, C. Shi, E. Z. Liu and J. Li, *ACS Nano*, 2014, **8**, 1728.
15 G. Qu, J. Cheng, X. Li, D. Yuan, P. Chen, X. Chen, B. Wang and H. Peng, *Adv. Mater.*, 2016, **28**, 3646.
16 J. Lu, Z. Chen, Z. Ma, F. Pan, L. A. Curtiss and K. Amine, *Adv. Nat. Sci.: Nanosci. Nanotechnol.*, 2016, **11**, 1031.
17 Y. Li and J. Lu, *ACS Energy Lett.*, 2017, **2**, 1370.
18 Q. Liu, Z. Chang, Z. Li and X. Zhang, *Small Methods*, 2018, **2**, 1700231.
19 X. Xiao, H. Song, S. Lin, Y. Zhou, X. Zhan, Z. Hu, Q. Zhang, J. Sun, B. Yang, T. Li, L. Jiao, J. Zhou, J. Tang and Y. Gogotsi, *Nat. Commun.*, 2016, **7**, 11296.
20 C. Zhao, Y. Jin, W. Du, C. Ji and X. Du, *J. Electroanal. Chem.*, 2018, **826**, 217.
21 Y. Ma, A. Sumboja, W. Zang, S. Yin, S. Wang, S. J. Pennycook, Z. Kou, Z. Liu, X. Li and J. Wang, *ACS Appl. Mater. Interfaces*, 2019, **11**, 1988.
22 M. Yu, Z. Wang, C. Hou, Z. Wang, C. Liang, C. Zhao, Y. Tong, X. Lu and S. Yang, *Adv. Mater.*, 2017, **29**, 1602868.
23 R. D. McKerracher, Carlos Ponce de Leon, R. G. A. Wills, A. A. Shah and F. C. Walsh, *ChemPlusChem*, 2015, **80**, 323.
24 J. Xie, X. Wang, J. Lv, Y. Huang, M. Wu, Y. Wang and J. Yao, *Angew. Chem., Int. Ed.*, 2018, **57**, 16996.
25 B. J. Bergner, A. Schurmann, K. Peppler, A. Garsuch and J. Janek, *J. Am. Chem. Soc.*, 2014, **136**, 15054.
26 B. Sun, K. Kretschmer, X. Xie, P. Munroe, Z. Peng and G. Wang, *Adv. Mater.*, 2017, **29**, 1606816.
27 N. Xiao, G. Gourdin and Y. Wu, *Angew. Chem., Int. Ed.*, 2018, **57**, 10864.
28 X. Zhang, Q. Zhang, Z. Zhang, Y. Chen, Z. Xie, J. Wei and Z. Zhou, *Chem. Commun.*, 2015, **51**, 14636.
29 X. Hu, Z. Li, Y. Zhao, J. Sun, Q. Zhao, J. Wang, Z. Tao and J. Chen, *Sci. Adv.*, 2017, **3**, 1602396.
30 W. Ma, X. Liu, C. Li, H. Yin, W. Xi, R. Liu, G. He, X. Zhao, J. Luo and Y. Ding, *Adv. Mater.*, 2018, **30**, 1801152.
31 X.-G. Wang, Q. Zhang, X. Zhang, C. Wang, Z. Xie and Z. Zhou, *Small Methods*, 2019, **3**, 1800334.

32 H. D. Lim, H. Park, H. Kim, J. Kim, B. Lee, Y. Bae, H. Gwon and K. Kang, *Angew. Chem., Int. Ed.*, 2015, **54**, 9663.
33 J. Lu, L. Li, J. B. Park, Y. K. Sun, F. Wu and K. Amine, *Chem. Rev.*, 2014, **114**, 5611.
34 P. Tan, B. Chen, H. Xu, H. Zhang, W. Cai, M. Ni, M. Liu and Z. Shao, *Energy Environ. Sci.*, 2017, **10**, 2056.
35 A. Manthiram and L. Li, *Adv. Energy Mater.*, 2015, **5**, 1401302.
36 N. Imanishi and O. Yamamoto, *Mater. Today*, 2014, **17**, 24.
37 Z. Xie, X. Zhang, Z. Zhang and Z. Zhou, *Adv. Mater.*, 2017, **29**, 1605891.
38 H. Sun, Y. Zhang, J. Zhang, X. Sun and H. Peng, *Nat. Rev. Mater.*, 2017, **2**, 17023.
39 X. Wang, G. Sun, P. Routh, D.-H. Kim, W. Huang and P. Chen, *Chem. Soc. Rev.*, 2014, **43**, 7067.
40 L. Ma, S. Chen, Z. Pei, H. Li, Z. Wang, Z. Liu, Z. Tang, J. A. Zapien and C. Zhi, *ACS Nano*, 2018, **12**, 8597.
41 Y. Zhang, Y. Zhao, J. Ren, W. Weng and H. Peng, *Adv. Mater.*, 2016, **28**, 4524.
42 W. Weng, P. Chen, S. He, X. Sun and H. Peng, *Angew. Chem., Int. Ed.*, 2016, **55**, 6140.
43 S. Pan, J. Ren, X. Fang and H. Peng, *Adv. Energy Mater.*, 2016, **6**, 1501867.
44 X. Wang, J. Xie, M. A. Ghausi, J. Lv, Y. Huang, M. Wu, Y. Wang and J. Yao, *Adv. Mater.*, 2019, **31**, 1807807.
45 Y. Zhao, Y. Zhang, H. Sun, X. Dong, J. Cao, L. Wang, Y. Xu, J. Ren, Y. Hwang, I. H. Son, X. Huang, Y. Wang and H. Peng, *Angew. Chem., Int. Ed.*, 2016, **55**, 14384.
46 Y. H. Zhu, S. Yuan, D. Bao, Y. B. Yin, H. X. Zhong, X. B. Zhang, J. M. Yan and Q. Jiang, *Adv. Mater.*, 2017, **29**, 1603719.
47 J. Ni, S. Fu, Y. Yuan, L. Ma, Y. Jiang, L. Li and J. Lu, *Adv. Mater.*, 2018, **30**, 1704337.
48 J. Ren, Y. Zhang, W. Bai, X. Chen, Z. Zhang, X. Fang, W. Weng, Y. Wang and H. Peng, *Angew. Chem., Int. Ed.*, 2014, **53**, 7864.
49 Y. Jing and Z. Zhou, *ACS Catal.*, 2015, **5**, 4309.
50 J. Pan, H. Li, H. Sun, Y. Zhang, L. Wang, M. Liao, X. Sun and H. Peng, *Small*, 2018, **14**, 1703454.
51 X. Cheng, J. Pan, Y. Zhao, M. Liao and H. Peng, *Adv. Energy Mater.*, 2018, **8**, 1702184.
52 D. Kundu, R. Black, B. Adams, K. Harrison, K. Zavadil and L. F. Nazar, *J. Phys. Chem. Lett.*, 2015, **6**, 2252.
53 C. Shu, J. Long, S. X. Dou and J. Wang, *Small*, 2019, **15**, 1804701.
54 M. J. Tan, B. Li, P. Chee, X. Ge, Z. Liu, Y. Zong and X. J. Loh, *J. Power Sources*, 2018, **400**, 566.
55 T. Liu, J. J. Xu, Q. C. Liu, Z. W. Chang, Y. B. Yin, X. Y. Yang and X. B. Zhang, *Small*, 2017, **13**, 1602952.
56 J. Fu, Z. P. Cano, M. G. Park, A. Yu, M. Fowler and Z. Chen, *Adv. Mater.*, 2017, **29**, 1604685.
57 L. Wang, X. Fu, J. He, X. Shi, T. Chen, P. Chen, B. Wang and H. Peng, *Adv. Mater.*, 2019, **31**, 1901971.
58 X. Xu, S. Xie, Y. Zhang and H. Peng, *Angew. Chem., Int. Ed.*, 2019, **58**, 1902425.
59 J. Park, M. Park, G. Nam, J. S. Lee and J. Cho, *Adv. Mater.*, 2015, **27**, 1396.
60 Q. C. Liu, J. J. Xu, D. Xu and X. B. Zhang, *Nat. Commun.*, 2015, **6**, 7892.
61 Q. C. Liu, L. Li, J. J. Xu, Z. W. Chang, D. Xu, Y. B. Yin, X. Y. Yang, T. Liu, Y. S. Jiang, J. M. Yan and X. B. Zhang, *Adv. Mater.*, 2015, **27**, 8095.
62 Y. Zhang, L. Wang, Z. Guo, Y. Xu, Y. Wang and H. Peng, *Angew. Chem., Int. Ed.*, 2016, **55**, 4487.
63 Y. Xu, Y. Zhao, J. Ren, Y. Zhang and H. Peng, *Angew. Chem., Int. Ed.*, 2016, **55**, 7979.
64 L. Wang, Y. Zhang, J. Pan and H. Peng, *J. Mater. Chem. A*, 2016, **4**, 13419.
65 Y. Zhang, Y. Jiao, L. Lu, L. Wang, T. Chen and H. Peng, *Angew. Chem., Int. Ed.*, 2017, **56**, 13741.
66 X. Hu, Z. Li and J. Chen, *Angew. Chem., Int. Ed.*, 2017, **56**, 5785.
67 J. Zhou, X. Li, C. Yang, Y. Li, K. Guo, J. Cheng, D. Yuan, C. Song, J. Lu and B. Wang, *Adv. Mater.*, 2018, **30**, 1804439.
68 M. Hilder, B. Winther-Jensen and N. B. Clark, *J. Power Sources*, 2009, **194**, 1135.
69 Z. Pan, J. Yang, W. Zang, Z. Kou, C. Wang, X. Ding, C. Guan, T. Xiong, H. Chen, Q. Zhang, Y. Zhong, M. Liu, L. Xing, Y. Qiu, W. Li, C. Yan, Y. Zhang and J. Wang, *Energy Storage Mater.*, 2019, **23**, 375.
70 S. Qu, Z. Song, J. Liu, Y. Li, Y. Kou, C. Ma, X. Han, Y. Deng, N. Zhao, W. Hu and C. Zhong, *Nano Energy*, 2017, **39**, 101.
71 X. Bi, R. Wang, K. Amine and J. Lu, *Small Methods*, 2018, **3**, 1800247.
72 P. Gu, M. Zheng, Q. Zhao, X. Xiao, H. Xue and H. Pang, *J. Mater. Chem. A*, 2017, **5**, 7651.
73 J. Fu, R. Liang, G. Liu, A. Yu, Z. Bai, L. Yang and Z. Chen, *Adv. Mater.*, 2019, **31**, 1805230.
74 J. Pan, Y. Y. Xu, H. Yang, Z. Dong, H. Liu and B. Y. Xia, *Adv. Sci.*, 2018, **5**, 1700691.
75 L. Grande, E. Paillard, J. Hassoun, J. B. Park, Y. J. Lee, Y. K. Sun, S. Passerini and B. Scrosati, *Adv. Mater.*, 2015, **27**, 784.
76 A. C. Luntz and B. D. McCloskey, *Chem. Rev.*, 2014, **114**, 11721.
77 X. Ren and Y. Wu, *J. Am. Chem. Soc.*, 2013, **135**, 2923.
78 Z. Ma, X. Yuan, L. Li, Z.-F. Ma, D. P. Wilkinson, L. Zhang and J. Zhang, *Energy Environ. Sci.*, 2015, **8**, 2144.
79 Z. Guo, D. Zhou, X. Dong, Z. Qiu, Y. Wang and Y. Xia, *Adv. Mater.*, 2013, **25**, 5668.
80 J. Lu, Y. Lei, K. C. Lau, X. Luo, P. Du, J. Wen, R. S. Assary, U. Das, D. J. Miller, J. W. Elam, H. M. Albishri, D. A. El-Hady, Y. K. Sun, L. A. Curtiss and K. Amine, *Nat. Commun.*, 2013, **4**, 2383.
81 Z. Geng, Y. Liu, X. Kong, P. Li, K. Li, Z. Liu, J. Du, M. Shu, R. Si and J. Zeng, *Adv. Mater.*, 2018, **30**, 1803498.
82 L. Zhang, X. Ren, Y. Luo, X. Shi, A. M. Asiri, T. Li and X. Sun, *Chem. Commun.*, 2018, **54**, 12966.
83 S. Zaromb, *J. Electroanal. Chem.*, 1962, **109**, 1125.
84 J. Ma, C. Qin, Y. Li, F. Ren, Y. Liu and G. Wang, *Mater. Res. Express*, 2019, **6**, 085528.
85 K. M. Abraham and Z. Jiang, *J. Electroanal. Chem.*, 1996, **143**, 1.

86 Q. Xu, H. Jiang, Y. Li, D. Liang, Y. Hu and C. Li, *Appl. Catal., B*, 2019, **256**, 117893.
87 L. Ma, S. Chen, Z. Pei, Y. Huang, G. Liang, F. Mo, Q. Yang, J. Su, Y. Gao, J. A. Zapien and C. Zhi, *ACS Nano*, 2018, **12**, 1949.
88 Q. Wang, Y. Ji, Y. Lei, Y. Wang, Y. Wang, Y. Li and S. Wang, *ACS Energy Lett.*, 2018, **3**, 1183.
89 S. Liu, Z. Wang, S. Zhou, F. Yu, M. Yu, C. Y. Chiang, W. Zhou, J. Zhao and J. Qiu, *Adv. Mater.*, 2017, **29**, 1700874.
90 S. Li, C. Cheng, X. Zhao, J. Schmidt and A. Thomas, *Angew. Chem., Int. Ed.*, 2018, **57**, 1856.
91 C. Li, M. Wu and R. Liu, *Appl. Catal., B*, 2019, **244**, 150.
92 Z. Zhao, X. Fan, J. Ding, W. Hu, C. Zhong and J. Lu, *ACS Energy Lett.*, 2019, **4**, 2259.
93 Y. Li, C. Zhong, J. Liu, X. Zeng, S. Qu, X. Han, Y. Deng, W. Hu and J. Lu, *Adv. Mater.*, 2018, **30**, 1703657.
94 F. Meng, H. Zhong, D. Bao, J. Yan and X. Zhang, *J. Am. Chem. Soc.*, 2016, **138**, 10226.
95 Z. Yang, J. Ren, Z. Zhang, X. Chen, G. Guan, L. Qiu, Y. Zhang and H. Peng, *Chem. Rev.*, 2015, **115**, 5159.
96 S. Pan, H. Lin, J. Deng, P. Chen, X. Chen, Z. Yang and H. Peng, *Adv. Energy Mater.*, 2015, **5**, 1401438.
97 J. Fu, F. M. Hassan, C. Zhong, J. Lu, H. Liu, A. Yu and Z. Chen, *Adv. Mater.*, 2017, **29**, 1702526.
98 T. Zhou, W. Xu, N. Zhang, Z. Du, C. Zhong, W. Yan, H. Ju, W. Chu, H. Jiang, C. Wu and Y. Xie, *Adv. Mater.*, 2019, **31**, 1807468.
99 K. Kordek, L. Jiang, K. Fan, Z. Zhu, L. Xu, M. Al-Mamun, Y. Dou, S. Chen, P. Liu, H. Yin, P. Rutkowski and H. Zhao, *Adv. Energy Mater.*, 2019, **9**, 1802936.
100 L. Ma, S. Chen, D. Wang, Q. Yang, F. Mo, G. Liang, N. Li, H. Zhang, J. A. Zapien and C. Zhi, *Adv. Energy Mater.*, 2019, **9**, 1803046.
101 Y. Qiao, P. Yuan, Y. Hu, J. Zhang, S. Mu, J. Zhou, H. Li, H. Xia, J. He and Q. Xu, *Adv. Mater.*, 2018, **30**, 1804504.
102 X. Han, W. Zhang, X. Ma, C. Zhong, N. Zhao, W. Hu and Y. Deng, *Adv. Mater.*, 2019, **31**, 1808281.
103 Y. Xu, Y. Zhang, Z. Guo, J. Ren, Y. Wang and H. Peng, *Angew. Chem., Int. Ed.*, 2015, **54**, 15390.
104 Z. Pan, H. Chen, J. Yang, Y. Ma, Q. Zhang, Z. Kou, X. Ding, Y. Pang, L. Zhang, Q. Gu, C. Yan and J. Wang, *Adv. Sci.*, 2019, **6**, 1900628.
105 L. Zhu, D. Zheng, Z. Wang, X. Zheng, P. Fang, J. Zhu, M. Yu, Y. Tong and X. Lu, *Adv. Mater.*, 2018, **30**, 1805268.
106 P. Yu, L. Wang, F. Sun, Y. Xie, X. Liu, J. Ma, X. Wang, C. Tian, J. Li and H. Fu, *Adv. Mater.*, 2019, **31**, 1901666.
107 C. Su, H. Cheng, W. Li, Z. Liu, N. Li, Z. Hou, F. Bai, H. Zhang and T. Ma, *Adv. Energy Mater.*, 2017, **7**, 1602420.
108 S. Zeng, X. Tong, S. Zhou, B. Lv, J. Qiao, Y. Song, M. Chen, J. Di and Q. Li, *Small*, 2018, **14**, 1803409.
109 Y. Xu, P. Deng, G. Chen, J. Chen, Y. Yan, K. Qi, H. Liu and B. Y. Xia, *Adv. Funct. Mater.*, 2019, **29**, 1906081.
110 Y. Lian, W. Yang, C. Zhang, H. Sun, Z. Deng, W. Xu, L. Song, Z. Ouyang, Z. Wang, J. Guo and Y. Peng, *Angew. Chem., Int. Ed.*, 2019, **58**, 1.
111 W. Wang, M. Tang, Z. Zheng and S. Chen, *Adv. Energy Mater.*, 2019, **9**, 1803628.
112 W. Zang, A. Sumboja, Y. Ma, H. Zhang, Y. Wu, S. Wu, H. Wu, Z. Liu, C. Guan, J. Wang and S. J. Pennycook, *ACS Catal.*, 2018, **8**, 8961.
113 Y. Jiang, Y. P. Deng, R. Liang, J. Fu, D. Luo, G. Liu, J. Li, Z. Zhang, Y. Hu and Z. Chen, *Adv. Energy Mater.*, 2019, **9**, 1900911.
114 T. V. Tam, S. G. Kang, M. H. Kim, S. G. Lee, S. H. Hur, J. S. Chung and W. M. Choi, *Adv. Energy Mater.*, 2019, **9**, 1900945.
115 W. Liu, B. Ren, W. Zhang, M. Zhang, G. Li, M. Xiao, J. Zhu, A. Yu, L. Ricardez-Sandoval and Z. Chen, *Small*, 2019, **15**, 1903610.
116 Y. Zhong, Z. Pan, X. Wang, J. Yang, Y. Qiu, S. Xu, Y. Lu, Q. Huang and W. Li, *Adv. Sci.*, 2019, **6**, 1802243.
117 Q. Jin, B. Ren, J. Chen, H. Cui and C. Wang, *Appl. Catal., B*, 2019, **256**, 117887.
118 H. Qiu, X. Du, J. Zhao, Y. Wang, J. Ju, Z. Chen, Z. Hu, D. Yan, X. Zhou and G. Cui, *Nat. Commun.*, 2019, **10**, 5374.
119 J. Zheng, Q. Zhao, T. Tang, J. Yin, C. Quilty, G. Renderos, X. Liu, Y. Deng, L. Wang, D. Bock, C. Jaye, D. Zhang, E. Takeuchi, K. Takeuchi, A. Marschilok and L. Archer, *Science*, 2019, **366**, 645.
120 X. Zhang, X. Chen, L. Hou, B. Li, X. Cheng, J. Huang and Q. Zhang, *ACS Energy Lett.*, 2019, **4**, 411.
121 L. Kang, M. Cui, F. Jiang, Y. Gao, H. Luo, J. Liu, W. Liang and C. Zhi, *Adv. Energy Mater.*, 2018, **8**, 1801090.
122 Y. Zeng, X. Zhang, R. Qin, X. Liu, P. Fang, D. Zheng, Y. Tong and X. Lu, *Adv. Mater.*, 2019, **31**, 1903675.
123 Q. Guan, Y. Li, X. Bi, J. Yang, J. Zhou, X. Li, J. Cheng, Z. Wang, B. Wang and J. Lu, *Adv. Energy Mater.*, 2019, **9**, 1901434.
124 L. Wang, N. Li, T. Wang, Y. Yin, Y. Guo and C. Wang, *Electrochim. Acta*, 2017, **244**, 172.
125 F. Wan, L. Zhang, X. Dai, X. Wang, Z. Niu and J. Chen, *Nat. Commun.*, 2018, **9**, 1656.
126 Y. Zeng, X. Zhang, Y. Meng, M. Yu, J. Yi, Y. Wu, X. Lu and Y. Tong, *Adv. Mater.*, 2017, **29**, 1700274.
127 C. Wang, K. Xia, H. Wang, X. Liang, Z. Yin and Y. Zhang, *Adv. Mater.*, 2019, **31**, 1801072.
128 M. Liao, L. Ye, Y. Zhang, T. Chen and H. Peng, *Adv. Electron. Mater.*, 2019, **5**, 1800456.
129 X. Fan, J. Liu, Z. Song, X. Han, Y. Deng, C. Zhong and W. Hu, *Nano Energy*, 2019, **56**, 454.
130 M. Wang, N. Xu, J. Fu, Y. Liu and J. Qiao, *J. Mater. Chem. A*, 2019, **7**, 11257.
131 J. Fu, J. Zhang, X. Song, H. Zarrin, X. Tian, J. Qiao, L. Rasen, K. Li and Z. Chen, *Energy Environ. Sci.*, 2016, **9**, 663.
132 N. Zhao, F. Wu, Y. Xing, W. Qu, N. Chen, Y. Shang, M. Yan, Y. Li, L. Li and R. Chen, *ACS Appl. Mater. Interfaces*, 2019, **11**, 15537.
133 J. Fu, D. U. Lee, F. M. Hassan, L. Yang, Z. Bai, M. G. Park and Z. Chen, *Adv. Mater.*, 2015, **27**, 5617.
134 A. Poosapati, K. Negrete, N. Jang, L. Hu, Y. Lan and D. Madan, *MRS Commun.*, 2019, **9**, 1015.
135 Y. Li, X. Fan, X. Liu, S. Qu, J. Liu, J. Ding, X. Han, Y. Deng, W. Hu and C. Zhong, *J. Mater. Chem. A*, 2019, **7**, 25449.

136 H.-W. Kim, J.-M. Lim, H.-J. Lee, S.-W. Eom, Y. T. Hong and S.-Y. Lee, *J. Mater. Chem. A*, 2016, **4**, 3711.
137 A. Poosapati, E. Jang, D. Madan, N. Jang, L. Hu and Y. Lan, *MRS Commun.*, 2019, **9**, 122.
138 M. Li, B. Liu, X. Fan, X. Liu, J. Liu, J. Ding, X. Han, Y. Deng, W. Hu and C. Zhong, *ACS Appl. Mater. Interfaces*, 2019, **11**, 28909.
139 Z. Cao, H. Hu, M. Wu, K. Tang and T. Jiang, *J. Mater. Chem. A*, 2019, **7**, 17581.
140 X. Cheng, J. Zhang, J. Ren, N. Liu, P. Chen, Y. Zhang, J. Deng, Y. Wang and H. Peng, *J. Phys. Chem. C*, 2016, **120**, 9685.
141 X. Xu, J. Chen, S. Cai, Z. Long, Y. Zhang, L. Su, S. He, C. Tang, P. Liu, H. Peng and X. Fang, *Adv. Mater.*, 2018, **30**, 1803165.
142 J. Lu, L. Cheng, K. C. Lau, E. Tyo, X. Luo, J. Wen, D. Miller, R. S. Assary, H. H. Wang, P. Redfern, H. Wu, J. B. Park, Y. K. Sun, S. Vajda, K. Amine and L. A. Curtiss, *Nat. Commun.*, 2014, **5**, 4895.
143 D. Aurbach, B. D. McCloskey, L. F. Nazar and P. G. Bruce, *Nat. Energy*, 2016, **1**, 16128.
144 D. Zhai, K. C. Lau, H. H. Wang, J. Wen, D. J. Miller, J. Lu, F. Kang, B. Li, W. Yang, J. Gao, E. Indacochea, L. A. Curtiss and K. Amine, *Nano Lett.*, 2015, **15**, 1041.
145 A. Dai, Q. Li, T. Liu, K. Amine and J. Lu, *Adv. Mater.*, 2019, **31**, 1805602.
146 G. Tan, L. Chong, R. Amine, J. Lu, C. Liu, Y. Yuan, J. Wen, K. He, X. Bi, Y. Guo, H. H. Wang, R. Shahbazian-Yassar, S. Al Hallaj, D. J. Miller, D. Liu and K. Amine, *Nano Lett.*, 2017, **17**, 2959.
147 Y. Qin, J. Lu, P. Du, Z. Chen, Y. Ren, T. Wu, J. T. Miller, J. Wen, D. J. Miller, Z. Zhang and K. Amine, *Energy Environ. Sci.*, 2013, **6**, 519.
148 Y. B. Yin, X. Y. Yang, Z. W. Chang, Y. H. Zhu, T. Liu, J. M. Yan and Q. Jiang, *Adv. Mater.*, 2018, **30**, 1703791.
149 S. Xu, Y. Yao, Y. Guo, X. Zeng, S. D. Lacey, H. Song, C. Chen, Y. Li, J. Dai, Y. Wang, Y. Chen, B. Liu, K. Fu, K. Amine, J. Lu and L. Hu, *Adv. Mater.*, 2018, **30**, 1704907.
150 C. Chen, S. Xu, Y. Kuang, W. Gan, J. Song, G. Chen, G. Pastel, B. Liu, Y. Li, H. Huang and L. Hu, *Adv. Energy Mater.*, 2019, **9**, 1802964.
151 W. J. Kwak, K. C. Lau, C. Shin, K. Amine, L. A. Curtiss and Y. Sun, *ACS Nano*, 2015, **9**, 4129.
152 Y. Hou, Y. Liu, Z. Zhou, L. Liu, H. Guo, H. Liu, J. Wang and J. Chen, *Electrochim. Acta*, 2018, **259**, 313.
153 Y. B. Yin, J. J. Xu, Q. C. Liu and X. B. Zhang, *Adv. Mater.*, 2016, **28**, 7494.
154 L. Wang, J. Pan, Y. Zhang, X. Cheng, L. Liu and H. Peng, *Adv. Mater.*, 2018, **30**, 1704378.
155 H. Xue, S. Wu, J. Tang, H. Gong, P. He, J. He and H. Zhou, *ACS Appl. Mater. Interfaces*, 2016, **8**, 8427.
156 X. Zou, Q. Lu, Y. Zhong, K. Liao, W. Zhou and Z. Shao, *Small*, 2018, **14**, 1801798.
157 Q. C. Liu, T. Liu, D. P. Liu, Z. J. Li, X. B. Zhang and Y. Zhang, *Adv. Mater.*, 2016, **28**, 8413.
158 T. Liu, Q. C. Liu, J. J. Xu and X. B. Zhang, *Small*, 2016, **12**, 3101.
159 J. Kang, J. Kim, S. Lee, S. Wi, C. Kim, S. Hyun, S. Nam, Y. Park and B. Park, *Adv. Energy Mater.*, 2017, **7**, 1700814.
160 X. Yang, J. Xu, Z. Chang, D. Bao, Y. Yin, T. Liu, J. Yan, D. Liu, Y. Zhang and X. Zhang, *Adv. Energy Mater.*, 2018, **8**, 1702242.
161 X. Y. Yang, J. J. Xu, D. Bao, Z. W. Chang, D. P. Liu, Y. Zhang and X. B. Zhang, *Adv. Mater.*, 2017, **29**, 1700378.
162 K. Yoon, K. Shin, J. Park, S. Cho, C. Kim, J. Jung, J. Cheong, H. Byon, H. Lee and I. Kim, *ACS Nano*, 2018, **12**, 128.
163 J. Long, Z. Hou, C. Shu, C. Han, W. Li, R. Huang and J. Wang, *ACS Appl. Mater. Interfaces*, 2019, **11**, 3834.
164 X. Yang, X. Feng, X. Jin, M. Shao, B. Yan, J. Yan, Y. Zhang and X. Zhang, *Angew. Chem., Int. Ed.*, 2019, **58**, 16411.
165 Z. Sun, S. Jin, H. Jin, Z. Du, Y. Zhu, A. Cao, H. Ji and L. Wan, *Adv. Mater.*, 2018, **30**, 1800884.
166 S. Chi, Y. Liu, W. Song, L. Fan and Q. Zhang, *Adv. Funct. Mater.*, 2017, **27**, 1700348.
167 A. Raji, R. Villegas Salvatierra, N. Kim, X. Fan, Y. Li, G. A. L. Silva, J. Sha and J. M. Tour, *ACS Nano*, 2017, **11**, 6362.
168 D. Lin, Y. Liu, Z. Liang, H. W. Lee, J. Sun, H. Wang, K. Yan, J. Xie and Y. Cui, *Adv. Nat. Sci.: Nanosci. Nanotechnol.*, 2016, **11**, 626.
169 Y. Yin, Z. Yu, Z. Ma, T. Zhang, Y. Lu, T. Ma, F. Zhou, H. Yao and S. Yu, *Natl. Sci. Rev.*, 2019, **6**, 247.
170 X. Wang, Z. Pan, J. Yang, Z. Lyu, Y. Zhong, G. Zhou, Y. Qiu, Y. Zhang, J. Wang and W. Li, *Energy Storage Mater.*, 2019, **22**, 179.
171 Q. Liu, J. Xu, S. Yuan, Z. Chang, D. Xu, Y. Yin, L. Li, H. Zhong, Y. Jiang, J. Yan and X. Zhang, *Adv. Mater.*, 2015, **27**, 5241.
172 T. Liu, X. Feng, X. Jin, M. Shao, Y. Su, Y. Zhang and X. Zhang, *Angew. Chem., Int. Ed.*, 2019, **131**, 18408.
173 B. Liu, W. Xu, J. Tao, P. Yan, J. Zheng, M. Engelhard, D. Lu, C. Wang and J. Zhang, *Adv. Energy Mater.*, 2018, **8**, 1702340.
174 C. Yan, X. Cheng, Y. Yao, X. Shen, B. Li, W. Li, R. Zhang, J. Huang, H. Li and Q. Zhang, *Adv. Mater.*, 2018, **30**, 1804461.
175 C. Zhao, J. Liang, Y. Zhao, J. Luo, Q. Sun, Y. Liu, X. Lin, X. Yang, H. Huang, L. Zhang, S. Zhao, S. Lu and X. Sun, *J. Mater. Chem. A*, 2019, **7**, 24947.
176 G. Huang, J. Han, C. Yang, Z. Wang, T. Fujita, A. Hirata and M. Chen, *NPG Asia Mater.*, 2018, **10**, 1037.
177 Z. Guo, J. Li, Y. Xia, C. Chen, F. Wang, A. Tamirat, Y. Wang, Y. Xia, L. Wang and S. Feng, *J. Mater. Chem. A*, 2018, **6**, 6022.
178 D. Safanama and S. Adams, *ACS Energy Lett.*, 2017, **2**, 1130.
179 J. Yi, Y. Liu, Y. Qiao, P. He and H. Zhou, *ACS Energy Lett.*, 2017, **2**, 1378.
180 X. Lei, X. Liu, W. Ma, Z. Cao, Y. Wang and Y. Ding, *Angew. Chem., Int. Ed.*, 2018, **57**, 16131.
181 H. Kim, T. Y. Kim, V. Roev, H. C. Lee, H. J. Kwon, H. Lee, S. Kwon and D. Im, *ACS Appl. Mater. Interfaces*, 2016, **8**, 1344.
182 Y. Liu, P. He and H. Zhou, *Adv. Energy Mater.*, 2018, **8**, 1701602.

183 N. Feng, P. He and H. Zhou, *Adv. Energy Mater.*, 2016, **6**, 1502303.
184 W. Xu, J. Wang, F. Ding, X. Chen, E. Nasybulin, Y. Zhang and J.-G. Zhang, *Energy Environ. Sci.*, 2014, **7**, 513.
185 Z. Jian, Y. Chen, F. Li, T. Zhang, C. Liu and H. Zhou, *J. Power Sources*, 2014, **251**, 466.
186 P. Hartmann, C. L. Bender, M. Vracar, A. K. Durr, A. Garsuch, J. Janek and P. Adelhelm, *Nat. Mater.*, 2013, **12**, 228.
187 J. L. Ma, F. L. Meng, Y. Yu, D. P. Liu, J. M. Yan, Y. Zhang, X. B. Zhang and Q. Jiang, *Nat. Chem.*, 2019, **11**, 64.
188 J. L. Ma, F. L. Meng, D. Xu and X. B. Zhang, *Energy Storage Mater.*, 2017, **6**, 1.
189 S. Xu, S. K. Das and L. A. Archer, *RSC Adv.*, 2013, **3**, 6656.
190 W. Zhang, C. Hu, Z. Guo and L. Dai, *Angew. Chem., Int. Ed.*, 2020, **59**, 3470.
191 X. Wang, X. Zhang, Y. Lu, Z. Yan, Z. Tao, D. Jia and J. Chen, *ChemElectroChem*, 2018, **5**, 3628.
192 B. Huang and G. Frapper, *J. Am. Chem. Soc.*, 2018, **140**, 413.
193 H. Lim, H. Lim, K. Park, D. Seo, H. Gwon, J. Hong, W. Goddard, H. Kim and K. Kang, *J. Am. Chem. Soc.*, 2013, **135**, 9733.
194 Y. Hou, J. Wang, L. Liu, Y. Liu, S. Chou, D. Shi, H. Liu, Y. Wu, W. Zhang and J. Chen, *Adv. Funct. Mater.*, 2017, **27**, 1700564.
195 W. Yin, A. Grimaud, I. Azcarate, C. Yang and J.-M. Tarascon, *J. Phys. Chem. C*, 2018, **122**, 6546.
196 A. Khurram, M. He and B. M. Gallant, *Joule*, 2018, **2**, 1.
197 K. Takechi, T. Shiga and T. Asaoka, *Chem. Commun.*, 2011, **47**, 3463.
198 Y. Liu, R. Wang, Y. Lyu, H. Li and L. Chen, *Energy Environ. Sci.*, 2014, **7**, 677.
199 S. R. Gowda, A. Brunet, G. M. Wallraff and B. D. McCloskey, *J. Phys. Chem. Lett.*, 2013, **4**, 276.
200 Z. Zhang, Q. Zhang, Y. Chen, J. Bao, X. Zhou, Z. Xie, J. Wei and Z. Zhou, *Angew. Chem., Int. Ed.*, 2015, **127**, 6550.
201 L. Qie, Y. Lin, J. W. Connell, J. Xu and L. Dai, *Angew. Chem., Int. Ed.*, 2017, **56**, 6970.
202 C. Lv, C. Yan, G. Chen, Y. Ding, J. Sun, Y. Zhou and G. Yu, *Angew. Chem., Int. Ed.*, 2018, **57**, 6073.
203 X. Zhang, C. Wang, H. Li, X.-G. Wang, Y.-N. Chen, Z. Xie and Z. Zhou, *J. Mater. Chem. A*, 2018, **6**, 2792.
204 Z. Zhang, X. G. Wang, X. Zhang, Z. Xie, Y. N. Chen, L. Ma, Z. Peng and Z. Zhou, *Adv. Sci.*, 2018, **5**, 1700567.
205 S.-M. Xu, Z.-C. Ren, X. Liu, X. Liang, K.-X. Wang and J.-S. Chen, *Energy Storage Mater.*, 2018, **15**, 291.
206 Z. Zhang, Z. Zhang, P. Liu, Y. Xie, K. Cao and Z. Zhou, *J. Mater. Chem. A*, 2018, **6**, 3218.
207 Y. Mao, C. Tang, Z. Tang, J. Xie, Z. Chen, J. Tu, G. Cao and X. Zhao, *Energy Storage Mater.*, 2018, **18**, 405.
208 Y. Qiao, J. Yi, S. Wu, Y. Liu, S. Yang, P. He and H. Zhou, *Joule*, 2017, **1**, 359.
209 B. Ge, Y. Sun, J. Guo, X. Yan, C. Fernandez and Q. Peng, *Small*, 2019, **15**, 1902220.
210 H. Liang, Y. Zhang, F. Chen, S. Jing, S. Yin and P. Tsiakaras, *Appl. Catal., B*, 2019, **244**, 559.
211 H. Wang, K. Xie, Y. You, Q. Hou, K. Zhang, N. Li, W. Yu, K. Loh, C. Shen and B. Wei, *Adv. Energy Mater.*, 2019, **9**, 1901806.
212 Z. Guo, J. Li, H. Qi, X. Sun, H. Li, A. G. Tamirat, J. Liu, Y. Wang and L. Wang, *Small*, 2019, **15**, 1803246.
213 S. Li, Y. Dong, J. Zhou, Y. Liu, J. Wang, X. Gao, Y. Han, P. Qi and B. Wang, *Energy Environ. Sci.*, 2018, **11**, 1318.
214 Y. Xing, Y. Yang, D. Li, M. Luo, N. Chen, Y. Ye, J. Qian, L. Li, D. Yang, F. Wu, R. Chen and S. Guo, *Adv. Mater.*, 2018, **30**, 1803124.
215 J. Chen, K. Zou, P. Ding, J. Deng, C. Zha, Y. Hu, X. Zhao, J. Wu, J. Fan and Y. Li, *Adv. Mater.*, 2018, **31**, 1805484.
216 Q.-C. Zhu, S.-M. Xu, Z.-P. Cai, M. M. Harris, K.-X. Wang and J.-S. Chen, *Energy Storage Mater.*, 2017, **7**, 209.
217 S. Xu, C. Chen, Y. Kuang, J. Song, W. Gan, B. Liu, E. Hitz, J. Connell, Y. Lin and L. Hu, *Energy Environ. Sci.*, 2018, **11**, 3231.
218 C. Wang, Q. Zhang, X. Zhang, X. G. Wang, Z. Xie and Z. Zhou, *Small*, 2018, **14**, 1800641.
219 Y. Li, J. Zhou, T. Zhang, T. Wang, X. Li, Y. Jia, J. Cheng, Q. Guan, E. Liu, H. Peng and B. Wang, *Adv. Funct. Mater.*, 2019, **29**, 1808117.
220 X. Li, J. Zhou, J. Zhang, M. Li, X. Bi, T. Liu, T. He, J. Cheng, F. Zhang, Y. Li, X. Mu, J. Lu and B. Wang, *Adv. Mater.*, 2019, **31**, 1903852.
221 L. Guo, B. Li, V. Thirumal and J. Song, *Chem. Commun.*, 2019, **55**, 7946.
222 T. Shiga, Y. Kato, M. Inoue and Y. Hase, *ACS Sustainable Chem. Eng.*, 2019, **7**, 14280.
223 R. Pipes, A. Bhargav and A. Manthiram, *Adv. Energy Mater.*, 2019, **9**, 1900453.
224 J. Li, H. Zhao, H. Qi, X. Sun, X. Song, Z. Guo, A. G. Tamirat, J. Liu, L. Wang and S. Feng, *Adv. Funct. Mater.*, 2019, **29**, 1806863.
225 C. Li, Z. Guo, B. Yang, Y. Liu, Y. Wang and Y. Xia, *Angew. Chem., Int. Ed.*, 2017, **129**, 9254.
226 J. Ma, D. Bao, M. Shi, J. Yan and X. Zhang, *Chem*, 2017, **2**, 525.
227 P. Andrei, J. P. Zheng, M. Hendrickson and E. J. Plichta, *J. Electrochem. Soc.*, 2012, **159**, A770.
228 K. G. Gallagher, S. Goebel, T. Greszler, M. Mathias, W. Oelerich, D. Eroglu and V. Srinivasan, *Energy Environ. Sci.*, 2014, **7**, 1555.

